ABSTRACT

STUDY OF HINDERED INTERNAL ROTATION IN SOME SUBSTITUTED AMIDES BY NUCLEAR MAGNETIC RESONANCE SPECTROSCOPY

By

William Chung-Tsing Tung

A Varian HA-100 high-resolution nuclear magnetic resonance (NMR) spectrometer was used for measuring the proton magnetic resonance spectra of several symmetrically and asymmetrically N,N-disubstituted amides over a wide range of temperatures. Due to inconsistencies in the Varian temperature charts, the ethylene glycol and methanol chemical-shift thermometers were carefully recalibrated.

A detailed description and discussion of the two currently most popular approximation methods used in the study of the relationship between the rate of internal rotation about the central C-N bond of symmetrically disubstituted amides and the various observed line-shape parameters, are presented. The theoretical two-site exchange line-shape equation was programmed to fit the experimental spectra to a set of line-shape parameters by a least-squares method. The best sets of parameters were extracted from the observed line shapes by this curve fitting procedure and the

theoretical spectra were plotted for visual comparison with experimental spectra. Both computer programs were written for the CDC-3600 computer.

In the case of symmetrically disubstituted amides, all three methods (intensity-ratio, peak-separation and total line-shape) were used to study the rate of internal rotation as a function of temperature. The results of these studies are reported and discussed. Deuterated N,N-dimethylformamide (DMF) was used to eliminate the effect of spin-spin interaction between the formal proton and the protons of N-methyl groups and so obtain a more reliable rotational energy barrier for DMF. A superposition technique was also used to estimate the effect of spin-spin coupling on the energy barrier of this amide using the digital computer.

A study of factors influencing the rotational energy barrier obtained for N,N-dimethylcarbamoylchloride has been made. It is shown that the methods of preparing and handling the sample, as well as the method of referencing the NMR signals, have an important effect on the values obtained for the energy barrier.

The total line-shape analysis method was also applied to evaluate the energy barriers of N-methyl-N-ethylacetamide, N-methyl-N-n-butylacetamide, N-methyl-N-isopropylacetamide, N-methyl-N-cyclohexylactamide and N-methyl-N-benzylformamide. The results qualitatively indicate that the order of the values of the energy barriers of these asymmetrically disubstituted amides is parallel to the order of polarity

of the N-alkyl groups.

The observed spectra of N-methyl-N-n-butyltrimethylacetamide, N-methyl-N-α-naphthylacetamide and N-methyl-N-phenylacetamide indicate that either the rates of internal rotation about the central C-N bonds of these amides were too fast, even at quite low temperature (-20°C), to be detected or the bulky N-substituted groups lead to a single stable isomer in the accessible temperature range.

The frequency factors obtained in this laboratory are in the range of 10^{+12} to 10^{17} sec^{-1}. These are somewhat higher than those reported earlier (3,4), but they are in good agreement with the more recent values. The high values are attributed to the increase of entropy in going from the ground state of a disubstituted amide molecule to the transition state.

The rotational energy barriers in a number of N,N-dimethylamides have been redetermined using the total line-shape analysis method. The new values are, in general, much higher than those reported from intensity-ratio or peak-separation studies. The effect of substituents on the barriers has been discussed.

The effect of solvents on the rotational energy barrier in DMF has been investigated. It is found that solvents of lower dielectric constant than the amide itself lower the barrier. These solvents appear to break up the dimers and polymeric species which are important in the pure amides and which tend to raise the barriers to internal rotation.

STUDY OF HINDERED INTERNAL ROTATION IN SOME SUBSTITUTED AMIDES BY NUCLEAR MAGNETIC RESONANCE SPECTROSCOPY

By

William Chung-Tsing Tung

A THESIS

Submitted to
Michigan State University
in partial fulfillment of the requirements
for the degree of

DOCTOR OF PHILOSOPHY

Department of Chemistry

1968

ACKNOWLEDGMENTS

It is with sincere appreciation that I acknowledge the encouragement and counsel of Professor M. T. Rogers under whose direction this investigation was conducted.

I also wish to express my gratitude to the National Institutes of Health, Division of General Medical Sciences and the American Chemical Society, Petroleum Research Fund, for support of this work.

To Debbie, my wife, I want to offer my everlasting appreciation for her constant encouragement and understanding during this phase of my education.

TABLE OF CONTENTS

TABLE OF CONTENTS - Cont'd. Page

LIST OF TABLES

LIST OF TABLES - cont'd.

LIST OF TABLES - cont'd.

LIST OF TABLES - cont'd.

LIST OF FIGURES

LIST OF FIGURES - cont'd.

LIST OF FIGURES - cont'd.

INTRODUCTION

Rotation about the central C-N bond of amides and substituted amides is not free and the energy barrier restricting rotation is believed to arise, in part at least, from the partial double-bond character of this bond (1). The only general method for measuring these rotational energy barriers depends on detailed analysis of the nuclear magnetic resonance line shapes at various temperatures.

Phillips (2) proved that the doublet observed for the N-methyl protons of N,N-dimethylamides was the result of a chemical shift difference between the two methyl groups A and B.

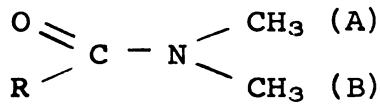

He also noted that the components of the doublet gradually coalesce on raising the temperature and that the resulting single line becomes narrower at high temperatures. Gutowsky and Holm (3) developed a theory relating the proton line shape to the rate of rotation about the C-N bond and evaluated the rotational energy barriers in N,N-dimethylformamide (DMF) and N,N-dimethylacetamide (DMA) from

measurements of the rates of rotation at different temperatures. Application of the Arrhenius equation (rate = $Ae^{-E_a/RT}$) to this rate process permitted values of the rotational energy barrier E_a and the frequency factor A to be evaluated.

Because of the general interest in the origin of rotational energy barriers, and also because the NMR method provides the only precise method for studying a series of substituted amides, many investigations have been made since 1956. Rogers and Woodbrey (4) showed that the original peak-separation method (3) was not capable of great precision and developed an intensity-ratio method which was used to study substituent effects on the rotational energy barriers in symmetrically N,N-disubstituted amides. They also studied the effect of solvents on these barriers (5).

Allerhand and Gutowsky (6) developed the spin-echo method for determining rates of internal rotation in amides and applied it to determining the rotational energy barriers in N,N-dimethylcarbamoyl chloride (DMCC) and in N,N-dimethyltrichloroacetamide (DMTCA). This method has the advantage that it greatly extends the range of temperatures which can be studied. Their values were consistently higher than those of Rogers and Woodbrey and detailed investigation showed that the intensity-ratio method is subject to certain systematic errors in unfavorable cases. It became clear that only by detailed fitting of observed line shapes to

those calculated with variable sets of parameters could reliable rate constants be obtained.

The present research program consists of three parts: (1) Re-examination of the high-resolution NMR method for determining rotational energy barriers and development of computer techniques for total line-shape analysis, (2) Application of the methods so developed for treating proton exchange between two sites, without any approximations or assumptions, to a re-examination of the symmetrically N,N-disubstituted amides, and (3) Extension of the total line-shape analysis techniques to the measurement of rotational energy barriers in a series of unsymmetrically N,N-disubstituted amides which had not been previously studied.

HISTORICAL BACKGROUND

High-resolution nuclear magnetic resonance (NMR) spectroscopy may be used to determine the rates of many processes. In 1953 Gutowsky and McCall (7) showed that for protons exchanging between two sites the rate of exchange may be related quantitatively to the line shape provided the rate falls within certain limits. Since then the NMR method has been used to measure the rates of many proton interchange processes.

In his book Pauling (1) postulated that rotation about the central C-N bond of amides would be restricted since the bond should have considerable double-bond character and this was confirmed by Phillips (2) from an NMR study of N,N-dimethylamides. Phillips (8) also discussed several types of molecules in which internal rotations could be studied by the NMR method. Phillips (2) showed that peaks corresponding to the two methyl groups A and B in N,N-dimethylformamide (I) were chemically shifted in the NMR spectrum and that these peaks coalesced at higher temperatures to a single peak located at the average position. From a theoretical study, Gutowsky and Holm (3) showed that the apparent peak separation $\delta\nu$ of the partially coalesced doublet could be related to the lifetime 2τ of a given set

of protons at one site. They were able to evaluate the rate of interchange of methyl protons in I between sites A and B, and so the rate of interchange between isomers I and II, for two amides. This may be considered a first order rate process with rate constant $k = 2\tau$.

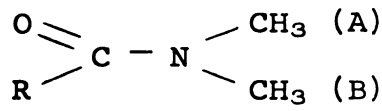

I

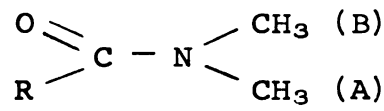

II

Treating the interchange as a rate process governed by the Arrhenius equation

$$k = Ae^{-E_a/RT} ,$$

they obtained values for the energy barrier E_a hindering rotation about the central C-N bonds in N,N-dimethylformamide (DMF) (I, R=H) and in N,N-dimethylacetamide (DMA) (I, R= CH_3) of 7 ± 3 and 12 ± 2 kcal/mole, respectively. The large probable errors reflect the fact that the linewidths are comparable to the chemical shifts between the peaks at the low spectrometer frequency (ν_o= 17.735 Mhz) which they used.

Loewenstein and Meiboom (9) showed that the mean lifetime τ of exchangeable nuclei at a chemical site could be related to r, the ratio of maximum to central minimum v-mode intensities. Rogers and Woodbrey (4) developed the intensity-ratio method and applied it to the evaluation of internal rotation energy barriers in an extensive variety of

substituted amides. In addition they treated the process as governed by the absolute reaction rate theory equation

$$k = \kappa \frac{kT}{h} e^{-\frac{\Delta F^{\ddagger}}{RT}}$$

and obtained values of the parameters $\Delta F^{\ddagger}$, $\Delta H^{\ddagger}$ and $\Delta S^{\ddagger}$ of that theory assuming the transmission coefficient κ to be unity. They also studied the effect of solvent on the energy barriers (5).

Fraenkel and Franconi (10) compared actual with calculated line shapes through two parameters, the intensity ratio r and the width of the collapsed doublet S. By this method they evaluated the barrier to internal rotation in DMF and in the protonated species DMF-H^{+} and showed that the latter was larger by 3.1 kcal/mole. Their work indicated that protonation occurs on oxygen rather than nitrogen and this was later proved conclusively by Gillespie (11) from NMR studies of solutions of DMF and DMA in fluorosulfuric acid. Neuman (12) programmed the general line-shape equations of Rogers and Woodbrey (4) to obtain energy barriers from the intensity-ratio method for DMF, DMA and dimethylthioacetamide (DMTA) in formamide solution.

Allerhand and Gutowsky (6) applied the spin-echo technique to determine exchange rates in the N,N-dimethyltrichloroacetamide (DMTCA) and N,N-dimethylcarbamoyl chloride (DMCC). They showed that accurate values of the exchange rates for the protons could be obtained by determining the

decay amplitude of successive echoes in a Carr-Purcell train and the method has the advantage that it can be used to measure much more rapid exchange rates than can the high-resolution methods. It has the disadvantage that no other protons but the two exchanging sets can be present since the resolution is low. Reeves (13) extended this method to N,N-dimethyltrifluoroacetamide (DMTFA) and to N,N-dimethylformamide-d_1 to obtain new values for the energy barriers in these amides.

Fryer, Conti and Franconi (14) reviewed all work up to 1965 on energy barriers hindering internal rotation in amides. They showed that values obtained in various laboratories disagreed beyond the stated limits of error and they attempted to locate systematic sources of error and to develop other line-shape parameters. They were able to show that both the peak-separation method and the intensity-ratio method were subject to systematic errors particularly as a result of the inhomogeneous broadening of the lines in magnetic fields at present attainable.

It became clear about this time that the best way to obtain reliable values of exchange rates and of energy barriers from high-resolution NMR data would be to compare the complete experimental spectrum with spectra calculated using various parameters and select the parameters to give best agreement between theory and experiment. Allerhand et al. (15), showed that good agreement between high-resolution and spin-echo methods could be obtained for

energy barriers if adequate computer methods were used to treat the data in each case. It has become necessary to reinvestigate all the values of energy barriers obtained using the older methods since systematic errors led to values which were, in general, too low.

Neuman (16) used total line-shape analysis to reinvestigate the rotational barriers in DMCC and obtained a value, E_a = 16.9 ± 0.5 kcal/mole, somewhat higher than that reported by the spin-echo method (16) (E_a = 14.0 ± 0.9 kcal/mole). The same method was used (17) to obtain a new value for the rotational barrier in DMA-d_3, E_a = 19.6 ± 0.3 kcal/mole; the deuteration of the acetyl methyl protons eliminates the spin coupling across the C-N bond and improves the accuracy of the results. They used the line-shape equations of Gutowsky and Holm to generate values of signal intensity <u>versus</u> frequency for exchange between equally populated sites for various values of the exchange rate 2τ. The results were plotted and compared visually with experimental spectra; a computer program developed by Roberts and Gerig was used in their work. Conti and von Philipsborn (18) have also reinvestigated several amides using every precaution to eliminate systematic errors and report values of DMF, DMF-d_1, DMF-H^+ and DMF-d_1-H^+ which should be quite reliable. Unfortunately these new and carefully-obtained results from the high-resolution method still differ in several cases from those obtained by the best spin-echo

techniques and the source of these discrepancies is not known.

Although most of the research so far has concentrated on symmetrically disubstituted amides, the NMR method may also be used to obtain rotational barriers in unsymmetrically substituted materials. The earliest report of barriers in such compounds was that by Franconi (19) who reported E_a = 11, 12, and 11 kcal/mole for $C_6H_5CHCH_3NCH_3CHO$, $C_6H_5CH_2NCH_3CHO$ (MBF) and $(C_6H_5)_2CHNCH_3CHO$, respectively. Mannschreck (20) obtained the relative amounts of isomers I and II by the NMR method in a series of compounds $R_3CONR_1R_2$ where R_3 = 2,4,6-trimethylphenyl and R_1, R_2 are various alkyl groups. He evaluated (21) the rotational barriers for the particular compound with $R_1 = CH_3$, R_2 = benzyl, and R_3 = 2,4,6-trimethylphenyl in quinoline solution and reports $\Delta F^{\ddagger}$ = 23.1 kcal/mole. If R_3 = 2,4,6-tribromophenyl, $\Delta F^{\ddagger}$ = 23.5 kcal/mole. Gehring et al. (22), determined the barriers in several N-alkyl-N-vinyl-amides by the peak-separation method. Gutowsky, Jonas and Siddall (23) have made the only reliable study of any unsymmetrically substituted amide for MBF where E_a = 22.7 kcal/mole or 25 kcal/mole, depending on whether the formyl or benzyl doublets are analyzed. A direct measurement from the experimentally determined equilibrium constant gave the value 20.0 kcal/mole. An intensive study of conformational isomerism in the much more complex N-acetyl-N-methyl-2,4,6-trinitroaniline (24) has also been made.

The values which have been reported for energy barriers hindering internal rotation in pure substituted amides are listed in Table 1 while Table 2 lists values obtained in solution. Table 3 summarizes the data for the unsymmetrically substituted amides. In only a few cases have the values been determined by fitting the complete observed line shape to the theoretical expression. All values determined by other methods must be considered as only estimates subject to very large probable errors.

Table 1. Energy barriers restricting rotation about the central C-N bond of substituted amides.

Compound	E_a kcal/mole	$\Delta F^{\ddagger}$ kcal/mole	Log_{10} A	Method	Reference
Formamide (in acetone)	18.0			LB	90
N,N-Dimethylformamide	7.0		3 to 7	PS	3
	9.6		6.5	IR	10
	15.9			PS	69
	18.3	21.0	10.8	IR	10
	20.0		13.0	PS	91
	22.0	21.7	13.0	VAR(HA-100)	18
	26.0	21.6	16.0	VAR(A-60)	18
	26.0		16.0	VAR	14
	28.2		17.2	PS	22
DMF-d_1	22.0		--	SE	93
	27.4	23.0	16.0	VAR	18
DMF-H^+($100\%H_2SO_4$)	12.7		8.0	IR	10
DMF-H^+ (in TFA)	26.0	21.6	16.0	VAR	18
DMF-d_1-H^+ (in TFA)	24.0	21.0	15.0	VAR	18
N,N-Dimethylacetamide	12.0	17.8	7 to 10	PS	3
	23.0	18.7	16.0	VAR	14
	10.6	17.4	7.8	IR	4
	20.2	15.7	16.1	PS	22
DMA-d_3	19.6	18.2	13.8	TLS	17
N,N-Dimethylpropionamide	21.0		15.0	VAR	14
	9.2	16.7	7.3	IR	4
N,N-Dimethylisobutyramide		16.2			94
N,N-Dimethylbenzamide					
(CH_2Br_2 solution)	7.7	15.5	7.2	IR	4
($CHCl_3$ solution)	20.0		16.0	VAR	14
N,N-Dimethylcarbamyl-chloride	7.3	16.5	6.1	IR	4
	14.0	16.6	10.9	SE	6
	16.9	16.8	12.9	TLS	16

continued

Table 1 (cont'd.)

Compound	E_a kcal/mole	$\Delta F^{\ddagger}$ kcal/mole	Log_{10} A	Method	Reference
N,N-Dimethyltrifluoro-acetamide	20.6	18.6	14.3	SE	13
	9.3	17.6	6.8	IR	4
N,N-Dimethylcyclopro-panecarboxamide	12.3	16.1(319.7°K)	10.0	IR	94
N,N-Dimethyltrichloro-acetamide	17.0		15.0	VAR	14
	9.9	14.9	9.1	IR	4
	14.6	15.0	12.5	SE	6
N,N-Dimethylbutyramide	24.0		16.0	VAR	14
N,N-Diethylformamide	19.6			PS	95
	16.8			PS	69
N,N-Diethylacetamide	16.9			PS	95
	18.0			PS	69
N,N-Diethylaceto-acetamide	16.8			PS	95
N,N-Di-n-propylacetamide	17.0			PS	95
N,N-Diisopropylacetamide	7.5			PS	69
	15.7			PS	95
o-Methoxy-N,N-dimethyl-benzamide	26.0		17.0	VAR	14
N,N-Dimethylacrylamide	6.8	16.0	6.0	IR	4

PS = Peak Separation
IR = Intensity Ratio
SE = Spin-Echo
VAR = Various Methods
TLS = Total Line-Shape analysis
LB = Line Broadening

[a]All values of $\Delta F^{\ddagger}$ are at 298.2°K unless another value of temperature is given.

Table 2. Some rotational barriers for substituted amides in solution.

Compound	Solvent	E_a kcal/mole	$\Delta F^{\ddagger}$ kcal/mole	Log_{10} A	Method	Reference
DMF	Chloronaphthalene		20.6[a]		TLS	21
	Formamide	26.3		15.5	IR	12
	Acetone-d^6	16.8			PS	69
	$CFCl_3$	11.3			PS	69
	HMDS	9.4			PS	69
DMA	10% Formamide	24.7		16.4	IR	12
DMA-d^3	95% DMSO	18.6	20.0[b]	14.3	TLS	17
N,N-Dibenzylacetamide	38% CH_2Br_2	7.3	16.5[c]	6.1	IR	5
	38% CCl_4	6.4	16.3[d]	5.5	IR	5
N,N-Dimethylpropion-amide	10% CH_2Br_2	6.7	16.7[e]	5.4	IR	5
	11% CCl_4	6.3	16.0[f]	5.7	IR	5
N,N-Dimethylcarbamoyl chloride	10.7% CH_2Br_2	7.3	16.5[g]	6.0	IR	5
	11% $CHCl_3$	6.8	16.2[h]	5.9	IR	5
	10.4% $CHCl_3$	17.7	16.3[b]	13.8	TLS	16
N,N-Dimethyl-2,4,6-trimethylbenzamide	Chloronaphthalene	23.2	22.5[f]	13.3	TLS	21
N,N-Dimethyl-2,4,6-tribromobenzamide	Chloronaphthalene		22.6[h]		TLS	21
o-Nitro-N,N-dimethyl-benzamide	CCl_3CHCl_2	20.0		13.0	VAR	14
m-Nitro-N,N-dimethyl-benzamide	CD_3COCD_3	15.0		12.0	VAR	14
p-Nitro-N,N-dimethyl-benzamide	CD_3COCD_3	22.0		17.0	VAR	14
m-Methoxy-N,N-di-methylbenzamide	CD_3COCD_3	20.0		17.0	VAR	14
N,N-Dimethyliso-butyramide	o-$C_6H_4Cl_2$		16.2[i]		IR	94
N,N-Dimethylcyclo-propanecarboxamide	o-$C_6H_4Cl_2$	12.7	16.4[j]	10.1	IR	94

a, 401.2°K; b, 298.2°K; c, 343.7°K; d, 334.5°K; e, 338.3°K; f, 316.4°K; g, 325.9°K; h, 444°K; i, 299°K; j, 311.4°K.

Table 3. Rotational barriers in unsymmetrically N,N-disubstituted amides.

Compound	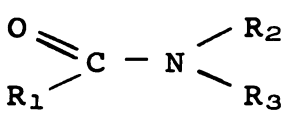		E_a kcal/ mole	$\Delta F^{\ddagger}$ kcal/ mole	Log_{10} A	Method	Reference
R_1	R_2	R_3					
H	CH_3	$-CH_2\phi$	25.0	20.9[a]	15.2	TLS	23
H	CH_3	$-CH_2\phi$	12.0		7.0	PS	96
H	CH_3	$-CHCH_3\phi$	11.5		7.0	PS	96
H	CH_3	$-CH\phi_2$	11.0		8.0	PS	96
H	CH_3	$-CH_2CH_2Cl$	30.0		17.4	PS	22
H	CH_3	$-CH=CH_2$	15.7		11.4	PS	22
H	$-CH_2CH_2Cl$	$-CH_2=CH_2$	21.0		14.7	PS	22
CH_3	$-CH_3$	$-CH_2-CH_2Cl$	22.7		16.2	PS	22
CH_3	CH_3	$-CH=CH_2$	14.0		13.2	PS	22
CH_3	H	$-2,4,6-(t-C_4H_9)_3\phi$		24.0[b]			92
Mesityl	CH_3	$-CH_2\phi$(in chloro-naphthalene)	23.5	23.0[c]	13.1	TLS	21
CH_3	CH_3	$-2,4,6-(NO_2)_3\phi$	19.7		14.0	TLS	24

a, 373.1°K
b, 298.2°K
c, 316.5°K

THEORETICAL BACKGROUND

Introduction

Many atomic nuclei behave as though they are spinning charged bodies and the circulation of the charge produces a magnetic moment along the axis of rotation. Nuclei such as ^{1}H, ^{13}C, ^{15}N and ^{19}F are spherical, have no quadrupole moment and their spin quantum number $I = 1/2$. When these nuclei are placed in a magnetic field H, taken as the Z direction, they will line up with the field ($I_z = +1/2$) or against the field ($I_z = -1/2$). The energy difference between these two levels, ΔE, is proportional to the magnetic field strength H at the nucleus and is equal to $\gamma hH/2\pi$, where γ is the gyromagnetic ratio of the nucleus. As for other type of spectroscopy, NMR involves absorption of electromagnetic radiation whose energy ΔE is related to the frequency ν of the rf oscillator by the equation $\Delta E = h\nu$. To observe nuclear magnetic resonance absorption a fixed frequency can be applied and the field varied until the equation $\nu = \gamma H/2\pi$ is satisfied; energy is then absorbed by the nuclei. In a typical experiment this flow of energy induces a current in the receiver circuit which is detected and recorded.

In a uniform static field H_o the energies of the two spin states are separated by an energy $2\mu H_o$, where μ is the maximum component of the nuclear magnetic moment. For an assembly of nuclei ($I = 1/2$) at a certain thermal equilibrium temperature T the ratio of the populations of the two states is

$$\frac{N_2}{N_1} = \exp\left(\frac{-2\mu H_o}{kT}\right) \simeq 1 - \frac{2\mu H_o}{kT} \quad .$$

The probabilities of a given nucleus being in either the upper or lower state are $\frac{1}{2}(1-\frac{\mu H_o}{kT})$ and $\frac{1}{2}(1+H\frac{\mu H_o}{kT})$, respectively. The mean nuclear magnetic moment in the direction of the main field is

$$\bar{\mu} = \mu\left[\tfrac{1}{2}\left(1 + \frac{\mu H_o}{kT}\right) - \tfrac{1}{2}\left(1 - \frac{\mu H_o}{kT}\right)\right] = \frac{\mu^2 H_o}{kT}$$

and, in a unit volume containing N nuclei, the corresponding paramagnetic volume susceptibility is

$$\chi_o = \frac{N\bar{\mu}}{H_o} = \frac{N\mu^2}{kT} \quad .$$

Let n_- and n_+ be the number of nuclei in the upper and lower states, respectively; the difference $n = n_+ - n_-$ (excess number of nuclei per time) is a function of time. If n_e is denoted as this difference after equilibrium is reached the rate of change of populations can be expressed as

$$dn/dt = -(n - n_e)/T_1 \quad ,$$

where T_1, the spin-lattice relaxation time, is a measure of the rate at which the spin system comes into thermal equilibrium with the other degrees of freedom. The spin-lattice relaxation time is related to W, the mean of the two probabilities for the spin-state transitions upward $W_- \rightarrow W_+$ and downward $W_+ \rightarrow W_-$ by the expression

$$T_1 = \frac{1}{2W} = \frac{1}{(W_- \rightarrow W_+) + (W_+ \rightarrow W_-)} .$$

The experimentally observed line is always broader (covers a range of several frequencies) than the sharp signal at one frequency predicted by the quantum mechanical calculation. There are several causes for the broadening. First, it is due to spontaneous emission since the lower limit of any spectroscopic line width is determined by the finite lifetime of the upper state. The broadening caused by this is negligibly small (25). Second, the spin-lattice relaxation can cause line broadening. The finite lifetime of the two states is important because of the possibility of transitions between them being induced by the other molecular degrees of freedom. The line broadening can be estimated from the uncertainty principle $\Delta E \Delta t \sim \hbar$, and this implies that the uncertainty in the frequency of the absorption is $1/2\pi\Delta t$.

In the case of solids or highly viscous liquids the direct interaction of the magnetic dipoles causes greater broadening than that from the spin-lattice relaxation process.

Here the nuclei stay in the same relative positions for a long time but the nuclei are in a variety of fields because of the changing local magnetic field from the neighboring dipoles. This relaxation process is characterized by the spin-spin relaxation time T_2. In a fluid of low viscosity, molecules undergo random motion (Brownian movement) and it can be shown (26) that, providing this motion is very fast, the local dipolar fields average out to a very small value.

A third cause of line broadening is the interaction of the given nuclear moments with neighboring nuclei having an electric quadrupole moment ($I > 1/2$). Quadrupolar broadening is important for protons attached to nuclei such as nitrogen ($I = 1$ for ^{14}N) and often makes the absorption peaks for such protons difficult to detect.

A final cause of line broadening is the inhomogeneity always present in the static magnetic field H_0 over the volume of the sample. The observed spectrum at a fixed frequency can be considered as a superposition of the spectra from molecules at all different parts of the sample each in a slightly different static field. Line widths in high resolution NMR are ordinarily limited by the inhomogeneous broadening.

Chemical Shifts

The magnetic field strength at a particular nucleus is usually less than the strength of the applied field H_o, because the motions of the electrons result in a diamagnetic shielding effect. The local field experienced by the nucleus is $H = H_o(1 - \sigma)$, where σ is the screening constant and depends only on the position of the particular nucleus in the molecule. Consequently, the resonance signal produced by each kind of hydrogen will come at a different field strength. The difference in field strengths at which the signals are obtained for nuclei of the same kind, but located in different magnetic environments, is called the chemical shift. It is dependent on the field strength.

It has been shown (27) that the screening constant for the nucleus of atom A may be written as

$$\sigma^A = \sigma_d^{AA} + \sigma_p^{AA} + \sum_{B \neq A} \sigma^{AB} + \sigma^A_{ring} \qquad (a)$$

where σ_d^{AA} is the diamagnetic Langevin-type circulation of electrons on atom A. The contribution of the local diamagnetic currents on the hydrogen nucleus itself can be estimated from the Lamb formula

$$\sigma_d^{AA} = \frac{e^2}{3mc^2} \int \frac{\rho}{\gamma} \, d\tau \ .$$

Her
wit
whe
hyp
The
as

Th
gr
wh
(2
lo
th
In
zs
de
to
c
m
w
e
c
a
C
a
n

Here ρ is the electron density of the electrons associated with the hydrogen atom and may be represented by $\lambda\psi_{1s}^2$, where λ measures the effective number of electrons in the hydrogen 1s atomic orbital $\psi_{1s}(=\pi^{-\frac{1}{2}}e^{-r}$ in atomic units). The expression for σ_d^{AA} may then be integrated and expressed as

$$\frac{\lambda e^2}{3mc^2A_o} \quad .$$

The second term of Equation a results from the mixing of ground and excited electronic states by the magnetic field which produces a paramagnetic current on this atom. Pople (28) has shown that an excited state contributes to the local paramagnetic current on an atom if it corresponds to the transfer of an electron between p-orbitals or d-orbitals. It vanishes for electrons in a s-orbital since these have zero angular momentum. Fluorine chemical shifts are largely dominated by the paramagnetic term, but for hydrogen this term is generally small. The term $\Sigma\sigma^{AB}$ is the shielding contributed by the electrons of all the other atoms in the molecule while σ_{ring}^{A} is the contribution from a ring current which cannot be localized on individual atoms. The combined effects of the diamagnetic and paramagnetic currents on other atoms is largest if the electrons on a near-neighbor atom have a large and anisotropic magnetic susceptibility. Consider a nucleus of spin I at a distance R from an axially symmetric anisotropic molecular grouping whose magnetic susceptibility is $\chi_{\parallel}$ along the z axis and $\chi_{\perp}$ along

the x and y axes. If the line from the nucleus to the group makes an angle θ with the z axis and the field H is along the z axis (as indicated in the diagram), then it may be shown that (5)

$$\sigma_{zz} = \chi_{\parallel} (1-3\cos^2\theta)/R^3$$

$$\sigma_{yy} = \chi_{\perp}/R^3$$

$$\sigma_{xx} = \chi_{\perp} (1-3\sin^2\theta)/R^3$$

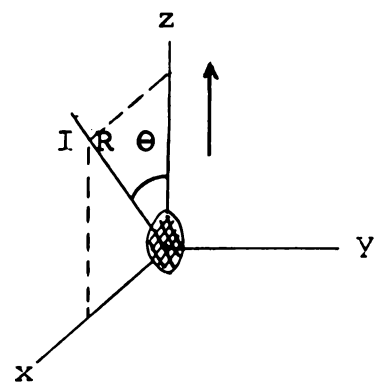

and the average correction to the screening for a molecule in solution becomes

$$\Delta\sigma = (\chi_{\parallel} - \chi_{\perp})(1-3\cos^2\theta)/3R^2 \ .$$

The ring current contribution has been evaluated (28) for aromatic ring systems. When the magnetic field is applied perpendicular to the plane of the ring a circulation of the π electrons is induced which is equivalent to a current. The ring acquires an induced magnetic moment in a direction opposite to the applied field. If the applied field is in any other direction the induced moment will be different and σ_{ring} is quite anisotropic. Pople has shown that $\Delta\sigma = \sigma_{\parallel} - \sigma_{\perp}$ may be written

$$\Delta\sigma = \frac{e^2}{2mc^2} \ \frac{R^2}{(R+d)^3} \ ,$$

where R is the ring radius, and d is C-H bond length for the particular case of aromatic hydrocarbons.

Complete calculation of the chemical shielding for a molecule is rarely possible since the required wave functions are not usually known. Only for protons in very simple molecules have accurate quantum mechanical calculations been possible. However, various empirical schemes have been proposed to correlate chemical shifts.

Primas, Arndt and Ernst (29) postulate that the chemical shift of a particular nucleus can be considered as the sum of several characteristic contributions from the various groups; the chemical shift can be estimated empirically from

$$\tau = T_o + \Sigma C_j T_j$$

Where τ is the τ value of a hydrogen nucleus, $T_o = 9,067$, T_j is the contribution from a group and C^j is the number of times such a group occurs in the molecule. In their paper, detailed information concerning the choice of parameters T_o and T_j is given.

Maslov (30) devised a semiempirical method for calculation of chemical shifts and magnetic shielding constants. He used an "equation of weighted averages":

$$B_i = \frac{1}{S} \Sigma \delta_j B_j ,$$

where $S = \Sigma \delta_j$ is the valency of the coordinating group, common for all representatives of the chosen family of molecules which are related in structure. B_i and B_j are the value of a particular property, such as chemical shift and

magnetic shielding constant, for molecules j which are given in the paper, and for molecule i which is unknown. This method has advantages over simple additivity relationships. He gives extensive tables of B_j values for various families of organic molecules.

Many other workers have tried to correlate qualitatively chemical shifts and molecular properties. Packer (31) has found that the ^{31}P chemical shifts in $(CF_3)_2PX$ compounds depend linearly on the electronegativity of the X group, and that deviations from this relationship are probably due to the magnetic anisotropy of the P-X bond.

Solvent Effects on Chemical Shifts

When molecules are dissolved in a solvent there are additional contributions to the chemical shifts of solute nuclei from the solvent molecules. The commonly used expression for the chemical shift δ observed for a particular species in solution is (32,33):

$$\delta = \delta_B + \delta_A + \delta_W + \delta_E + \delta_C$$

where the contributions to δ are: δ_B from the bulk magnetic susceptibility of the solution; δ_A from the anisotropic diamagnetic susceptibility of the solvent molecules; δ_W from van der Waals interactions with the neighboring molecules; δ_E from the polar effect caused by the charge distribution in the neighboring molecules which leads to an

elec

pert

scre

sol

sol

thi

and

giv

of

2-

sol

or

ne

di

ri

en

ar

electric field acting on the solute molecule thereby perturbating its electron structure and hence magnetic screening constant, and δ_C from the formation of solute-solvent complexes.

In the presence of the external magnetic field the solvent molecules will be diamagnetically polarized and this polarization may produce a magnetic field at the nucleus and consequently contribute to the screening constant of the given nucleus. This secondary field depends upon the shape of the sample. It is zero for a spherical sample and is $2\pi\chi v/3$ for a cylindrical sample.

The anisotropic term σ_A, depends on the shape of the solvent molecules, their magnetic anisotropy and their orientation with respect to the solute molecule and the magnetic field. Solvent molecules such as benzene, which have disc-like shapes, will have large induced moments when the ring is at right angles to the field, and since their shape enables them to lie closer to the solute molecule when they are in the configuration a_1 than in the configuration a_2

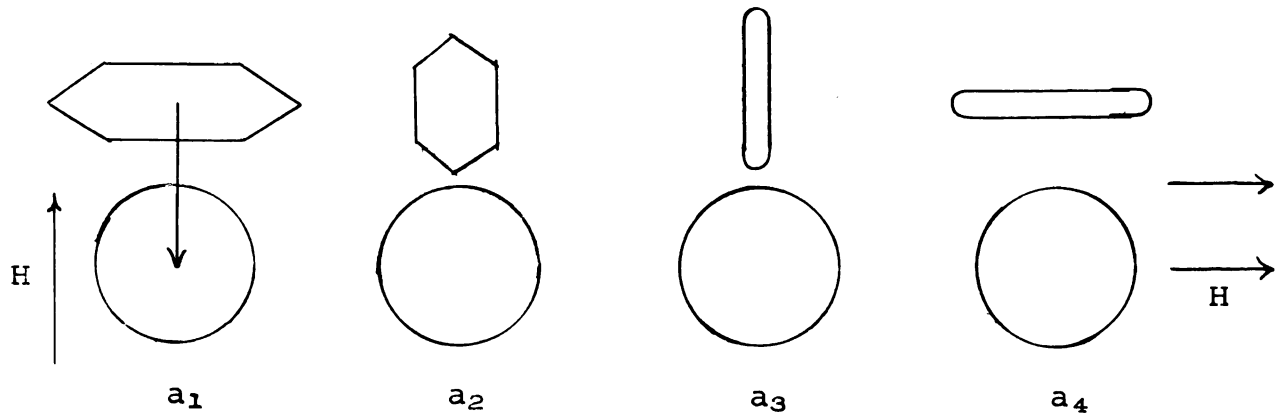

the contribution of a_1 may be expected to dominate. This would lead to a mean diminution of the external field at the solute protons and, consequently, a resulting shift to high field because the secondary magnetic field due to the induced magnetic moment is proportional to the inverse third power of the separation.

Using the same argument, rod-like solvent molecules such as carbon disulfide and acetylene, whose largest magnetic susceptibility is along the axis of the rod, would lead to a low-field shift. The arrangement a_4 becomes the most significant one and leads to an enchancement of the applied field.

For a disc-like solvent molecule close to a solute molecule the screening constant is $\sigma_A = -2n(\chi_{\parallel} - \chi_{\perp})/3R^3$, where $\chi_{\parallel}$ and $\chi_{\perp}$ are the magnetic susceptibilities parallel and perpendicular to the symmetry axis, $\vec{R}$ (whose magnitude R must be large in comparison to the molecular dimension) is the vector from the origin of the solvent molecule to the center of the solute molecule, and n is the number of solvent molecules which are considered close enough to contribute to σ_A. The magnitude of $\vec{R}$ is $\vec{R}\cdot\vec{1}/\cos\theta$, where $\vec{1}$ is the unit vector along the molecular symmetry axis of the solvent molecule and θ is the angle between $\vec{R}$ and $\vec{1}$. Likewise the screening constant for the case of rod-like solvent molecule is expressed as $\sigma_A = +n(\chi_{\parallel} - \chi_{\perp})/3R^3$.

Schug (33) assumed that liquid solutions are completely random in nature and that the anisotropic shift is therefore

directly proportional to the volume fraction of the anisotropic species; he then tried to calculate the anisotropic shift σ_A produced by cylindrically symmetrical solvent molecules. He found that including all the anisotropic molecules in the solution, rather than nearest neighbors only, provided theoretical anisotropic shifts comparable to those observed.

In case of polar solutes the interactions between the solvent and solute molecules perturb their electronic structures and the resulting distortion leads to a solvent dependent nuclear screening constant term, the van der Waals term. This arises because the electronic environment of the nucleus is distorted by the interaction between the solute and solvent molecules causing the solute electrons to be attracted by the neighboring molecules. The diamagnetic screening is therefore reduced and nuclear resonance occurs at lower field strength. This contribution can be expressed as (34,35):

$$\sigma_W = \frac{3}{4} \phi \, h \left(\frac{2n^2-2}{2n^2+1}\right) \left(\frac{1}{a^3}\right) \left(\frac{\nu_1 \nu_2}{\nu_1 + \nu_2}\right) ,$$

where n is the refractive index of the solvent, a is the solvent molecular radius, h is Planck's constant, ν_1 and ν_2 are the mean absorption frequencies of the solvent and solute, and ϕ corresponds to a bonded hydrogen atom.

For polar solutes the observed large solvent chemical shifts are due to the effect of the reaction field. This is

a secondary electric field arising in the polar or polarizable solvents under the influence of solute molecules which carry a permanent dipole moment. The model used by Onsager (36) and Buckingham (37) assumes that the entire molecule is reduced to a point dipole in the center of a cavity surrounded by an isotropic, homogeneous, polarizable continuous medium of fixed dielectric constant. They (37) showed that the electric field at a particular nucleus arising from a polar group in the remainder of the molecule can lead to chemical shifts proportional to the first power of the field strength. The change in the proton screening constant of a proton of an X-H bond when it is subject to an electric field **E** is equal to

$$\Delta\sigma = -2 \times 10^{-12}E_z - 10^{-18}E^2 ,$$

where E_z is the component of **E** (e.s.u.) in the bond direction. An electric field in the X-H direction would be expected to draw the electronic charge between the nuclei toward the X atom, thereby causing its resonance to occur at lower magnetic field strength, while a field in the H-X direction leads to resonance at higher fields.

Spin-Spin Splitting

A systematic study of multiplet splitting by Gutowsky and McCall (38) showed that fine structure may arise in any molecule containing two or more nuclei which resonate at

different field strengths; that is, if the nuclei are either of different isotopic species or are chemically shifted. The multiplet fine structure is caused by mutual magnetic interactions between the nuclear spins giving rise to a set of values of the total magnetic field at a given nucleus. The interactions are transmitted by the bonding electrons (39) and the magnitude of the interaction is the spin-spin coupling constant J.

The interaction can be divided theoretically into three parts (40,41). In the first of these one nuclear magnetic moment induces orbital electronic currents which consequently induces magnetic fields at the site of the second nucleus. In the second, the electron spins interact with the magnetic moment of one nucleus producing an electron spin polarization which is then transferred to the adjoining nuclei. However the two parts just mentioned are very small in comparison with the third part which is the Fermi contact interaction and is the most significant contribution to the overall spin-spin coupling. In this the interaction between nuclear moments and the spins of electrons in s-orbitals produces an electron spin polarization proportional to the density of the s electron at the nucleus. In molecular orbital theory the spin coupling constant, J_{AB}, may be written in terms of the wave functions of the ground and excited states ψ_i, ψ_j. Summing over occupied and unoccupied levels for i and j, respectively,

$$J_{AB} \alpha - \sum_{i}^{occ} \sum_{j}^{unocc.} \frac{(\psi_i \psi_j)_A \ (\psi_i \psi_j)_B}{(\epsilon_j - \epsilon_i)}$$

where $(\epsilon_j-\epsilon_i)$ is the energy difference between the ground state ϵ_i and the unoccupied excited state ϵ_j and is always positive. From the above expression the sign of the coupling constant depends on whether the molecular orbital is symmetric or asymmetric. The symmetric molecular orbitals have the same sign at atom A and atom B, and the asymmetric molecular orbitals have different signs. For transitions from symmetric to symmetric or from asymmetric to asymmetric molecular orbitals, the contribution to J, the spin-spin coupling constant, is negative. Transitions from symmetric to asymmetric molecular orbitals, or vice versa, gives a positive contribution to the coupling constant.

Pople (41) used this molecular orbital theory in the study of spin-spin coupling between directly bonded atoms where the contact term is usually dominant. His calculations indicate that the coupling constant is negative when one of the atoms is fluorine. For long-range spin-spin interactions over four or five chemical bonds the theoretical study becomes much more difficult. It can be treated as a "particle in a box" problem. The linear paths are more energetically favorable than those with high curvature in the long-range delocalization of electrons (42). Hence long-range couplings are largest when a linear path can be drawn between the coupled nuclei to include the intervening bonds particularly when these latter form a conjugated system.

Double Irradiation

When two non-equivalent magnetic nuclei A and X are coupled together by indirect spin-spin interaction, the absorption peak for each nucleus is split into a multiplet. If one of these nuclei (X, say) can be made to transfer rapidly between its various spin states then the multiplet for the other nucleus (A) will average out to a single peak located at the center of the original multiplet. This process occurs naturally if one of the nuclei possesses an electric quadrupole moment since the fluctuating electric field gradients arising from molecular motions will induce transitions between the spin states of the nucleus with the quadrupole moment. The decoupling can also be induced artificially (43-45) by application of a second rf field at the resonance frequency of the X nucleus while observing the A nuclei at their resonance frequency. Sufficient rf power at the X resonance frequency will then induce transitions among the spin states of the X nuclei and the A resonance peaks will not show multiplet structure from coupling with X nuclei.

Bloom and Shoolery (46) have made a quantum mechanical analysis of the effects of radiofrequency fields on nuclear spin coupling. They were able to predict the nature of intermediate spectra between the unperturbed multiplets and the totally collapsed multiplets when the second radio-frequency was changed. The double resonance method has

been applied to the measurement of chemical shifts (44) and to the determination of the relative signs of coupling constants (48).

Bloch Formulation of the Nuclear Induction Experiment

To describe the time dependent variation of the components of the total nuclear magnetic moment per unit volume, Bloch used a set of phenomenological equations (26). First, a set of coordinates should be defined. Let Z be the direction of the magnetic field, with field strength H_0, and X be the direction of the rf field with angular frequency ω and amplitude $2H_1$. The three components of the total field vector H_1 are:

$$H_x = 2H_1 \cos\omega t \; ; \; Hy = 0 \; ; \; H_z = H_0 \qquad (1)$$

If the vector $\bar{M}=(M_x,M_y,M_z)$ is the resultant nuclear moment per unit volume, the primary purpose of the theory is to formulate the variation of this vector with the time.

Let the resultant angular momentum vector of all the nuclei in a unit volume be $\bar{A}$. Then, from the classical mechanical definition of torque, the torque acting on the nuclei is

$$\frac{d\bar{A}}{dt} = \bar{T} \qquad (2)$$

and $\bar{T}$ is also equal to $(\bar{M} \times \bar{H})$. The magnetic moment $\bar{M}$ is equal to the product of the angular momentum and the

gyromagnetic ratio,

$$\bar{M} = \gamma \bar{A} \ . \tag{3}$$

Combining equations 1, 2, and 3, the time variation of the total magnetic moment vector $\bar{M}$ (or macroscopic moment), can be written

$$\frac{d\bar{M}}{dt} = \gamma [\bar{M} \times H] \ . \tag{4}$$

For a set of nuclei with spin 1/2 in a steady magnetic field H_o along the Z direction the Z component of $(\bar{M} \times \bar{H})$ vanishes, and the X and Y components are

$$\frac{dM_x}{dt} = \omega_o M_y \tag{5}$$

$$\frac{dM_y}{dt} = -\omega_o M_x \tag{6}$$

$$\frac{dM_z}{dt} = 0 \tag{7}$$

where $\omega_o = \gamma H_o$ is the angular frequency of the Larmor precession.

By introducing appropriate damping terms, the relaxation effects can be added to above equations. M_z will vary and approach an equilibrium value of M_o. For N nuclei of spin 1/2 in a unit volume, M_o may be written

$$M_o = \frac{N\mu^2 H_o}{kT} = \chi_o H_o \ . \tag{8}$$

The rate of approach to equilibrium is dependent on the spin-lattice relaxation time T_1:

$$\frac{dM_z}{dt} = - \frac{M_z - M_0}{T_1} \quad . \tag{9}$$

For the same reason the X and Y components must also be modified. According to the solutions of Equations 5 and 6, the component perpendicular to H_0 rotates with the Larmor frequency about the Z axis. Individual nuclei will get out of phase due to relaxation effects and M_x and M_y will decay to zero. By analogy with the argument for the longitudinal component, the change of M_x and M_y will also have an exponential character governed by the equations,

$$\dot{M}_x = - (\frac{1}{T_2}) M_x \tag{10}$$

$$\dot{M}_y = - (\frac{1}{T_2}) M_y \tag{11}$$

where the time constant T_2 is called the transverse relaxation time.

Up to this point, the discussion is only concerned with the nuclei in a fixed field H_0 along the Z direction. In the NMR experiment an additional field H_1, perpendicular to H_0 and rotating with angular frequency ω, must also be considered. The vector H in Equation 4 then will have additional components $H_x = H_1 \cos\omega t$, $H_y = - H_1 \sin\omega t$ and $H_z = H_0$. The complete Bloch equations can be obtained by combining the contributions from Equations 9, 10, 11, and 4:

$$\dot{M}_x = \gamma (M_y H_0 + M_z H_1 \sin\omega t) - \frac{M_x}{T_2} \tag{12}$$

$$\dot{M}_y = \gamma (M_z H_1 \cos\omega t - M_x H_0) - \frac{M_z}{T_2} \tag{13}$$

$$M_z = \gamma(-M_x H_1 \sin\omega t - M_y H_1 \cos\omega t) - \frac{M_z - M_o}{T_1} \qquad (14)$$

Equations 12, 13, and 14 are derived with respect to a set of fixed axes; they can be transformed to a set of axes rotating with frequency ω about the Z axis. The new components of $\bar{M}$ are Mz, u, and v, where u and v are the in-phase and out-phase components of $\bar{M}$ since they are parallel and perpendicular to the direction of H_1, respectively. The relationships between components are

$$M_x = u\cos\omega t - v\sin\omega t \qquad (15)$$

$$M_y = u\sin\omega t - v\cos\omega t \qquad (16)$$

and

$$u = M_x \cos\omega t - M_y \sin\omega t \qquad (15\text{-a})$$

$$v = -M_x \sin\omega t - M_y \cos\omega t \ . \qquad (16\text{-a})$$

The Bloch equations in the rotating coordinate system can be obtained by substituting Equations 15 and 16 into the Bloch equations for the fixed coordinate system and are:

$$\frac{du}{dt} + \frac{u}{T^2} + (\omega_o - \omega)v = 0 \qquad (17)$$

$$\frac{dv}{dt} + \frac{v}{T_2} - (\omega_o - \omega)v + \gamma H_1 M_z = 0 \qquad (18)$$

$$\frac{dM_z}{dt} + \frac{M_z - M_o}{T_1} - \gamma H_1 v = o \qquad (19)$$

where $\omega_o - \omega = \gamma H_o - \omega$ and $\omega_1 = \gamma H_1$.

In most NMR experiments the steady state solutions of the above set of equations are of interest. They can be solved by requiring the time derivatives to be zero and M_z to be constant. The values of M_z, u, v then become:

$$u = M_o \frac{\gamma H_1 T_2^2(\omega_o - \omega)}{1 + T_2(\omega_o - \omega)^2 + \gamma^2 H_1^2 T_1 T_2} \tag{20}$$

$$v = -M_o \frac{\gamma H_1 T_2}{1 + T_2^2(\omega_o - \omega)^2 + \gamma^2 H_1^2 T_1 T_2} \tag{21}$$

$$M_z = M_o \frac{1 - T_2^2(\omega_o - \omega)^2}{1 + T_2^2(\omega_o - \omega)^2 + \gamma^2 H_1^2 T_1 T_2} . \tag{22}$$

The rate of absorption of energy per volume is $-M_x dH_x/dt$ and M_x can be obtained by reconverting the above components to the fixed laboratory axes. Then,

$$M_x = \frac{1}{2} M_o \gamma T_2 \frac{T_2(\omega_o-\omega) 2H_1 \cos\omega t + 2H_1 \sin\omega t}{1 + T_2^2(\omega_o-\omega)^2 + \gamma^2 H_1^2 T_1 T_2} \tag{23}$$

Inspecting $-M_x dH_x/dt$, it is seen that there is a term proportional to $\cos\omega t \sin\omega t$ which averages to zero and a term proportional to $\sin^2\omega t$ that averages to 1/2. The average rate of absorption of energy per unit value is then

$$\frac{\omega\gamma H_1^2 M_o T_2}{1 + T_2^2(\omega_o - \omega)^2 + \gamma H_1^2 T_1 T_2} . \tag{24}$$

This expression has a maximum value when ω is in the vicinity of the Larmor frequency. With a small oscillating magnetic field, $H_1 \ll 1/\gamma\sqrt{T_1 T_2}$, Equation 24 becomes

$$g(\nu) = \frac{\omega\gamma H_1^2 T_2 M_o}{1 + T_2^2(\omega_o-\omega)^2} \tag{25}$$

which has a peak value of $2T_2$. In Equation 25, $g(\nu)$ is called the line-shape function which in practice, however, cannot always be approximated by a Lorentz-type curve.

The Line-Shape Equation with Exchange

The Bloch equations can be directly generalized to include the effect of exchanging nuclei (49). Let nuclei X transfer back and forth between two different molecular environments A and B, where A and B are sites with different local fields giving two absorption peaks shifted by $+\delta\omega/2$ and $-\delta\omega/2$ from their average angular frequency $\delta\omega$. Time spent in the transition state can be assumed to be short and can be disregarded. The lifetimes of X at site A and site B are denoted by τ_A and τ_B, respectively. In other words, the probability of X at site A moving to site B is $1/\tau_A$, and for the reverse process in $1/\tau_B$. The rate of exchange of protons between the two sites can be expressed by the following equations (12):

$$\frac{dN_A}{dt} = -\frac{1}{\tau_A} N_A \tag{26}$$

$$\frac{dN_B}{dt} = -\frac{1}{\tau_B} N_B \tag{27}$$

$$\frac{P_A}{\tau_A} = \frac{P_B}{\tau_B} \tag{28}$$

$$\tau = \frac{\tau_A \tau_B}{\tau_A + \tau_B} \tag{29}$$

where N_A and N_B are the number of labeled X nuclei at site A and site B, t is the time, and p_A and p_B are the fractions of X nuclei at site A and site B at time t, respectively.

Having the above consideration in mind, the magnetizations can be written as the sum of the contributions of A and B systems:

$$u = u_A + u_B \tag{30}$$

$$v = v_A + v_B \tag{31}$$

$$M_z = M_z^A + M_z^B \quad , \tag{32}$$

where v, u and M_z denote the components of X nuclear magnetization which are in-phase and out-of-phase with the effective rotating components of RF field, and in the direction of the large stationary field, respectively.

The Bloch Equations 17, 18 and 19 can be modified to accommodate the kinetic effects and take the forms (46)

$$\dot{u}_A + \Delta\omega_A v_A = -u_A/\tau_{2A} + u_B/\tau_B \tag{33}$$

$$\dot{u}_B + \Delta\omega_B v_B = -u_B/\tau_{2B} + u_A/\tau_A \tag{34}$$

$$\dot{v}_A - \Delta\omega_A u_A = -v_A/\tau_{2A} + v_B/\tau_B - \omega_1 M_z^A \tag{35}$$

$$\dot{v}_A - \Delta\omega_B u_B = -v_B/\tau_{2B} + v_A/\tau_A - \omega_1 M_z^B \tag{36}$$

$$\dot{M}_z^A - \omega_1 v_A = M_0^A/\tau_{1A} - M_z^A/T_{1A} + M_z^B/\tau_B \tag{37}$$

$$\dot{M}_z^B - \omega_1 v_B = M_0^B/\tau_{1B} - M_z^B/T_{1B} + M_z^B/\tau_A \quad . \tag{38}$$

In the preceding equations M_o^A and M_o^B are the equilibrium Z magnetizations of X nuclei at site A and site B; $\Delta\omega_A$ and $\Delta\omega_B$ are the differences between ω_A, ω_B and ω, the angular frequency of the RF field, respectively. τ_{1_A} and τ_{2_A} can be defined as:

$$\frac{1}{\tau_{1_A}} = \frac{1}{T_{1_A}} + \frac{1}{\tau_A} \tag{39}$$

$$\frac{1}{\tau_{2_A}} = \frac{1}{T_{2_A}} + \frac{1}{\tau_A} \tag{40}$$

and similar definitions hold for τ_{1_B} and τ_{2_B}; T_{1_A} and T_{2_A} are the longitudinal and transverse relaxation times of nuclei X at site A, and T_{1_B} and T_{2_B} of nuclei X at site B.

By comparing Equations 33-40 with the original Bloch equations the reason for the modification made becomes evident. Equation 33 has two additional terms on the right hand side, $-u_A/\tau_A$ and u_B/τ_B. The first term measures the rate at which u_A decreases due to the chemical exchange of u magnetization out of A site; and the second term measures the rate at which u_A increases because of the chemical exchange of u magnetization from site B to site A. The same argument is also applicable to Equations 34 to 38.

In order to apply Equations 33 to 38 to reaction rate determinations, the assumption that the relaxation times T_{1_A}, T_{2_A}, T_{1_B} and T_{2_B} are independent of τ_A and τ_B must be made. This assumption is most readily realized when the X nuclear relaxation is due to time-dependent perturbations

which are of high frequency relative to τ_A^{-1} and τ_B^{-1}. The modified Bloch equations also imply the requirement that the X nuclear magnetizations of the A and B systems are independent of one another (except for the chemical kinetic exchange effect).

For slow passage in an NMR experiment

$$\dot{u}_A = \dot{u}_B = \dot{v}_A = \dot{v}_B = \dot{M}_z^A = \dot{M}_z^B = 0 \qquad (41)$$

which transforms the set of coupled differential Equations 33-38 to a complete set of ordinary simultaneous linear equations in six unknowns which can be solved numerically.

Equations 33 to 39 can be applied to the case of hindered internal rotation in disubstituted amides which is a typical two-site exchange problem. If the RF saturation is negligible, the total Z magnetization M_z becomes unaffected by the kinetic process (50):

$$M_z = M_z^A + M_z^B = M_o = M_o^A + M_o^B = \frac{M_o^A}{p_A} = \frac{M_o^B}{p_B} . \qquad (42)$$

By summing over all X nuclei, the RF magnetization can be written as

$$\bar{M} = u + iv = M_A + M_B = u_A + iv_A + u_B + iv_B \qquad (43)$$

Substituting Equations 28, 39, 40, 42 and 30-33 into the above expression the resulting equation is

$$\bar{M} = -i\omega_o M_o \left(\frac{\tau_A + \tau_B + (\tau_A\tau_B + p_A p_B)}{(1 + \tau_A\beta_A)\ (1 + \tau_B\beta_B) - 1}\right) \qquad (44)$$

where $\beta_A = \frac{1}{T_{2A}} - i\Delta\omega_B$ and $\beta_B = \frac{1}{T_{2_B}} - i\Delta\omega_A$. (45)

The real part of Equation 44 gives the dispersion u-mode line-shape equation and the imaginary part gives the absorption v-mode line-shape function in terms of the rate constant:

$$u = \frac{-\omega_1 M_o [QP - \{1 - \tau(p_B/T_{2A} + p_A/T_{2B})\}R]}{P^2 + R^2} \quad (46)$$

$$v = \frac{-\omega_1 M_o [P\{1 + \tau(p_B/T_{2A} + p_A/T_{2B})\} + QR]}{P^2 + R^2} \quad (47)$$

where

$$P = \tau[\frac{1}{T_{2A}T_{2B}} - \Delta\omega^2 + (\frac{\delta\omega}{2})^2] + \frac{p_A}{T_{2_B}} + \frac{p_B}{T_{2A}} = S - \tau\Delta\omega^2$$

$$Q = \tau[\Delta\omega - \frac{\delta\omega}{2}(p_A - p_B)]$$

and $R = \Delta\omega[1 + \tau(\frac{1}{T_{2A}} + \frac{1}{T_{2B}})] + \tau\frac{\delta\omega}{2}(\frac{1}{T_{2B}} - \frac{1}{T_{2A}}) +$

$$\frac{\delta\omega}{2}(p_A - p_B) .$$

When a set of line-shape parameters is known, the intensities at the corresponding values of ω can be calculated from Equation 47. Upon differentiating this equation with respect to $\Delta\omega$, the resulting equation has the following form:

$$2\tau^2 A\Delta\omega^5 + 3\tau^2 B\Delta\omega^4 + 4\tau^2 C\Delta\omega^3 + (BD-AE)\Delta\omega^2 + 2(CD-AF)\Delta\omega + (CE-BF) = 0 \quad (48)$$

where

and

Wit

sol

to

dou

onl

coa

con

52)

Equ

of

ess

two

$$A = \tau^2(\tau_A/T_{2_A} + p_B/T_{2_B}); \quad B = \tau^2\delta\omega(\frac{p_B}{T_{2_B}} - \frac{p_A}{T_{2_A}})$$

$$C = \tau(\frac{\delta\omega}{2})^2[1-(p_A - p_B)^2 + \frac{A}{\tau}] + \frac{\tau}{T_{2_A}T_{2_B}}[1 + p_A^2 + p_B^2 + \tau(\frac{p_B}{T_{2_A}} + \frac{p_A}{T_{2_B}})] + \tau p_A p_B (\frac{1}{T_{2_A}^2} + \frac{1}{T_{2_B}^2}) + \frac{A}{\tau^2}$$

$$D = [1 + \tau(\frac{1}{T_{2_A}} + \frac{1}{T_{2_B}})]^2 - 2\tau S$$

$$E = \delta\omega(D + 2\tau S)^{\frac{1}{2}}[p_A - p_B + \tau(\frac{1}{T_{2_B}} - \frac{1}{T_{2_B}})]$$

and $F = S^2 + \frac{E^2}{4}(D - 2\tau S)^{-1}$.

When Equation 48 is solved, one of two cases can occur. With a large value of τ (slow exchange) three of the five solutions of the fifth-order equation are real and correspond to the two maxima and the central minimum of the uncoalesced doublet. In case of small τ, in other words fast exchange, only one solution is real, the central maximum for the coalesced doublet.

Computer Programs for Exchange Calculations

In the last few years the application of electronic computers to the exchange problem has been reported (51,12, 52). T. Nakagawa (53) reported a computer program based on Equation 47 which gives intensities corresponding to a set of line-shape parameters. The program is very simple; it is essentially a couple of do-loops with no adjustments included. Two programs written by Gutowsky's group (53) and one by

Saunders (55) have been used on several NMR problems. Line shapes of fluorine magnetic resonance spectra and the conformational isomerization of 1,1-difluorocyclohexane have been studied with the first program (53). In this program the rate constant is the only variable parameter, and often the single-parameter curve fitting does not yield very satisfactory results because Equation 47, on which the program is based, makes the assumption that the values of the line widths and the peak separations in the absence of exchange hold for the entire temperature range. In this laboratory, as well as in several others (54,15,25), this assumption is found not to be valid. This point will be discussed quantitatively in the Discussion section of this report.

Saunders (55) program has been used to study exchange among many sites. A correction to the line-shape function for field inhomogeneity can be built into the computer program by use of the convolution integral; this permits the introduction of any desired line shape. Let the intensity function without correction be $Y'(\omega)$ and the desired function be $S(\omega)$, the corrected intensity function is then expressed as

$$Y'(\omega) = \int_{-\infty}^{\infty} S(\omega-\omega') I'(\omega') d\omega \quad . \tag{49}$$

Anet (56) used the approach mentioned above in the study of ring inversion in cyclohexane-d_{11}; he reported that the results from the programs with and without the convolution integral were almost identical.

All three principal methods (42,51) will be subject to a significant systematic error if each of the doublet peaks is itself a spin-spin multiplet from coupling with other protons; for instance, in N,N-dimethylformamide the two N-methyl peaks are each split into a doublet by spin coupling between the formyl proton and the methyl groups. With this complication the procedure for evaluation of the exchange rate constant must be modified. Four approaches can be used.

(1) Isotopic substitution: When the formyl proton in DMF is substituted by deuterium the coupling constant becomes negligibly small, because the ratio of the coupling constant of the two isotopes with the third nucleus is proprotional to the ratio of their gyromagnetic ratios which is 0.1535 for deuterium and hydrogen.

(2) Double irradiation: In the case of DMF the secondary doublet can be eliminated by irradiation at the frequency of the formyl proton using an external oscillator or noise generator. This method permits decoupling the protons when enough rf power can be introduced.

(3) Quantum mechanical approach: When two nonequivalent protons exchange between the two sites and couple with each other to form an AB spin system, the coupling complication can be resolved theoretically by using the density matrix method. The basic formulation is worked out by Kaplan (57) and Alexander (58,59). The theoretical line-shape equation

describing the two exchanging protons can be calculated by deriving the Boltzmann equation for the average density matrix, and the exchange process is described by exchanging the indices of the spin coordinates in the spin wave function. The equations derived with this approach have been used in several exchange problems (60,61,62). A very explicit application is the study of conformation and internal rotation in a nitroaromatic amine by Heidberg et al. (63). The equation used is:

$$v = C\left(\frac{\gamma_+ b_+ - Sa_+}{a_+^2 + b_+^2} + \frac{\gamma_- b_- - Sa_-}{a_-^2 + b_-^2}\right) \qquad (50)$$

where

$$a \pm = [(\omega_o-\omega) \pm \tfrac{1}{2}J]^2 - (\tau^{-1} + T_2^{-1})^2 - \delta^2 - \tfrac{1}{2}J^2 + \tau^{-2}$$

$$b \pm = 2[(\omega_o-\omega) \pm \tfrac{1}{2}J] (\tau^{-1} + T_2^{-1}) \mp J/\gamma$$

$$\gamma \pm = (\omega_o-\omega) \pm J$$

$$S = 2/\tau + 1/T_2 \ .$$

It describes the line shape for a system of two exchanging protons which couple with each other. If the coupling constant J in the equation is equal to zero Equation 50 will be reduced to a simpler form, identical to the classically derived Equation 47. This approach could be used for the disubstituted amides, but the quantum mechanical derivation becomes extremely complex because of the large number of spins in this problem and has never been reported.

(4) Superposition: The doublets at each N-methyl peak can be considered as the superposition of two sets of identical methyl doublets with centers separated by $(J_1 + J_2)/2$, where J_1 and J_2 are the coupling constants between the two methyl groups and the formyl proton. Method III can be modified to accommodate this improvement.

In order to evaluate the activation energy for the exchange process in N,N-disubstituted amides the classical Arrhenius rate equation (64,65) can be written as

$$\log \tau = \log \frac{1}{2A} + \frac{E_a}{2.303\ RT} \qquad (51)$$

Where τ is the inverse of twice the rate constant of the exchange process, R is the molar gas constant, A is the frequency factor and E_a is the activation energy, or the energy barrier of the system. The quantities A and E_a can be evaluated from the slope and the intercept of the best straight line when log τ is plotted vs. $10^3/T^{\circ}K$.

Assuming that this exchange process obeys the absolute rate equation (66), the free energy of activation $\Delta F^{\ddagger}$ for the internal rotation problem can be written as

$$\begin{aligned} \Delta F^{\ddagger}_{(T)} &= -RT \ln K^{\ddagger} \\ &= -RT \ln(\text{rate constant} \cdot h)/(\kappa kT) \\ &= 2.303RT \log 2\tau\kappa kT/h \\ &= 2.303\ RT(10.319 + \log T + \log 2\tau) \end{aligned} \qquad (52)$$

where h is Planck's constant, k is the Boltzmann constant and κ is the transmission coefficient, which is equal to unity when every activated complex breaks up to give products.

Chemical Shifts of the Methyl Proton Peaks

Much research has been done on the assignment of the peaks of the doublet to the respective methyl groups in N,N-dimethyl amides. The resonances corresponding to the two N-methyl groups of N,N-dimethylformamide can be distinguished because each is split into a closely-spaced doublet by spin-spin coupling with the formyl proton (67) and the coupling constants differ. The high-field signal in pure DMF is most strongly coupled to the formyl proton and so is trans to the formyl proton. In N,N-dimethylacetamide the two N-methyl resonance peaks may also be distinguished because the high-field signal is broader. Each component of the doublet is presumably an unresolved quartet with the coupling constants to the acetyl methyl proton different. The N-methyl resonance which shows the greater broadening must be trans to the acetyl methyl group.

A second method for assigning the N-methyl resonances is based on the fact that addition of an aromatic solvent produces large changes in the relative chemical shifts of the two N-methyl groups (67). As the concentration of the N,N-dimethylamides decreases, both N-methyl resonance signals are shifted to higher fields but the original lower-field

signal shifts by a much larger amount. At a certain concentration the doublet coalesces and further addition of solvent causes the original low-field signal to cross over the original high-field peak, with consequent change in the sign of the chemical shift between them.

This phenomenon can be explained by the fact that the amide molecules associate with the aromatic solvents in such a way that the nitrogen atom with its fractional positive charge is situated close to the region of high π electron density of the aromatic ring and with the negatively-charged carbonyl oxygen atom as far from the center of the ring as possible. The amide molecule retains its planar configuration so the solute and solvent molecules become parallel and coplanar as shown below:

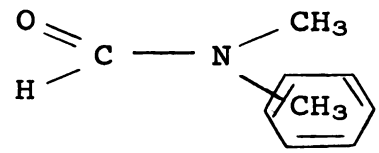

In this arrangement the N-methyl group <u>trans</u> to the carbonyl oxygen atom will be near the center of the ring and, consequently, the diamagnetic anisotropy of the benzene ring will affect this N-methyl group more than the other, tending to shift it to higher magnetic field. Hatton (67,68) measured the chemical shifts of N-methyl groups of DMF in both aromatic and non-aromatic solvents. In non-aromatic solvents the mean chemical shifts of the two peaks due to the N-methyl group do not change with respect to the internal

reference. However, the peak separation between them decreases as the mole fraction of the amide is reduced. This is probably due to the mutual interaction of the amide molecules by dipolar association.

Of considerable importance in the present studies of rates of internal rotation in the N,N-disubstituted amides is the question of whether or not the peak separation changes with temperature. It can only be precisely measured at temperatures low enough that exchange broadening is small. It has then been usual to use this value at all higher temperatures in the calculation of rate constants. However, Whittaker and Siegel (69) made measurements on the temperature dependence of this separation, over the accessible range, using solutions of amides in acetone-d_6, hexamethyldisiloxane and $CFCl_3$ as well as the pure amides. They noticed that the maximum value of chemical shift at low temperature is strongly dependent on the nature of the solvent. The peak separation decreases rapidly as concentration decreases, but different limiting values are reached at infinite dilution in different solvents. This behavior indicates the possibility of dimerization or hydrogen bond formation. They also found that the peak separation increases as the temperature decreases from the coalecence point but tends to level off at some intermediate temperature. When the temperature is reduced even further, the rate of increase of the peak separation may change indicating that effects other than internal rotation must

enter. They suggest that the correct peak separation $\delta\omega_o$ in the absence of exchange can be obtained by plotting the observed peak separation $\delta\omega$ vs. temperature. This will yield a plot of the following type:

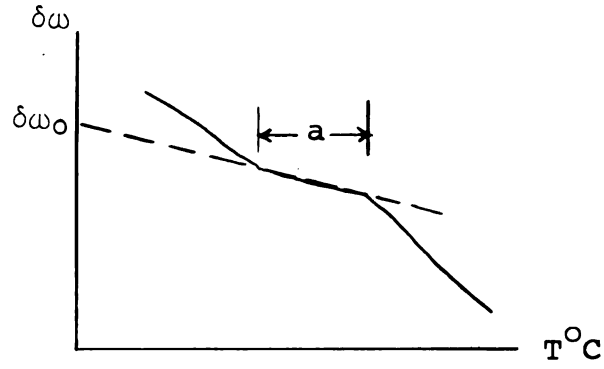

and the correct value of $\delta\omega_o$ is obtained by a 'reasonable' extrapolation (perhaps to the freezing point) of the linear portion "a" of the curve.

The unusual behavior of the $\delta\omega$ vs T^o curves may be explained qualitatively. The planar amide molecules tend to associate (68), and this association may change the magnetic anisotropy of the carbonyl bond since it has been shown (70) to be quite sensitive to the charge distribution in the bond.

The average half-life of a given dipolar interaction increases with decrease in thermal motion and increase viscosity. Consequently, the average magnetic anisotropy of a carbonyl bond increases with decrease in temperature and the chemical shift of the methyl groups should increase as temperature decreases. This explains the sudden change in slope at temperatures lower than "a". At high temperatures

the fast rotation about the C-N bond probably prohibits significant dipolar association because of the steric effects. Based on this mechanism, the E_a obtained from the high temperature data should be more reliable.

EXPERIMENTAL

Preparation of Amides

The compounds used in this investigation are listed in Table 4 , along with their boiling points and appropriate literature references. N-methyl-N -butylacetamide and N-methyl-N-cyclohexylacetamide are prepared (67) by the addition of one mole of acetyl chloride in ether (or benzene) slowly with stirring into an ether (or benzene) solution of two moles of the respective amine. Sub-zero temperatures should be maintained at all times, but freezing should be avoided. The mixture is then allowed to warm up to room temperature with stirring. After several hours, the amine chloride is dissolved in a minimum amount of water. The aqueous layer is then extracted three times by ether (or benzene) and the organic extract is combined with the original organic portion which contains the desired amide. The combined organic solution is then washed with minimum amount of 20% potassium carbonate solution, in small portions, until neutral. The organic layer is dried over anhydrous potassium carbonate overnight, and the amide collected by vacuum fractional distillation.

Table 4. Boiling points of substituted amides.

Compound	Observed B.P. °C.	Observed mm Hg.	Literature B.P. °C.	Literature mm Hg.	Reference
$HCON(CH_3)_2$	151.5	740	153.0	760	81,a
$CH_3CON(CH_3)_2$	44.0	3	166.1	760	82,b
$CCl_3CON(CH_3)_2$	85.2	5			c
$ClCON(CH_3)_2$	58.0	30	167.0	754	83,d
$CH_2{=}CHCON(CH_3)_2$	46.0	3	96-104	35	84,d
$C_2H_5CON(CH_3)_2$	58.5	10	175.5	765	85,c
$CH_3CON(CH_3)(C_2H_5)$	45.0	33	180	760	86,c
$CH_3CON(CH_3)(C\text{-}C_6H_{11})$	129-130	13	249	740	87,c
$CH_3CON(CH_3)CH(CH_3)_2$	60.5	17	69-70	13	88,c
$CH_3CON(CH_3)(n\text{-}C_4H_9)$	82.0	8	65.0	3	89,c

[a]Purchased from Fisher Scientific Company, Fair Lawn, N. J.
[b]Purchased from Eastman Organic Chemicals Dept., Rochester, N. Y.
[c]Prepared in this laboratory.
[d]Purchased from K and K Lab. Inc., Jamaica, N. Y.

an

aqu

ch

ly

bet

lay

eth

ori

bon

by

of

aqu

one

cee

pre

tet

spe

tub

amo

HMD

has

ver

At

N-methyl-N-ethylacetamide is prepared by addition of an aqueous solution of two moles of NaOH slowly into an aqueous solution of one mole of N-methyl-N-ethylamine hydrochloride. One mole of acetyl chloride is then added gradually to the above mixture. The temperature should be kept between 0 and 10°C throughout the experiment. The aqueous layer is separated and then extracted several times by either ether or benzene. The organic extract is combined with the original amide layer and dried over anhydrous potassium carbonate. The solvent is evaporated and the amide is collected by vacuum fractional distillation.

N-methyl-N-isopropylacetamide is prepared by addition of one mole of acetyl chloride slowly with stirring to an aqueous mixture of one mole of N-methyl-N-isopropylamide and one mole of sodium hydroxide. The temperature should not exceed 10°C. The remaining procedures are the same as for the preparation of N-methyl-N-ethylacetamide.

The purity of t-butylbenzene, trifluoroacetic acid, s-tetrachloroethane and hexamethyldisiloxane was checked by NMR spectra after vacuum fractional distillation. All the sample tubes are sealed at a pressure of 10^{-4} mm of Hg and a small amount of HMDS is added to the sample as an internal reference. HMDS is a good internal reference for this study because it has a higher boiling point (about 100°C) than the conventional reference, tetramethylsilane, TMS (b.p. 27°C). At room temperature the chemical shift of HMDS is 0.05 ±

0.005 ppm from TMS. After the sample tube is sealed, it is tested by heating in an oil bath to a temperature twenty degrees above the highest desired probe temperature. In general practice chemical shifts are measured against a reference compound and the most common reference compounds for protons are water, benzene, TMS and HMDS. The chemical shifts are given here as the dimentionless numbers

$$\delta = (H_c - H_r)H_o^{-1} \times 10^6 \text{ ppm}$$

where H_c is the resonance field for the nucleus in the particular molecular environment and H_r is the resonance field for the reference compound. Ocasionally an external reference was used to eliminate the solvent effect. This is done by sealing the reference compound in a capillary tube which in turn is supported in the center of the sample tube by Teflon plugs. The results using the external reference technique are not entirely satisfactory for two reasons. First, at high temperatures the vapor pressure of the sample tends to push the Teflon plugs upward out of the sample region. Second, the capillary tube can cause very high spinning noise, due to the high sensitivity of the 100MHz instrument. Also, the relative chemical shifts measured by the external reference technique must be corrected for the difference in the bulk diamagnetic susceptibility χ between the compound and the reference material. The correction factor for a cylindrical sample is

In s

be 2

it c

Bers

sphe

The

refe

cept

ing

whe

con

bet

min

bil

spe

MHz

pro

nal

Mag

$$\delta_{corr} = \delta_{obs} + \frac{2\pi}{3}(\chi_{ref}-\chi) .$$

In some cases the correction factor is found empirically to be 20-30% greater than the theoretical value $2\pi\Delta\chi/3$ (71,72). $\Delta\delta$ can be measured by the method (73) suggested by Frei and Berstein. They used two small reference containers, one spherical and one cylindrical in the regular 5mm sample tube. The difference between the two sharp signals from the two reference cells, is linearly dependent upon the volume susceptibility of the sample contained in the sample tube according to the expression

$$\delta_{cyl}(R) - \delta_{sph}(R) = [g_{cyl} - g_{sph}][\chi_v(R) - \chi_v(S)] ,$$

where the chemical shifts are in ppm and g is a geometrical constant which depends only on the shape of the interface between the reference and sample. $(g_{cyl}-g_{sph})$ can be determined by calibration with liquids of known volume susceptibility. In the ideal case it is equal to $\frac{2\pi}{3}$.

Spectrometer

A Varian HA-100 high-resolution proton-stabilized NMR spectrometer was used in this investigation. A V-4311(100 MHz) fixed frequency rf unit and a V-4333 variable temperature probe were used to obtain the proton magnetic resonance signals. A V-3506 flux stabilizer is used to stabilize the H_o magnetic field to about one part in 10^8. The V-4354A

internal-reference proton stabilization unit provides NMR stabilization by locking the magnetic field to a reference proton signal of the sample. Frequencies were counted with a Hewlett-Packard 5245L frequency counter.

Temperature Calibration

The temperature of the sample is controlled by a V-4341 variable temperature system which has a temperature range of -60-200°C. At ambient temperatures and above the nitrogen gas is heated inside the probe to the desired temperature and allowed to flow around the sample tube. For low temperature studies liquid nitrogen is used to cool the nitrogen gas. The temperature controller circuits limit the maximum temperature variation at the heat sensor to ± 1°C.

Since the temperature dial on the V-4341 has a calibration accuracy of only ± 3 degrees, ethylene glycol and methanol chemical-shift thermometers are used for more accurate work in the high-temperature range (60-160°C) and the low-temperature range (-40° to 40°C), respectively.

These two chemical-shift thermometers have been carefully calibrated in this laboratory using a copper-constantan thermocouple which was inserted in the spinning sample tube and the voltage output recorded on a Sargent recorder. A least-squares analysis of each set of data provided the necessary temperature-chemical shift correlation expressions. These correlations were used in all the following experiments

to provide precise values of the sample temperatures.

For the high-temperature range the resulting expression is

$$T^{\circ}K = -(\delta)1.017 + 464.9 \qquad (A)$$

where δ is the difference between the two chemical shifts in ethylene glycol. For the low-temperature range the calibration equation is

$$T^{\circ}K = -(\delta)1.076 + 464.7 \qquad (B)$$

where δ is the difference between the two chemical shifts in the methanol spectrum.

A cross check has been made between the above calibrated temperatures and the temperatures from the calibration charts provided by Varian, and the results are listed below:

Ethylene glycol $\Delta\delta$	Varian	Eq. A	Methanol $\Delta\delta$	Varian	Eq. B
155 cps	32°C	34.3°C	146 cps	37.5°C	34.5°C
159	28	30.2	150.5	32	29.8
163	24	26.1	154.5	27	25.5
167	20	22.06	158	23	21.7

All the results in a given row are from the same temperature setting on the V-4341 unit. Columns 2 and 5 are obtained from the charts provided by Varian Associates and it is evident that these two columns are not consistent in the

region where they overlap (20 to 40°C). The values in columns 3 and 6 are obtained from Equations A and B, respectively, and are quite consistent, so these two equations can be used with confidence.

In addition to using the differences of the chemical shifts of ethylene glycol and methanol, Glew (74) used a mixture of 3 mole percent tetramethylsilane, 61 mole percent m-chlorophenol and 36 mole percent trifluoroacetic acid as an NMR thermometer. This mixture is useful in the temperature range -10 to +30°C. The analytical expression for this thermometer is

$$T^{\circ}C = 87.961 - 1.0736(\delta_{OH} - \delta_{ArH})$$

where δ_{OH} and δ_{ArH} are the phenolic and the aromatic ring proton chemical shifts in cps, respectively. The sensitivity of this thermometer is claimed to be 1.8 times greater than that of methanol but it was not used in this work. Duerst (75) has a similar thermometer which employs a mixture of 51.8% water, 48.1% methanol and 0.1% HCl, by weight. The temperature and chemical shift relationship is

$$T^{\circ}C = 160.0 - 90.5\ (S)$$

where S is the peak separation in ppm between the two sharp signals.

RESULTS

Computer Methods in NMR Studies of Rate Processes

Methods for Evaluating Rotational Energy Barriers in Amides

Several methods have been used in the last ten or eleven years to determine the energy barriers for internal rotation in molecules from NMR data. Three of them will be discussed here.

Method I--The Intensity-ratio Method

Woodbrey and Rogers (4,50) imposed the requirements $\frac{1}{T_{2A}} \ll \delta\omega \gg \frac{1}{T_{2B}}$, $p_A = p_B$, and $\tau_A = \tau_B = 2\tau$ on Equations 47 and 48 to obtain an expression for rate constant $1/2\tau$ in terms of the ratio r of the maxima to central minimum of the doublet:

$$\frac{1}{2\tau} = \frac{\pi\delta\omega}{\sqrt{2}} [r + (r^2 - r)^{\frac{1}{2}}]^{-\frac{1}{2}}. \qquad (53)$$

The method then consists of measurement of the intensities of the maxima and of the minimum of the doublet corresponding to the two different magnetic environments for the N-methyl groups in the N,N-disubstituted amides. The intensity ratio is obtained at each temperature and, combining

it

ra

int

us

Up

Th

mo

la

in

er

br

Al

sta

wi

I/

the

sid

and

A s

bar

for

it with the peak separation in the absence of exchange, the rate constant $1/2\tau$ can be evaluated from Equation 53.

This method is, in general, used for exchanges with intermediate rates and the applicable temperature range is usually only about 25 degrees. For obvious reasons, the upper temperature limit is the coalescence temperature. The intensity ratio can be measured quite accurately in the moderately-fast exchange region but the errors are the largest in the slow-exchange region where small fluctuations in the base line and the central minimum will cause a large error in the value of the intensity ratio. Inhomogeneous broadening also tends to cause systematic errors.

A mathematical evaluation of this method was made by Allerhand and Gutowsky (15) who showed that, for a given $\delta\omega T_2^{\circ}$ product, the percent error in calculating the rate constant increases with decreasing exchange rate and decreases with an increasing value of the $\delta\omega T_2^{\circ}$ product.

In the case where the natural line widths $1/T_{2A}$ and $1/T_{2B}$ are comparable in magnitude to the peak separation in the absence of exchange, the overlap effect should be considered. Woodbrey and Rogers (50) substituted $2\Delta\omega = \delta\omega_{obs}$ and $\tau \rightarrow \infty$ into Equation 48 to solve for a corrected $\delta\omega$. A slight improvement may be made on the value of the energy barrier when the value of $\delta\omega$ corrected for overlap is used.

The improved intensity-ratio method can be programmed for the digital computer and the computation procedures are

summarized as follows:

1. Substitute $\tau \rightarrow \infty$, p_A, T_{2A}, T_{2B} and $\delta\omega_\infty$ into Equation 48 to calculate the corrected peak separation in the absence of exchange.

2. Use the corrected peak separation $\delta\omega$, the line shape parameters mentioned above and Equation 48 to solve for the precise positions of the maxima and the minimum, varying τ each time by a small increment.

3. For each set of frequencies found in step 2 above, the corresponding relative intensities of the maxima and minimum can be obtained from Equation 47 so the ratios of the maxima and the minimum are obtained.

4. Compare all the calculated intensity ratios from step 3 with the experimental intensity ratios and choose the one closest to the experimental value . The corresponding τ is the best value for that particular experimental spectrum.

It is obvious that this computation is very time consuming because it requires the computer to solve a large number of fifth-order equations. A computer program, BARRIER, has been written for this calculation. For a typical experimental spectrum, 250 τ values ranging from 10^{-4} to 10^5 are used, requiring 20 minutes time on the Control Data 3600 computer. This procedure is seen to be rather impractical, particularly in view of the systematic

errors inherent in the intensity-ratio method.

This program is not included as an Appendix since it was not extensively used in this research; however, the program is available.

Method II--Peak-Separation Method

The peak-separation method was developed by Gutowsky and Holm (3). When the line widths $\frac{1}{T_2}$ are small compared to the peak separations $\delta\omega$ in the absence of exchange the $\frac{1}{T_2}$ terms can be neglected in Equation 48. Neglecting overlap, the experimentally observed peak separation $\delta\omega_e$ can be expressed as

$$(\frac{\delta\omega_e}{\delta\omega}) = \pm\sqrt{1 - \frac{2}{\tau^2 d\omega^2}} \quad . \tag{54}$$

When Equation 50 is written in terms of cycles/sec the equation has the following form

$$\frac{1}{\tau} = \frac{\pi}{\sqrt{2}}\sqrt{\delta\nu^2 - \delta\nu_e^2} \quad . \tag{55}$$

In this method the frequency separation in the proton magnetic resonance spectrum of the N-methyl doublet at different temperatures is measured. From Equation 55 the corresponding rate of internal rotation $1/2\tau$ can be calculated for each temperature. Fitting the data to an Arrhenius-type rate equation, $1/2\tau = Ae^{-E_a/RT}$, the energy barrier E_a and the frequency factor A can then be obtained from the slope

and the intercept of the straight line plot of log $1/2\tau$ *vs.* $1/T^{o}K$. The least-squares method may be used to obtain the best values of E_a and A.

The program NMRTAU was written for the CDC-3600 computer to carry out the above operations. It prints out τ values at each temperature, and the values of E_a and log A evaluated by the peak separation method, using a least-squares fit of the data (Appendix III).

$\delta\omega_e$ becomes decreasingly sensitive to rate of exchange as the exchange becomes slower. At very low temperatures, where the exchange is quite slow, the error in determining $\delta\omega_e$ becomes large. The other shortcoming is that the major change in the peak separation with exchange rate takes place over a very narrow temperature range, $0.45 \leq \tau\delta\omega \leq 2$. For fast exchange, the rate constant obtained from Equation 55 is always inaccurate (48). The peak separation method is, therefore, not a reliable technique for obtaining precise kinetic data.

Method III--Total Line-Shape Analysis

From Table 1 values of the internal rotation energy barrier for a given amide are seen to vary widely, depending on which particular approximation method (intensity-ratio method or peak-separation method) was used. Both are subject to large systematic errors and disadvantages. The most logical and desirable method is to determine the exchange rate from the high resolution NMR spectra by using Equation 47

directly, without further assumptions or approximations.

When a set of adjustable line-shape parameters τ, p_A, $\delta\omega$, $1/T_{2A}$, $1/T_{2B}$, and $\Delta\omega$ are substituted into Equation 47, the complete spectrum can be calculated. The computer program NMRFIT (Appendix I) will compute the spectrum based on any given set of the above parameters. The calculated spectrum is then compared with the experimental spectrum and the computer will continue to search for the best combination of the parameters until the value of $\sum_i$ (calculated intensity$_i$ - observed intensity$_i$)^2 is not improved by further changes. The program NMRFIT is thus able to extract the best combination of the above parameters to fit a given experimental spectrum. It must be kept in mind that NMRFIT is only a numerical operation and it is possible that the iteration procedure may stop before reaching the best fit. This is possible if it is trapped in a local minimum. To avoid such a situation the input parameters should be as close to the true values as possible.

The best parameters selected by NMRFIT are then used as input in the program NMRPLOT (Appendix II) which will plot out the entire calculated spectrum so it can be checked visually against the experimentally determined spectrum.

Treatment of Data

The line-shape Equation (47) was derived from the modified Bloch equations and kinetic considerations. The ideal approach for extracting line-shape parameters from the

experimental spectrum is to substitute a number of sets of parameters into the theoretical equation, calculating a theoretical spectrum in each case, comparing these with the observed spectrum and identifying the set of parameters which will provide the best fit. The comparison can be done either visually or mathematically. The most common mathematical criterion used is the least-squares curve fitting procedure (76,77,78).

The ordinary least-squares operation involves three steps (79). First, suppose the line-shape equation is

$$Y_i = AX_i + BU_i + CZ_i + DW_i \tag{56}$$

where Y_i is the intensity at a particular frequency, and A, B, C, D are the line-shape parameters such as peak separation, half-width at half-height and exchange rate constant. The other variables X_i, U_i, Z_i and W_i are simple functions of the frequency. Second, the sum of the squares of the absolute deviations of the calculated values of Y from those observed should be minimized:

$$Y_i - (AX_i + BU_i + CZ_i + DW_i) = Dev \tag{57}$$

$$\Sigma[Y_i - (AX_i + BU_i + CZ_i + DW_i)]^2 = (Dev)^2 \tag{58}$$

$$\frac{\partial \Sigma(Dev)^2}{\partial A} = \Sigma(-2)[Y_i - (AX_i + BU_i + CZ_i + DW_i)]X_i = 0 \tag{59}$$

Differentiation of $\Sigma(Dev)^2$ respect with B, C, and D yields

$$\Sigma X_i Y_i = A\Sigma X_i^2 + BZU_i X_i + C\Sigma Z_i X_i + D\Sigma W_i X_i \tag{60}$$

$$\Sigma U_i Y_i = A\Sigma X_i U_i + B\Sigma U_i^2 + C\Sigma Z_i U_i + D\Sigma W_i U_i \quad (61)$$

$$\Sigma Z_i Y_i = A\Sigma X_i Z_i + B\Sigma U_i Z_i + C\Sigma Z_i^2 + D\Sigma W_i Z_i \quad (62)$$

$$\Sigma W_i Y_i = A\Sigma X_i W_i + B\Sigma U_i W_i + C\Sigma Z_i W_i + D\Sigma W_i^2 \quad (63)$$

Third, Equations 60, 61, 62 and 63 can be solved simultaneously for the values of line-shape parameters, A, B, C and D, which will give the best fit.

The ordinary least-squares treatment of data occasionally gives experimentally impossible results and, in other cases, reasonable values for the parameters can only be obtained by treating part of the data rather than the entire set of values.

Instead of solving the above set of equations directly, an alternate procedure can be used. The estimated parameters are substituted into the line-shape equation in such an order that the least certain parameter will be adjusted first. An arbitrary adjustment increment or variation function is assigned to each parameter. The sum of the squares of the differences between the calculated and observed intensities is compared with that obtained in the previous trial (80). If this sum is smaller than the previous sum, it indicates that the correction adjustment is in the right direction, otherwise the sign and magnitude of the previous adjustment increment are changed. This procedure was programmed and the description of the program and the flow chart are given in Appendix I.

High-resolution Spectra

The proton magnetic resonance spectra reported on the following pages are obtained from the HA-100 MHz high-resolution spectrometer at room temperature. The chemical shifts were measured in ppm from the internal reference HMDS, chosen as zero. Indication will be given when other reference compounds are used.

The spectra of N,N-dimethylformamide, N,N-dimethylacetamide, N,N-dimethylcarbamyl chloride and N,N-dimethyltrichloroacetamide can be found in Woodbrey's thesis (50). In the spectra of these compounds the two $N-CH_3$ groups give rise to a doublet. The signal at the higher field is due to the methyl group which is in a position trans to the carbonyl oxygen atom, while the one at the lower field is due to the cis methyl group. In the case of N,N-dimethylformamide, the two peaks of the original doublet are further split into doublets by the formyl proton. The coupling constants are 0.7 and 0.9 cps for the low and high field peaks, respectively. This additional splitting is not observed for the other amides mentioned above.

N,N-Dimethylpropionamide

The proton magnetic resonance spectrum of N,N-dimethylpropionamide is given in Figure 1. One N-methyl group has a resonance signal at 2.91 ppm and that of other N-methyl is located at 2.77 ppm. The quartet between 2.333 ppm and 210.7

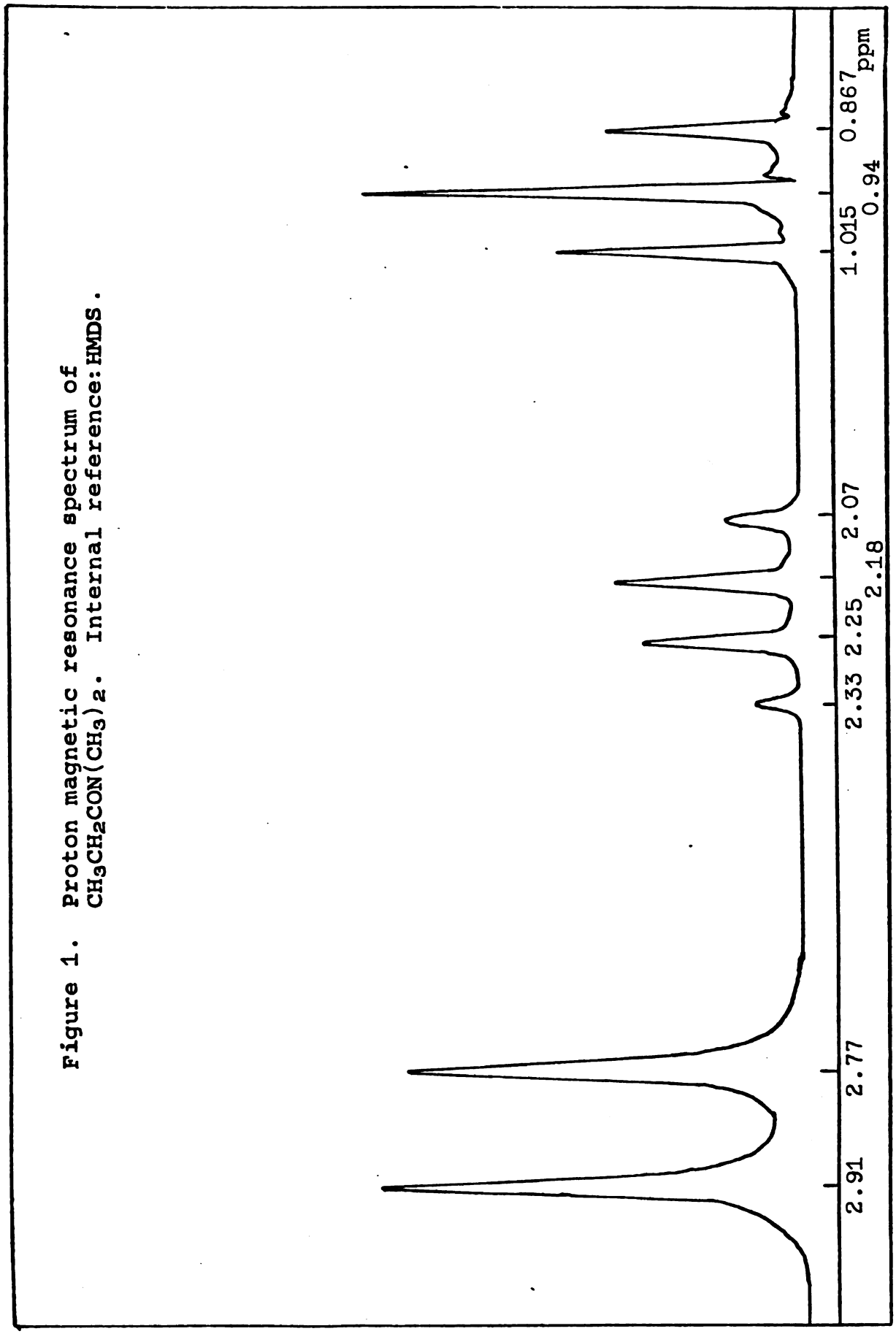

Figure 1. Proton magnetic resonance spectrum of $CH_3CH_2CON(CH_3)_2$. Internal reference:HMDS.

ppm is due to the methylene protons, whereas the triplet between 1.015 ppm and 0.867 ppm arises from the methyl protons of the ethyl group. These multiplets result from the spin-spin coupling between the methyl protons and the methylene protons of the ethyl group.

N,N-Dimethylacrylamide

The proton magnetic resonance spectrum of pure N,N-dimethylacrylamide is shown in Figure 2. The doublet at 2.98 ppm and 2.837 ppm arises from the two N-methyl groups. The peak at 2.837 ppm arises from the N-methyl group which is cis to the carbonyl oxygen atom. The line widths of the two peaks are about the same, because of the negligible spin-spin coupling with the proton of the vinyl group.

The remaining signals are from the protons of the vinyl group. Such a complicated spectrum arises when the chemical shifts and the spin-spin coupling constants are comparable and it can be analyzed by standard methods as an ABC spectrum.

Asymmetrical N,N-Disubstituted Amides

In this type of compound, the intensities of the two components of the N-methyl doublet are different, because the equilibrium proportions of the two isomers differ. The relative populations of the two rotational isomers are proportional to the relative intensities of the two N-methyl peaks.

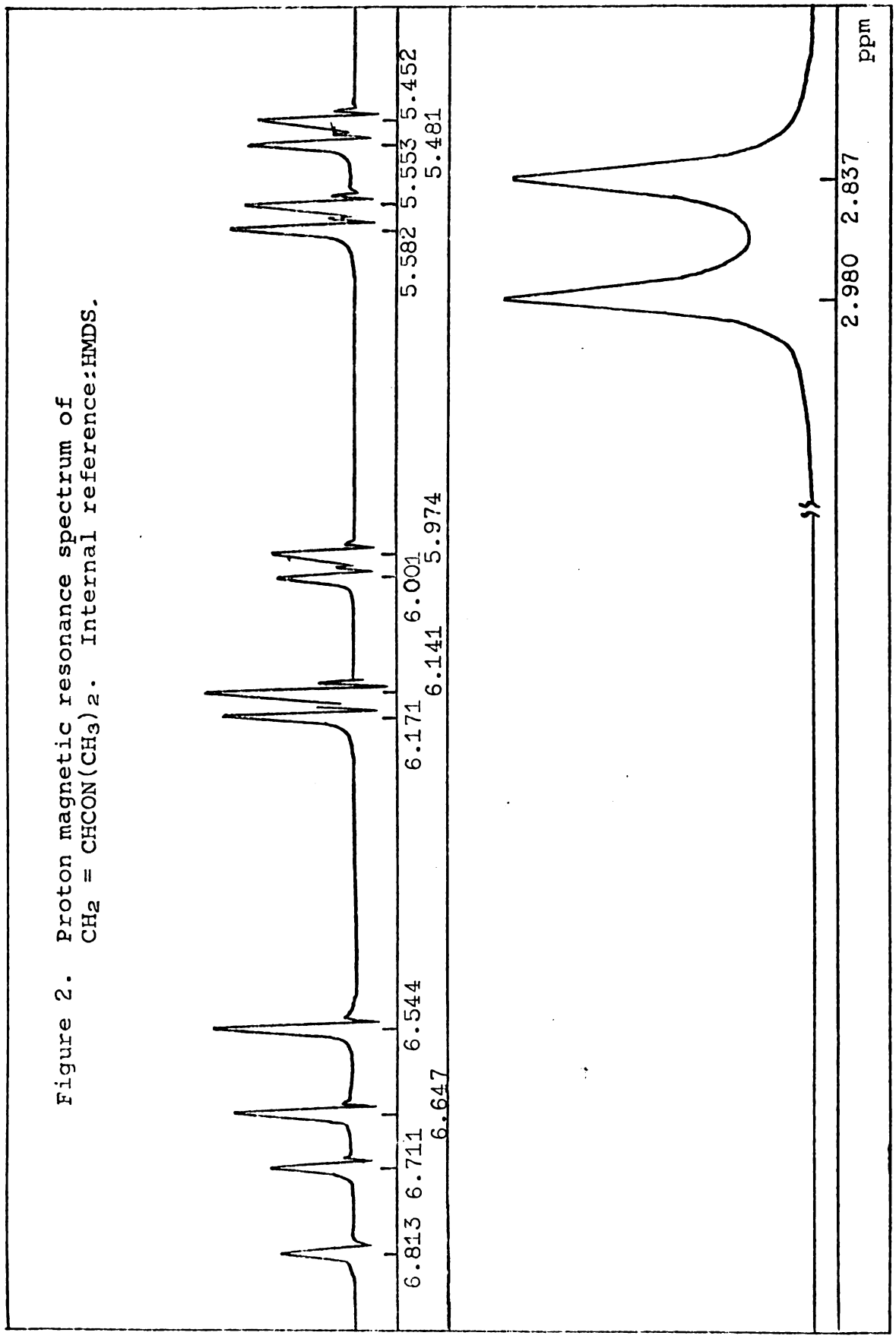

Figure 2. Proton magnetic resonance spectrum of $CH_2 = CHCON(CH_3)_2$. Internal reference:HMDS.

N-Ethyl-N-methylacetamide

The proton magnetic resonance spectrum of N-ethyl-N-methylacetamide is shown in Figure 3. The resonance peaks at 1.92 ppm and 1.895 ppm arise from the CH_3-CO groups of the two rotational isomers. The quartet at 3.27 ppm is from the N-methylene protons and the 'doublet' splitting of this quartet is from the two rotational isomers. The methyl signal at 2.901 ppm and the N-C-CH_3 triplet at 1.040 ppm are assigned to the respective N-alkyl groups which are in a position trans to the carbonyl oxygen atom, while N-methyl peak at 2.741 ppm and the N-C-CH_3 triplet at 0.935 ppm are associated with groups located cis to the carbonyl oxygen. The different line widths of the two methyl peaks are probably a result of weak spin-spin coupling with the O=C-CH_3 protons. The difference in spin-spin coupling constants is averaged out at elevated temperature, and consequently the line widths become equal.

N-n-Butyl-N-methylacetamide

The proton magnetic resonance spectrum of pure N-n-butyl-N-methylacetamide is shown in Figure 4. The triplet at 3.225 ppm is from the N-CH_2 protons and the rather large line width of this triplet is probably caused by the superposition of two triplets from the two rotational isomers. The doublet at 1.94 ppm and 1.885 ppm is from the acetyl protons of the two rotational isomers. The N-methyl peak at 2.74 has been assigned to the group which is in a position

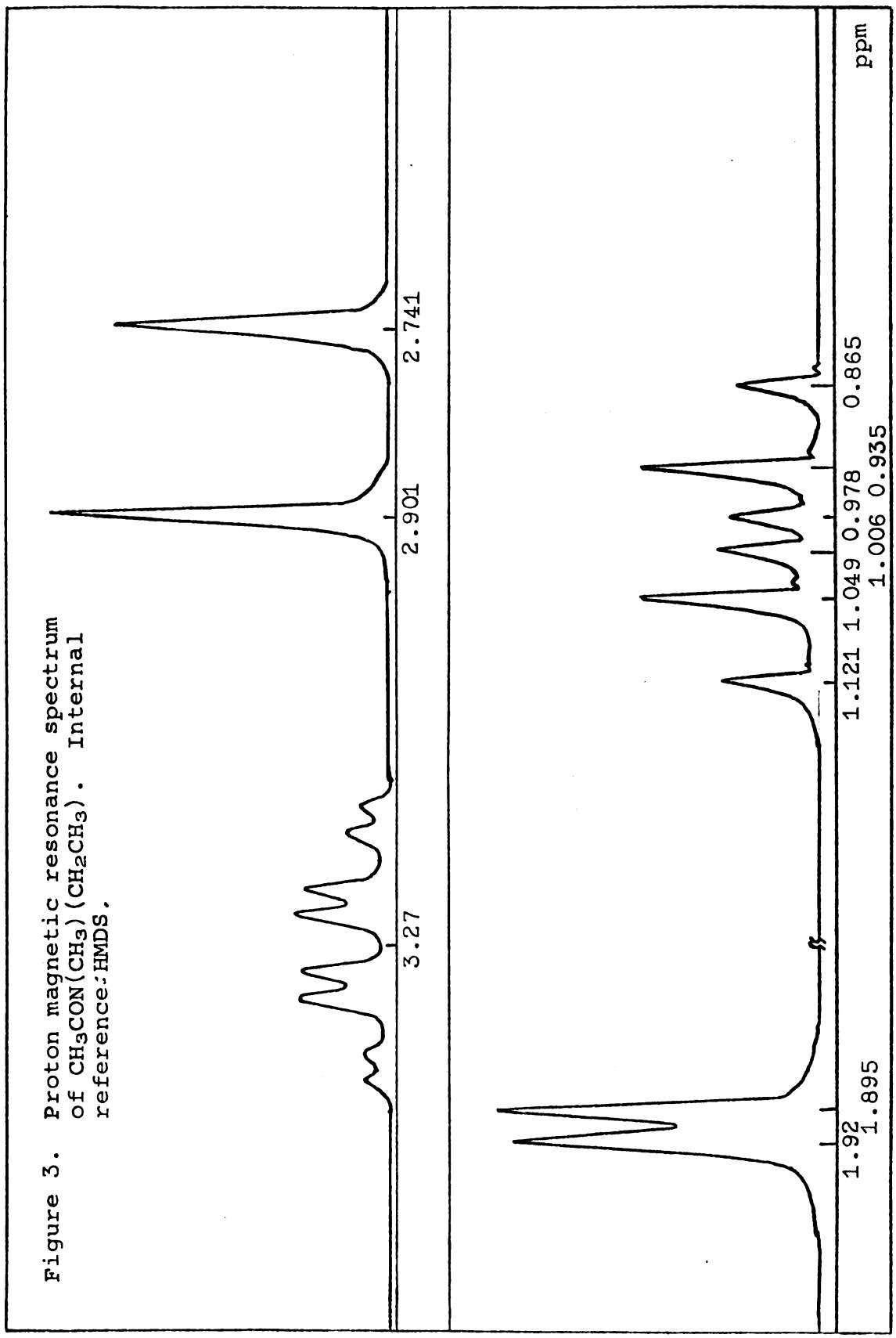

Figure 3. Proton magnetic resonance spectrum of $CH_3CON(CH_3)(CH_2CH_3)$. Internal reference: HMDS.

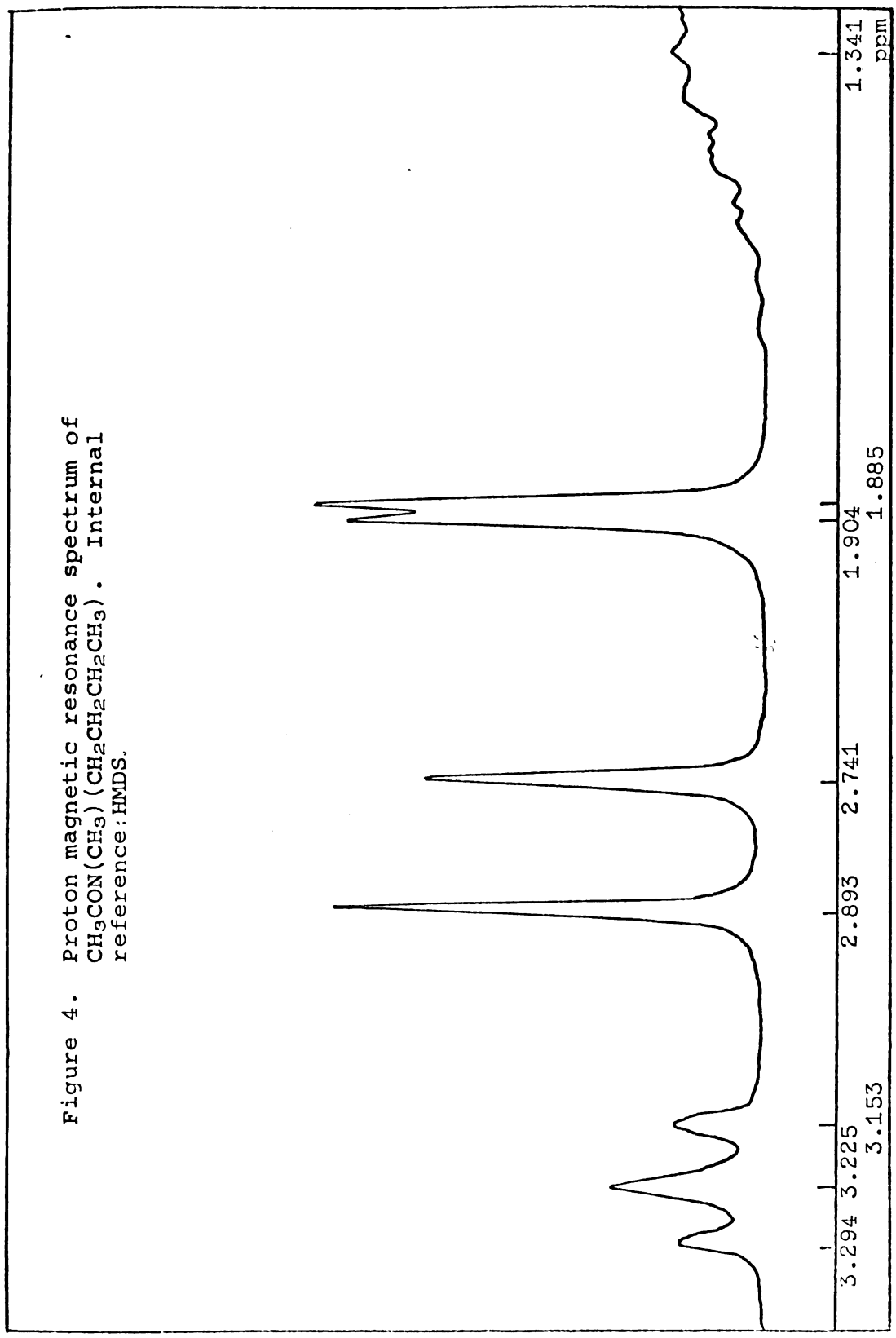

Figure 4. Proton magnetic resonance spectrum of $CH_3CON(CH_3)(CH_2CH_2CH_2CH_3)$. Internal reference: HMDS.

cis to the carbonyl oxygen atom and the trans N-methyl peak is located at 2.893 ppm. The unresolved signal at 1.341 ppm is from the N-C-CH_2-CH_3 protons.

N-Cyclohexyl-N-methylacetamide

The proton magnetic resonance spectrum of N-cyclohexyl-N-methylacetamide is shown in Figure 5. The peaks of the acetyl protons of the two rotational isomers are located at 1.942 ppm and 1.89 ppm. The N-methyl peak at 2.644 ppm is assigned to the group which is cis to the carbonyl oxygen atom, while the peak at 2.752 is assigned to the N-methyl group trans to the carbonyl oxygen atom. The two broad and weak peaks at 4.245 ppm and 3.508 ppm are from the protons at the 1-position of the cyclohexyl rings of the two rotational isomers.

N-Isopropyl-N-methylacetamide

The proton magnetic resonance spectrum of the N-isopropyl-N-methylacetamide is shown in Figure 6. The acetyl proton peaks are at 1.928 ppm and 1.876 ppm. The N-C-$(CH_3)_2$ resonance peaks appears as two doublets at 1.112, 0.99 ppm and 1.047, 0.916 ppm. The N-methyl peak at 2.609 ppm and the methine septet at 4.726 ppm are assigned to the isomer in which these groups are located cis to the carbonyl oxygen atom, while the N-methyl peak 2.726 ppm and the methine septet at 4.016 ppm are assigned to the isomer in which the respective groups are trans to the oxygen atom. The relative

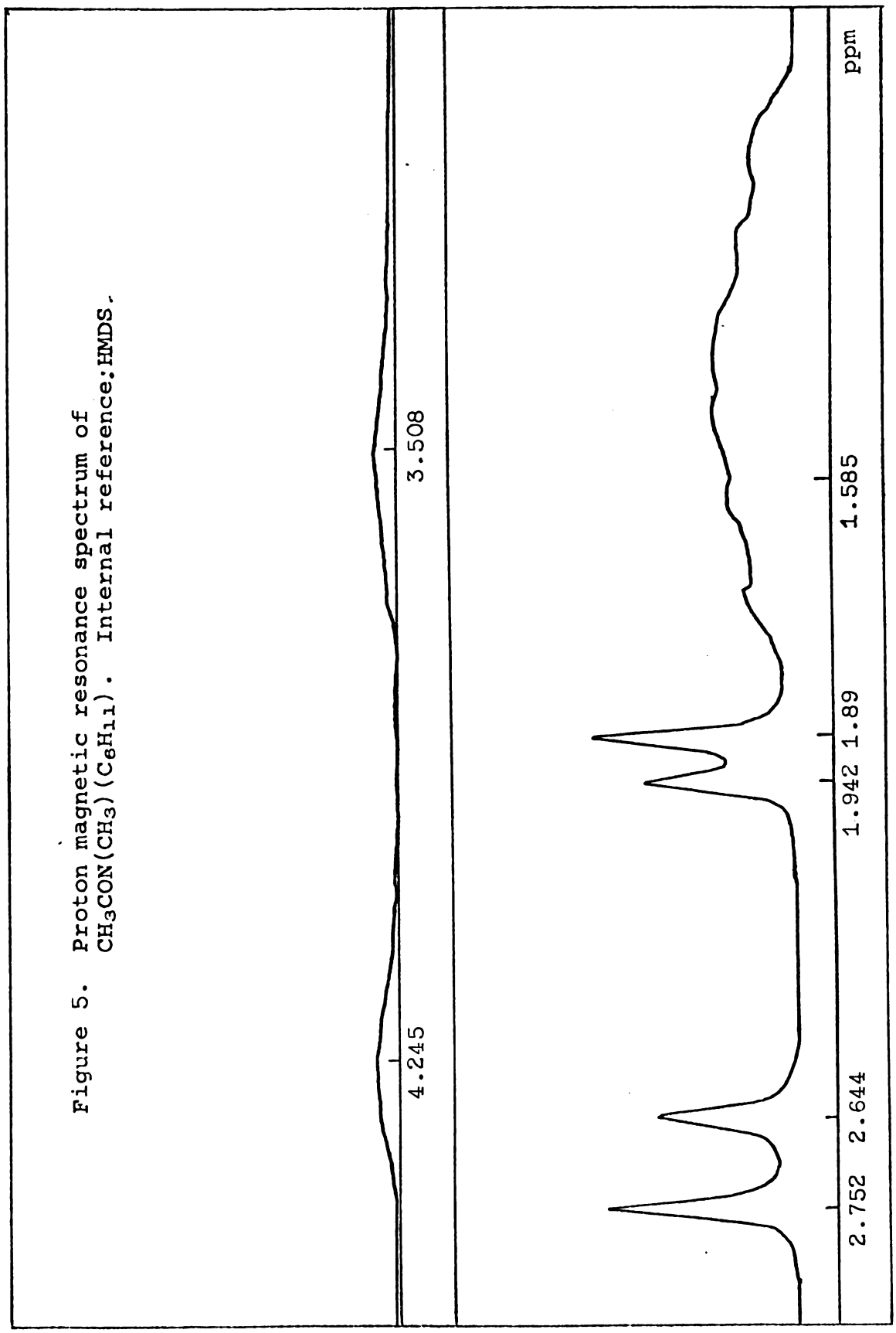

Figure 5. Proton magnetic resonance spectrum of $CH_3CON(CH_3)(C_6H_{11})$. Internal reference:HMDS.

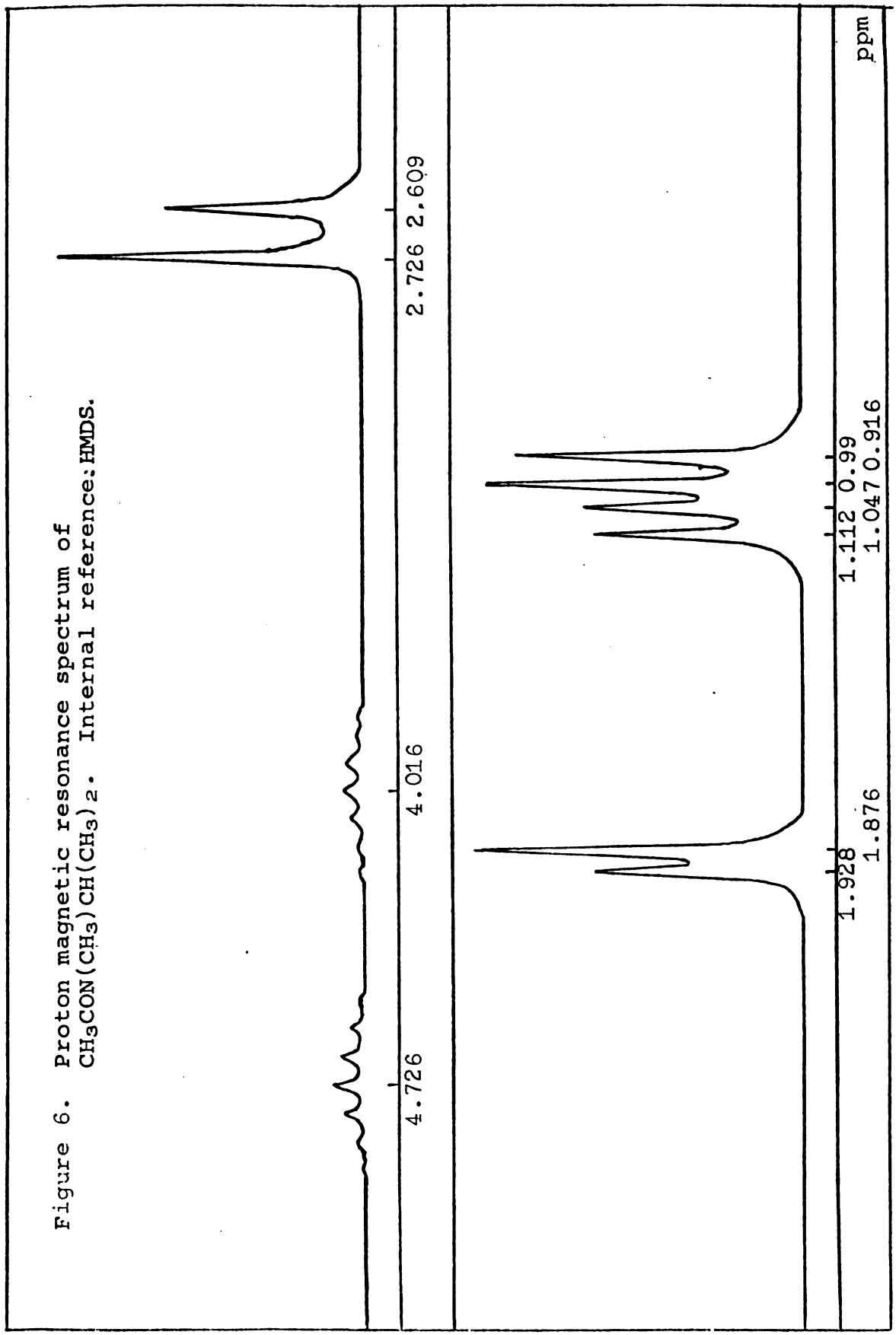

Figure 6. Proton magnetic resonance spectrum of $CH_3CON(CH_3)CH(CH_3)_2$. Internal reference: HMDS.

population is about 60% for the isomer with the N-methyl group trans to the carbonyl oxygen atom.

N-Methyl-N-benzylformamide

The proton magnetic resonance spectrum of N-methyl-N-benzylformamide is shown in Figure 7. The peaks from the N-methyl protons and benzyl protons cis to the carbonyl oxygen atom are located at 1.321 ppm and 3.168 ppm, respectively, while those from the N-methyl protons and benzyl protons trans to the carbonyl oxygen atom are at 1.348 and 3.168 ppm, respectively. The low field doublet is from the formyl protons in the two rotational isomers. The unresolved signal at 5.956 ppm is from the ring protons.

N-n-Butyl-N-methyltrimethylacetamide

The proton magnetic resonance spectrum of N-n-butyl-N-methyltrimethylacetamide is shown in Figure 8. In this spectrum only one set of N-alkyl resonances is found. The N-methyl resonance is located at 2.937 ppm and the $N-CH_2$ triplet is at 3.272 ppm. The high-field strong single peak is from the t-butyl protons. The unresolved high field signals are assigned to the protons of the $N-C-CH_2-CH_2-CH_3$ group. No doublet appears for the N-methyl group when the sample temperature is increased from -20°C to 80°C indicating that there is only one isomer in this temperature range.

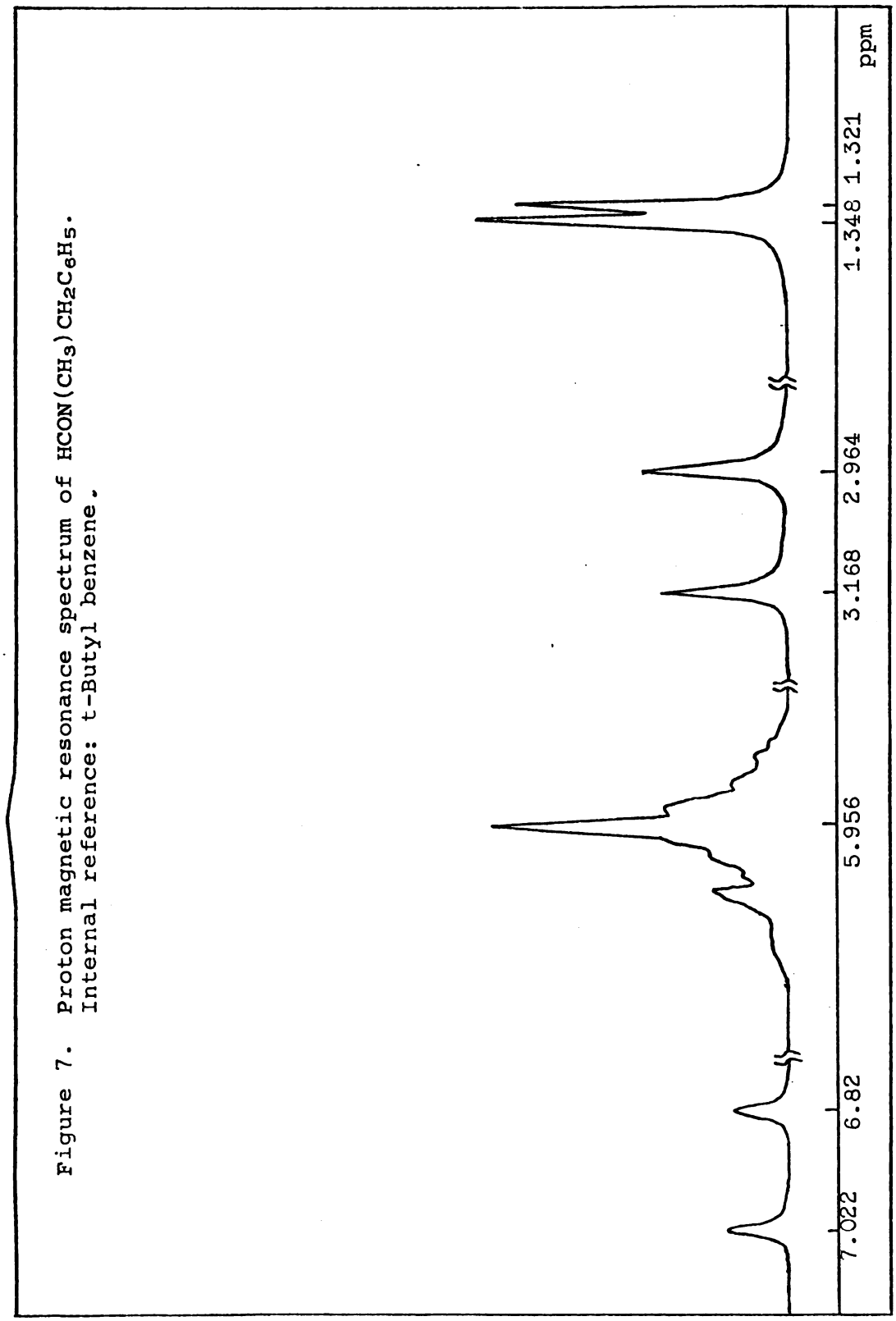

Figure 7. Proton magnetic resonance spectrum of $HCON(CH_3)CH_2C_6H_5$.
Internal reference: t-Butyl benzene.

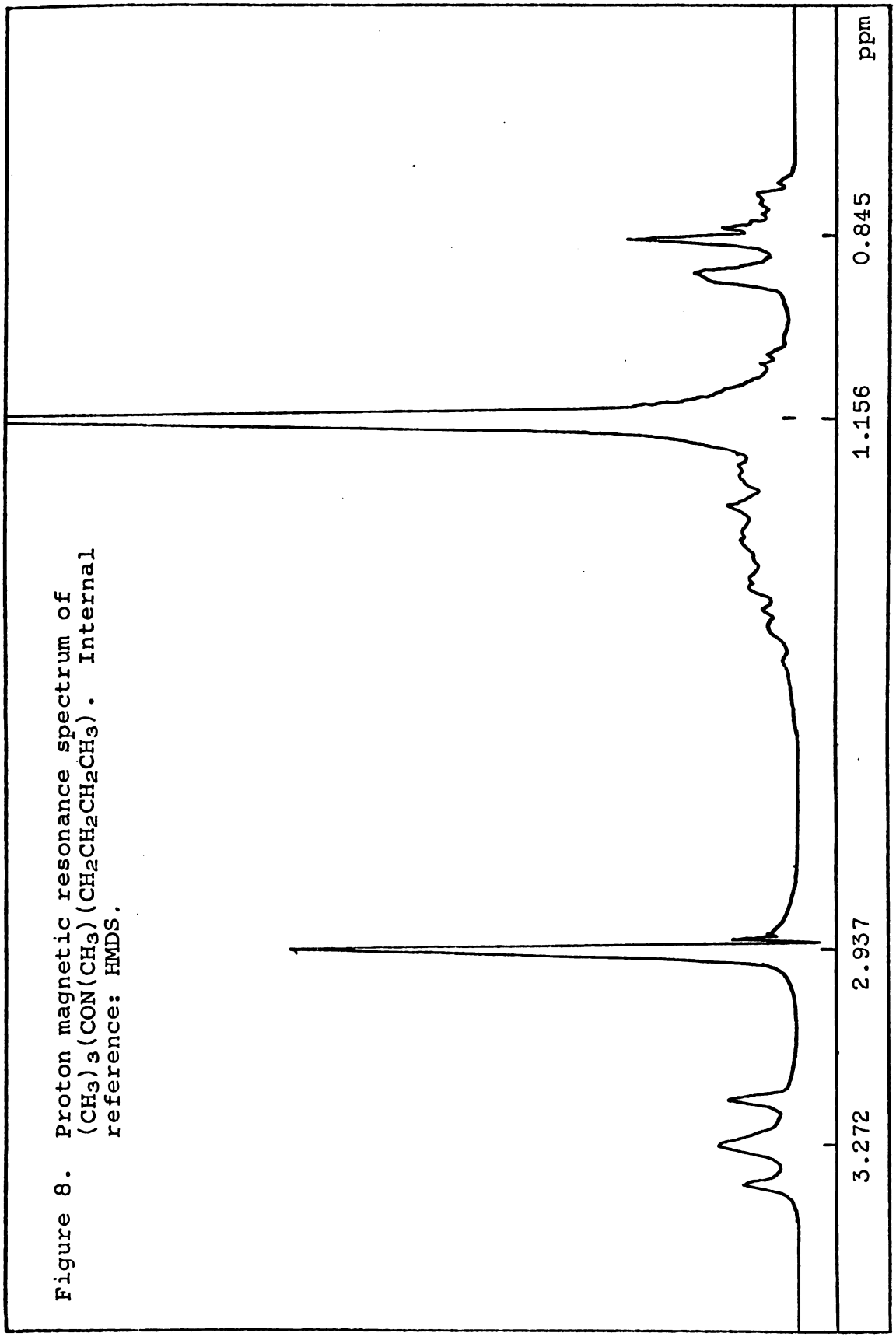

Figure 8. Proton magnetic resonance spectrum of $(CH_3)_3(CON(CH_3)(CH_2CH_2CH_2CH_3)$. Internal reference: HMDS.

N

o

F

a

g

7

t

t

N

p

A

-

a

r

7

b

r

N

Ta

N-Methyl-N-α-naphthylacetamide

The proton magnetic resonance spectrum of the solution of N-methyl-N-α-naphthylacetamide in $CHCl_3$ is shown in Figure 9. Only one peak is found for the N-methyl protons at 3.46 ppm and the proton signal from the acetyl methyl group is located at 1.863 ppm. The solvent peak is at 7.648 ppm. When the sample temperature is varied from -20°C to 65°C, no evidence for the existence of a second rotational isomer was obtained.

N-Methyl-N-phenylacetamide

The proton magnetic resonance spectrum of N-methyl-N-phenylacetamide in CCl_4 solution is shown in Figure 10. Again only one isomer is found in the temperature range -20°C to 60°C. The resonance peaks at 3.126 ppm and 1.706 are assigned to N-methyl protons and acetyl methyl protons, respectively. The unresolved ring signal is located between 7.241 ppm and 7.174 ppm.

Hindered Internal Rotation of Substituted Amides

The hindered internal rotations about the central C-N bond of some N,N-disubstituted amides were studied, and the results are reported as follows:

N,N-Dimethylformamide

The experimental and calculated data are tabulated in Table 7 and Figure 14. The internal rotation of pure

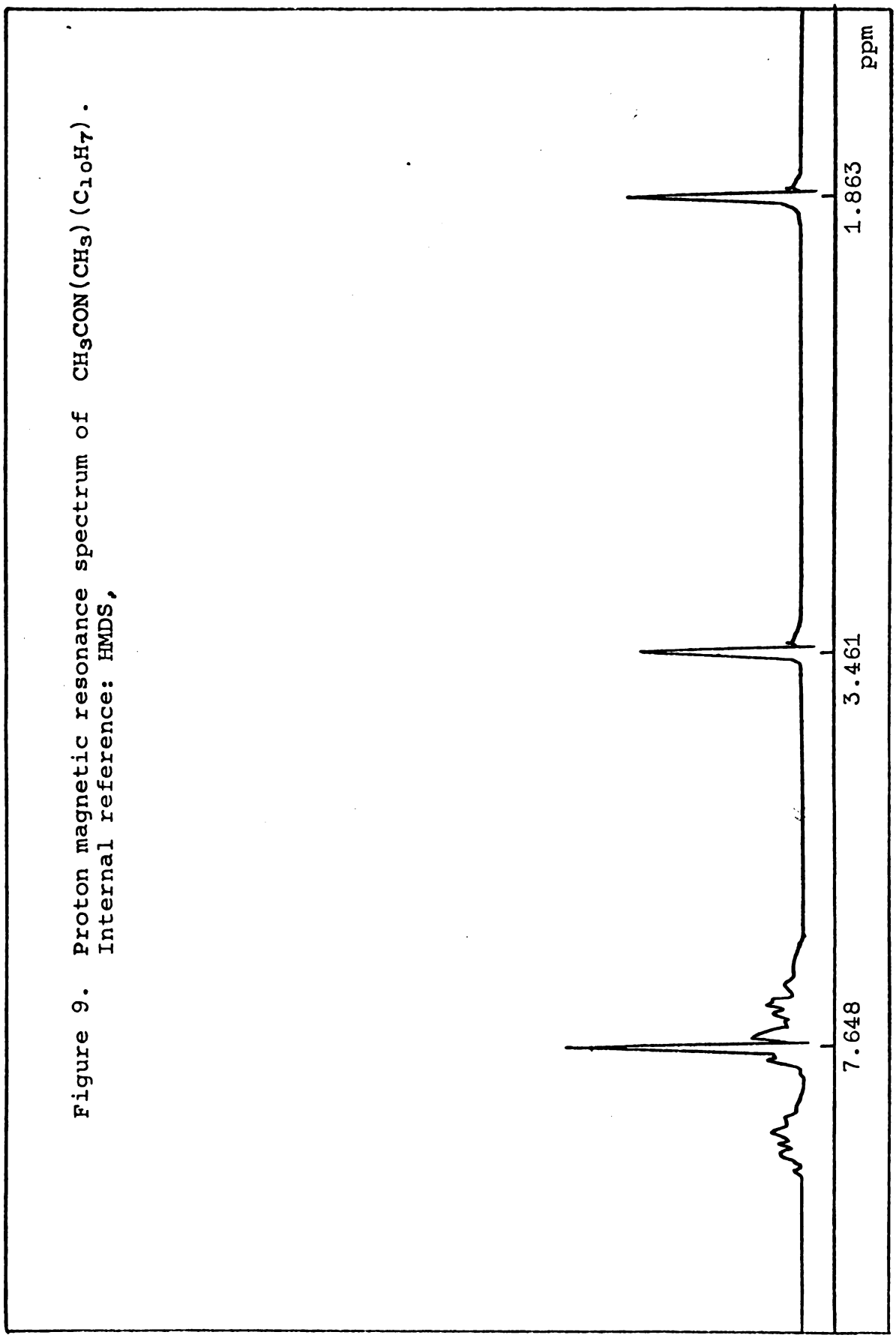

Figure 9. Proton magnetic resonance spectrum of $CH_3CON(CH_3)(C_{10}H_7)$.
Internal reference: HMDS.

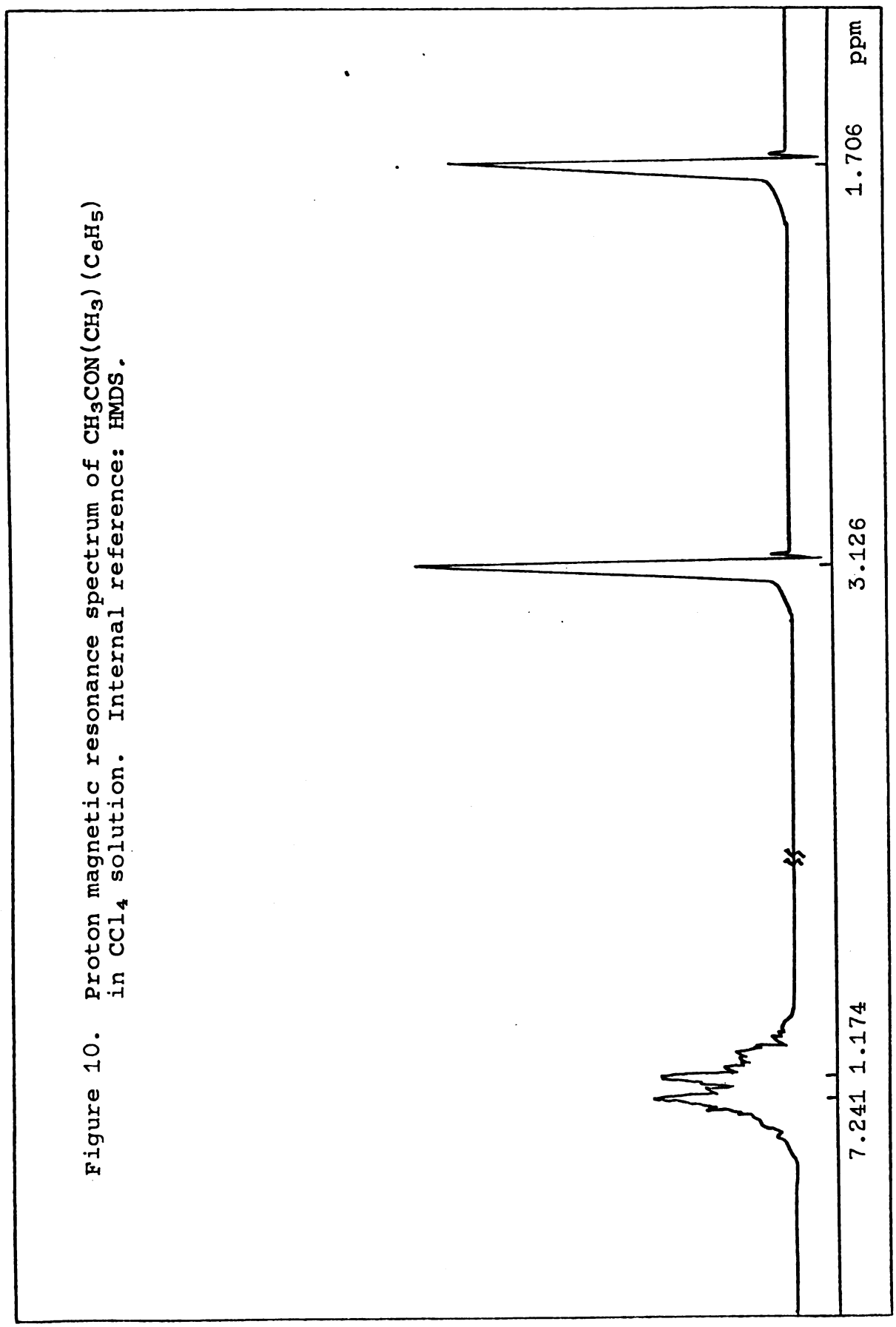

Figure 10. Proton magnetic resonance spectrum of $CH_3CON(CH_3)(C_6H_5)$ in CCl_4 solution. Internal reference: HMDS.

DMF-d_1 and its solutions in F_3CCOOH, S-$C_2H_2Cl_4$ and ϕ-$C(CH_3)_3$ were also studied and the results are tabulated in Tables 5, 9, 11, and 13, respectively. These data are plotted as $\log_{10} \tau$ against $10^3/T^oK$ in Figures 13, 15, 16, and 17.

N,N-Dimethylacetamide

This compound has been studied in both the pure form and in solution in F_3CCOOH. The calculated and experimental data are tabulated in Tables 15, 17, and 19, respectively. The data obtained by total line-shape analysis (T.L.S.) are plotted as $\log_{10} \tau$ against $10^3/T^oK$ in Figures 19 through 21.

N,N-Dimethylpropionamide

The results for DMP were evaluated by all three methods and tabulated in Table 21 and the results from T.L.S. are plotted as $\log_{10} \tau$ against $10^3/T^oK$ in Figure 22.

N,N-Dimethylacrylamide

The data are tabulated in Table 23, and the results from T.L.S. are plotted as $\log_{10} \tau$ against $10^3/T^oK$ in Figure 23.

N,N-Dimethyltrichloroacetamide

The results for DMTCA are tabulated in Tables 25 and 27 and the T.L.S. outputs are plotted as $\log_{10} \tau$ against $10^3/T^oK$ in Figures 24 and 25.

N,N-Dimethylcarbamoylchloride

The results for different samples of DMCC are tabulated in Tables 29 through 36, and the T.L.S. outputs are plotted as $\log_{10} \tau$ against $10^3/T^{\circ}K$ in Figures 26 through 31.

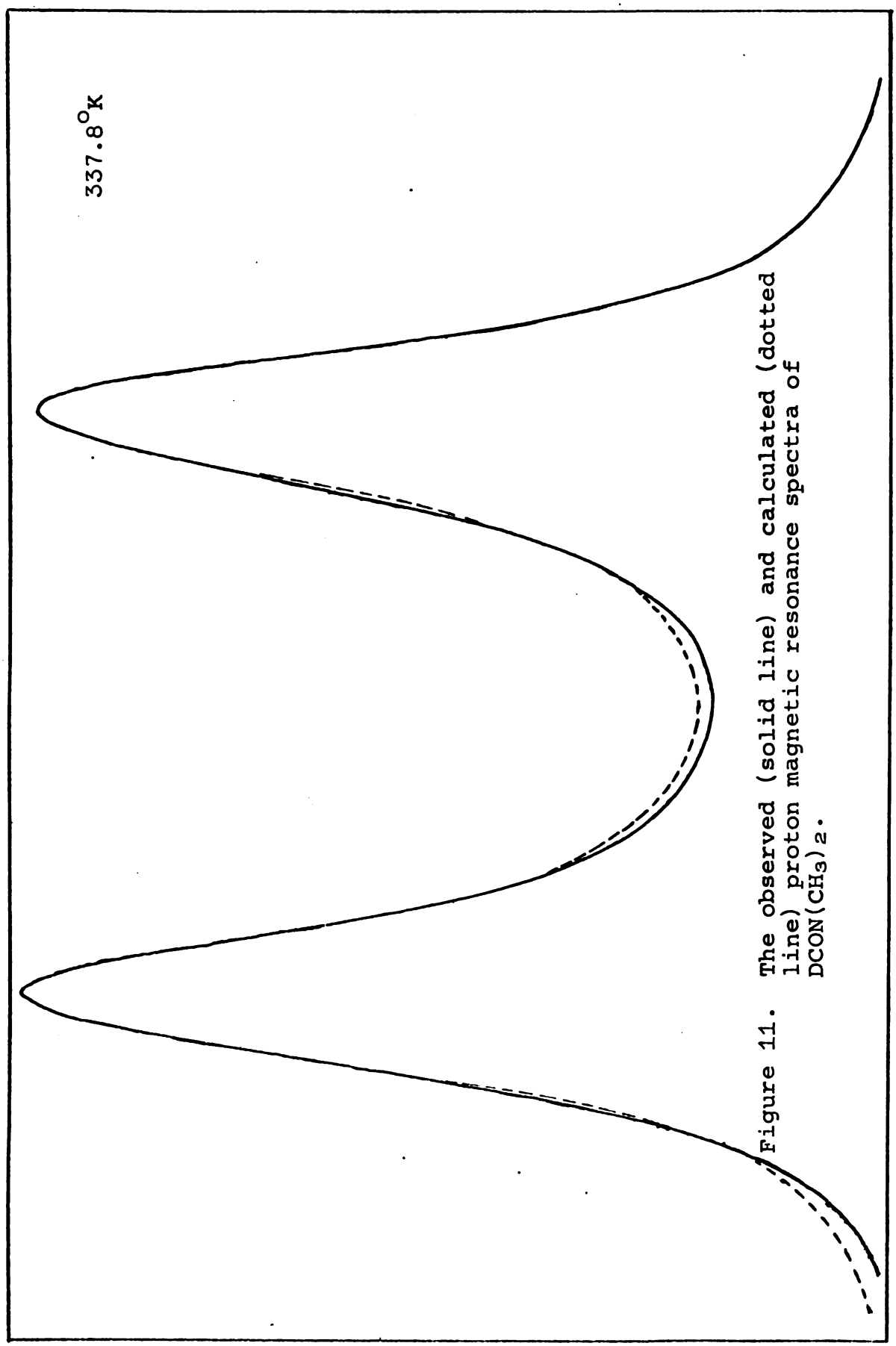

Figure 11. The observed (solid line) and calculated (dotted line) proton magnetic resonance spectra of $DCON(CH_3)_2$.

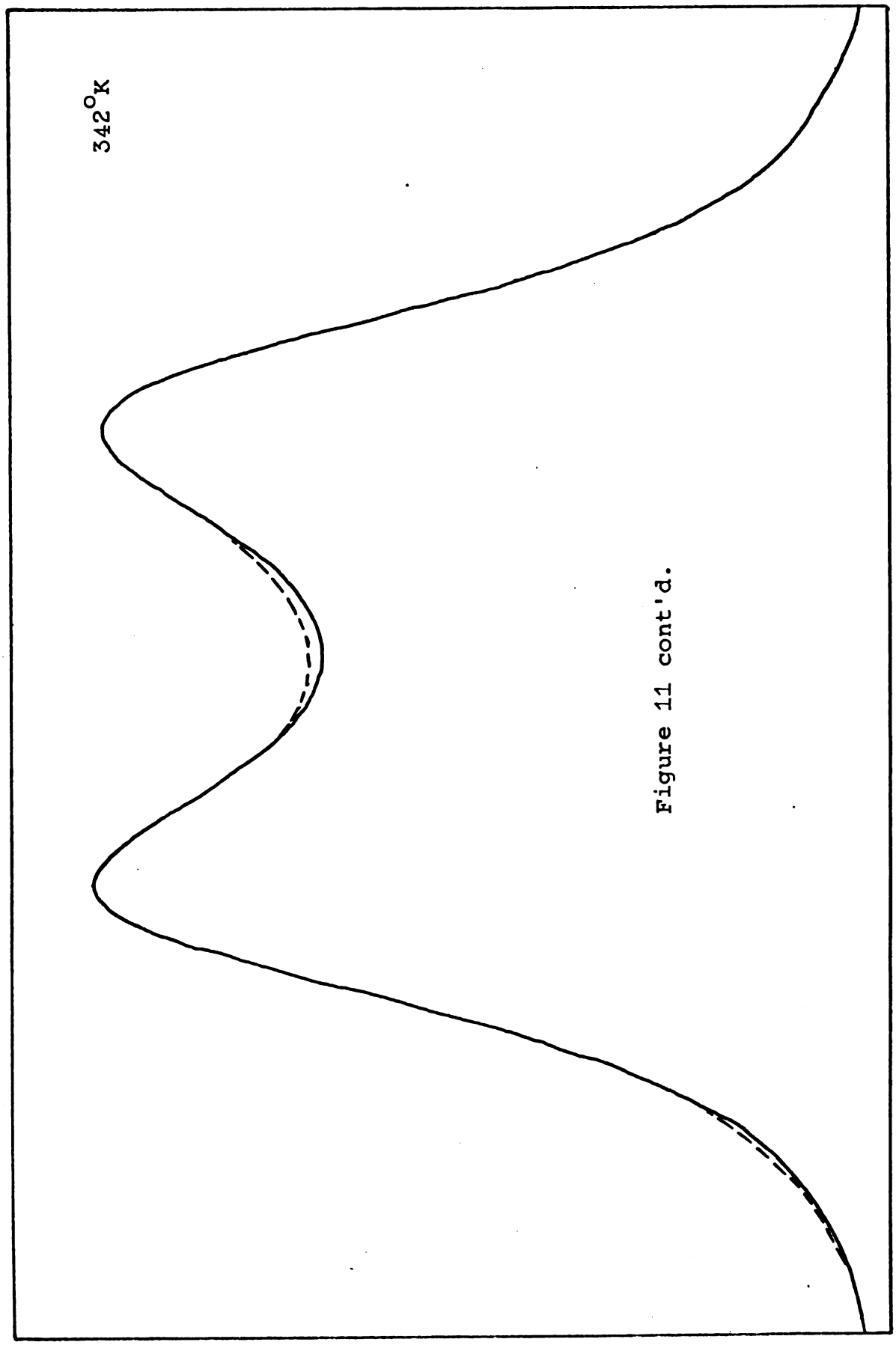

Figure 11 cont'd.

Figure 12. Temperature dependence of observed and calculated spectra of $DCON(CH_3)_2$.

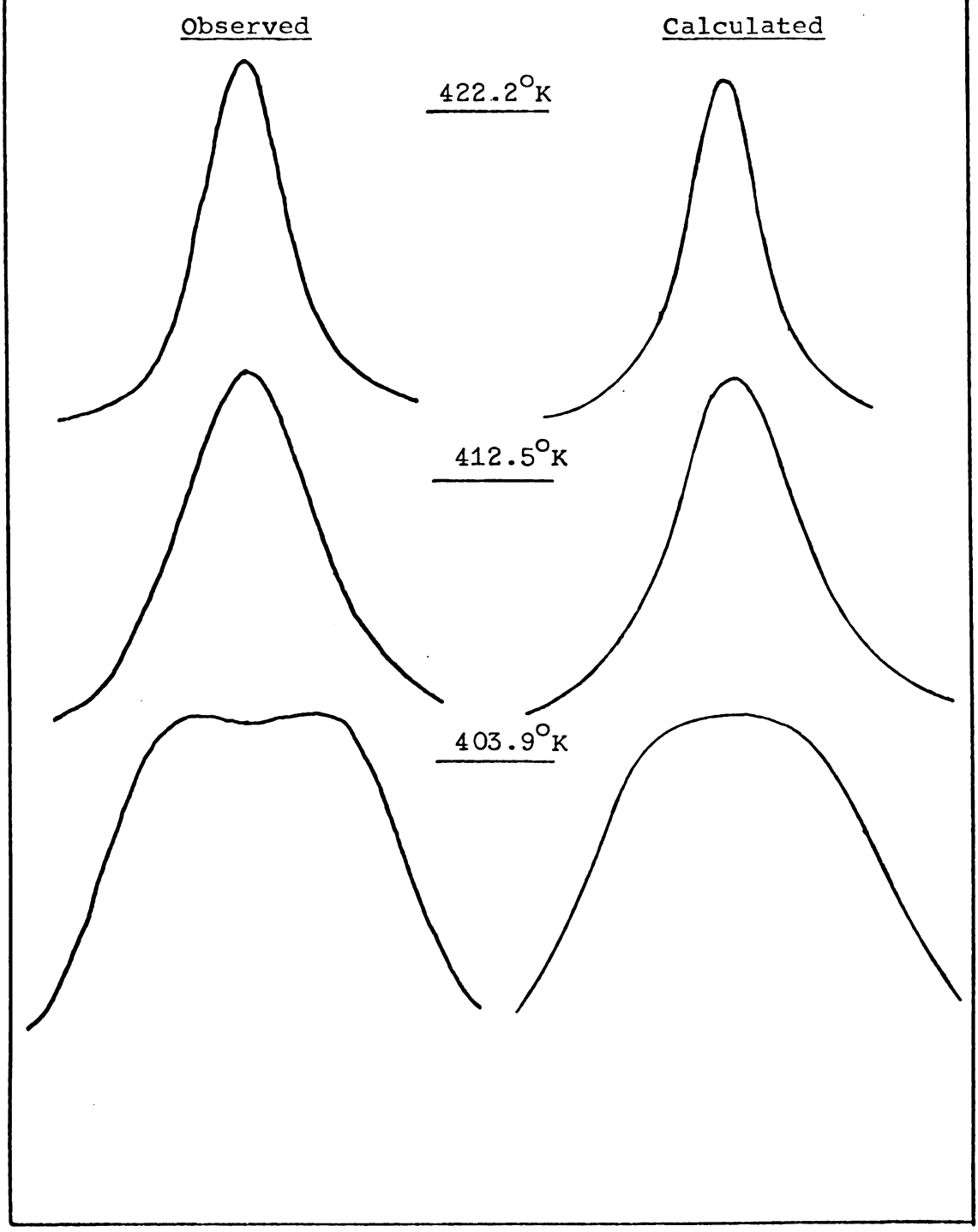

Figure 12 cont'd.

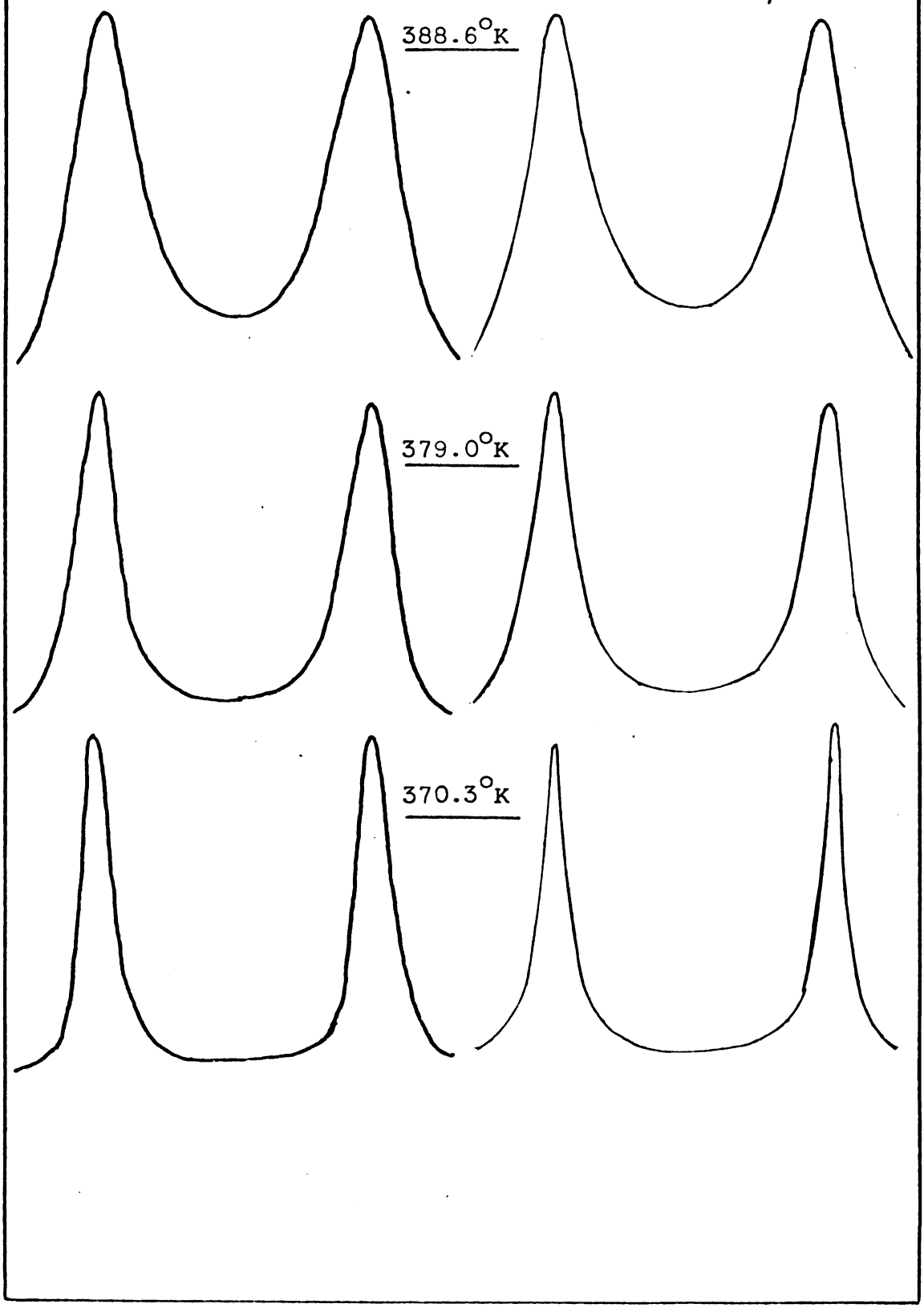

Table 5. Temperature dependence of the rate of internal rotation about the central C-N bond of pure $DCON(CH_3)_2$.***

$10^3/T^oK$	p_A	$\tau \times 10^2$sec I.R.*	$\tau \times 10^2$sec P.S.**	$\tau \times 10^2$sec T.L.S.++	Log τ^{++}	FR ++ rad/sec
3.171	0.47316			178.88	0.2526	
3.176	0.50139			139.18	0.1436	
2.7	0.51481	9.397	3.678	26.588	-0.575	97.037
2.675	0.50631	7.989	3.54	15.0	-0.824	96.687
2.639	0.50584	7.92	3.255	9.8489	-1.007	96.007
2.607	0.493	4.714	3.116	6.3179	-1.199	96.374
2.573	0.48789	4.098	2.887	4.0843	-1.287	96.04
2.514	0.50108	2.038	1.915	2.0583	-1.686	99.113
2.476	0.49975			1.3669	-1.864	105.31
2.454	0.49729			0.99539	-2.002	105.3
2.424	0.49231			0.55721	-2.254	119.5
2.398	0.49907			0.31906	-2.496	118.7
2.369	0.49527			0.24586	-2.609	118.14

* Intensity-ratio method
** Peak-separation method
*** TMS as internal reference
++ Total line-shape analysis method
FR = $\delta\omega_{oo}$
Coalescence point= $10^3/T_c^oK \cong 2.48$ deg^{-1}

Table 6. Thermodynamic and kinetic parameters for internal rotation about the central C-N bond of pure $DCON(CH_3)_2$, from different methods.

Method	E_a kcal/mole	Log 2_A	$\Delta F^{\ddagger}_{373.8^oK}$ kcal/mole
I.R.*	16.22	10.56	20.688
P.S.*	6.441	5.212	20.08
T.L.A.	27.19	16.67	21.156

*FR = $\delta\omega_{\infty}$ = 16.2 Hz.

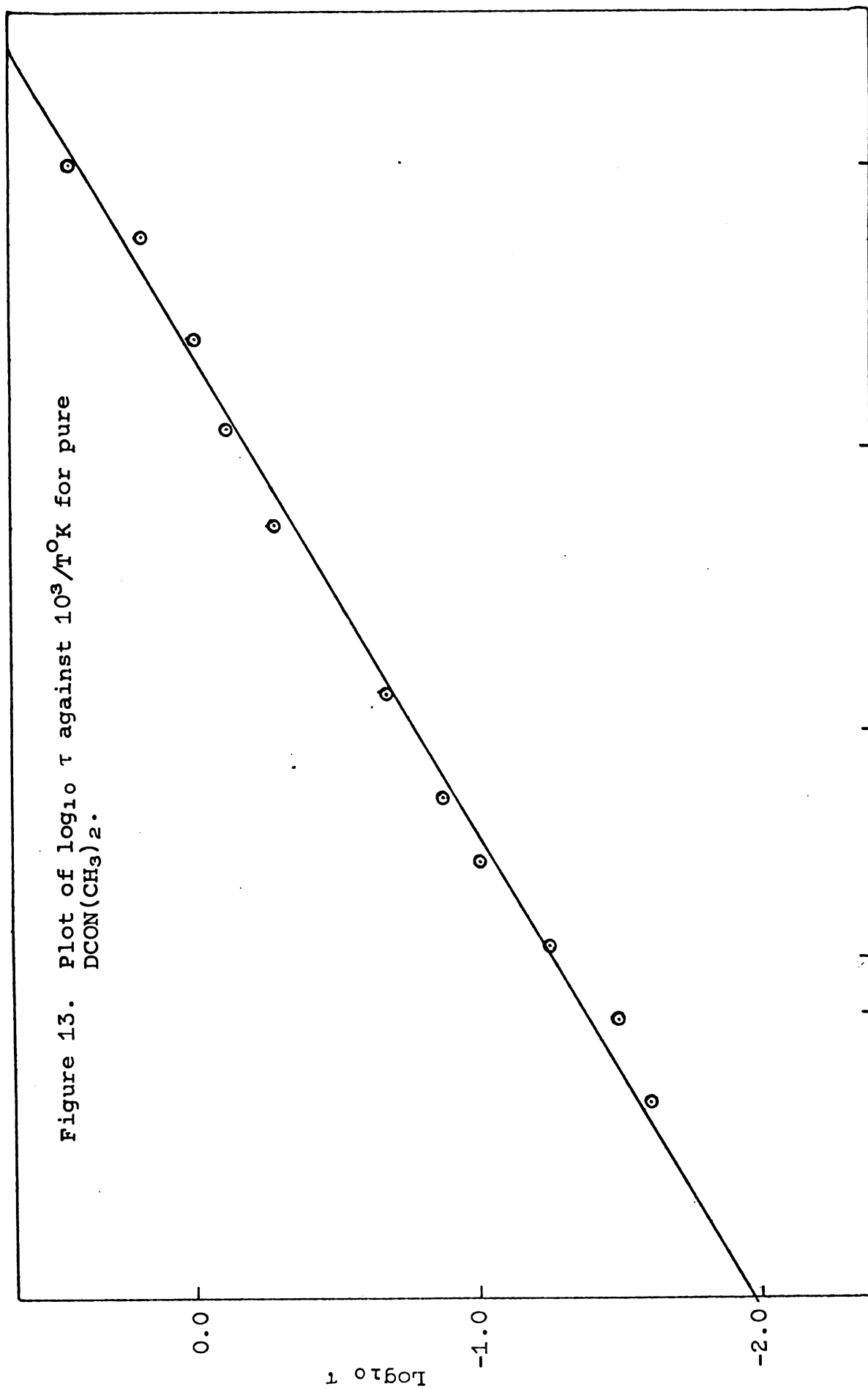

Figure 13. Plot of $\log_{10} \tau$ against $10^3/T^{\circ}K$ for pure $DCON(CH_3)_2$.

Table 7. Temperature dependence of the rate of internal rotation about the central C-N bond of pure $HCON(CH_3)_2$, with $C_6H_5C(CH_3)_3$ as internal reference.

$10^o/T^oK$	P_A *	$\tau \times 10^2$ sec I.R.	$\tau \times 10^2$ sec P.S.	$\tau \times 10^2$ sec T.L.S.	Log τ * T.L.S.	Log τ ** T.C.S.
2.7318	0.50136	8.576	2.395	19.355	-0.7132	-0.6667
2.6944	0.50369	7.012	2.329	14.875	-0.8276	-0.8297
2.6601	0.49833	5.716	2.299	10.157	-0.9932	-0.9948
2.626	0.49141	4.379	2.242	6.6942	-1.174	-1.171
2.5901	0.50644	3.192	2.12	4.27	-1.37	-1.367
2.5584	0.49726	2.429	1.929	3.1929	-1.496	-1.497
2.5268	0.50734	1.921	1.698	2.3896	-1.622	-1.67
2.4948	0.50663			1.4007	-1.854	-1.852
2.4635	0.50126			0.73042	-2.136	-2.136

*Spin-spin coupling is neglected.

**Spin-spin coupling is included by superposition.

Table 8. Thermodynamic and kinetic parameters for internal rotation about the central C-N bond of pure $HCON(CH_3)_2$ with $C_6H_5C(CH_3)_3$ as internal reference.

Method	Ea kcal/mole	Log 2A	$\Delta F^{\ddagger}_{375.9}$ kcal/mole
I.R.[+]	14.67	9.808	20.56
P.S.[+]	3.006	3.399	19.88
T.L.A.[*]	23.52	14.7	20.99
T.L.A.[**]	24.15	15.06	20.99

[+] FR = 15.8 Hz.

[*] With no spin-spin coupling correction.

[**] With spin-spin coupling correction by superposition.

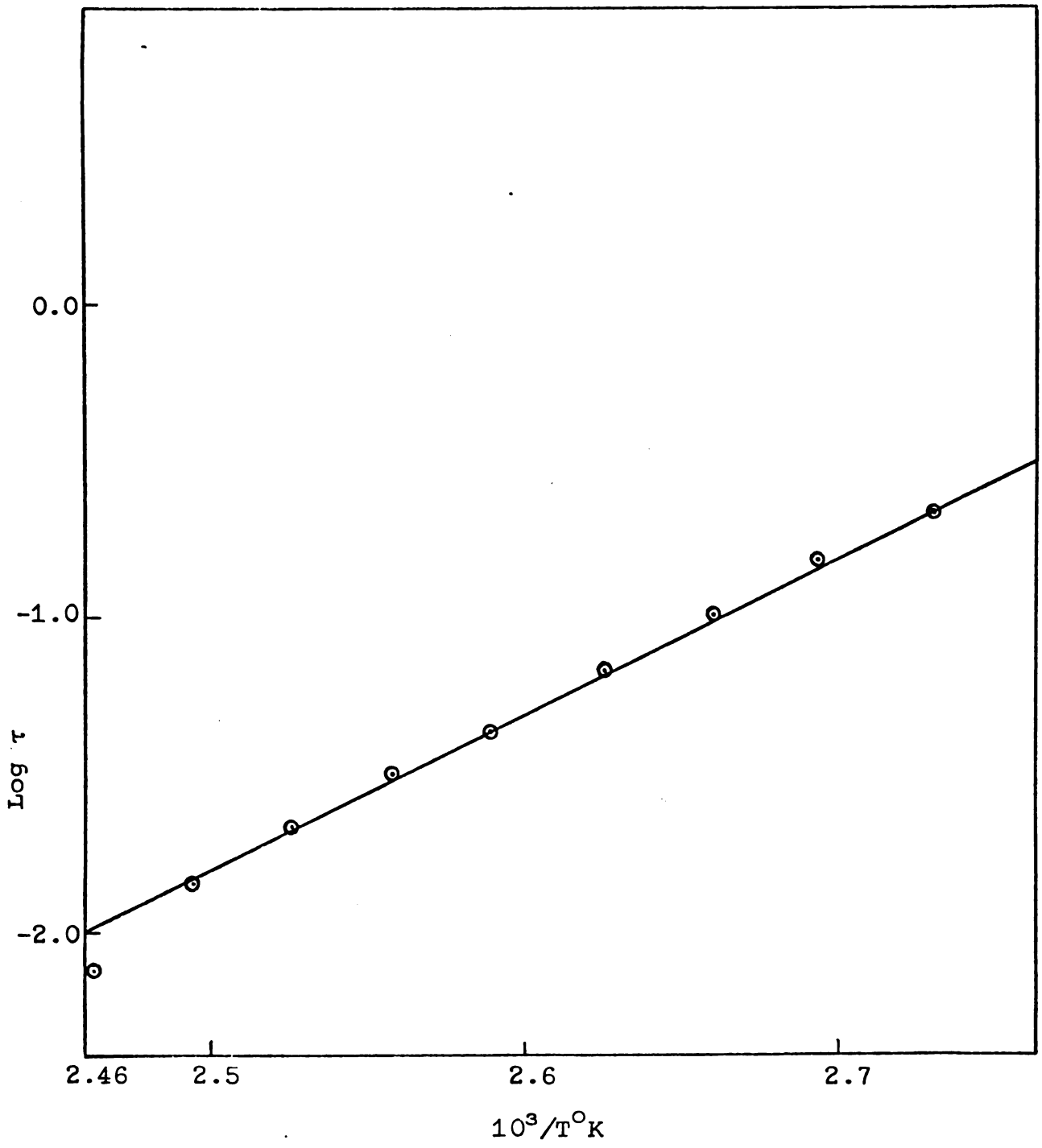

Figure 14. Plot of $\log_{10} \tau$ against $10^3/T^{\circ}K$ for pure $HCON(CH_3)_2$ with spin-spin coupling correction included by superposition, with $C_6H_5C(CH_3)_3$ as internal reference.

Table 9. Temperature dependence of the rate of internal rotation about the central C-N bond of pure $DCON(CH_3)_2$ in F_3CCOOH solution.

$10^3/T^oK$	p_A*	$\tau \times 10^2$ sec I.R.	$\tau \times 10^2$ sec P.S.	$\tau \times 10^2$ sec T.L.S.	Log τ *	FR* rad/sec.
3.028	0.50227	8.978	5.013	10.964	-0.96	79.589
3.003	0.49964	7.081	4.210	8.3015	-1.081	75.905
2.996	0.49208	6.549	4.301	8.2783	-1.082	78.93
2.959	0.50482	5.246	3.972	6.3428	-1.198	78.698
2.938	0.50562	4.437	3.455	5.1821	-1.285	75.839
2.917	0.49945	3.874	3.249	3.9775	-1.4	79.344
2.891	0.50150	3.229	2.838	3.3418	-1.476	77.161
2.877	0.50185	2.808	2.635	2.8888	-1.539	79.368
2.842	0.50004	2.241	2.164	2.1799	-1.662	79.74
2.802	0.49864			1.6293	-1.788	99.946
2.767	0.49965			1.1499	-1.939	83.673
2.729	0.49511			0.88509	-2.053	83.171

Coalescence point= $10^3/T_C^oK \cong 2.8$

* Results from T.L.S.

Table 10. Thermodynamic and kinetic parameters for internal rotation about the central C-N bond of $DCON(CH_3)_2$ in F_3CCOOH solution.

Method	E_a kcal/mole	Log 2A	$\Delta F^{\ddagger}_{337.9}$ kcal/mole
I.R.*	14.0	10.35	18.55
P.S.*	8.154	6.711	18.17
T.L.S.	16.78	12.09	18.48

* FR = 13.0 Hz.

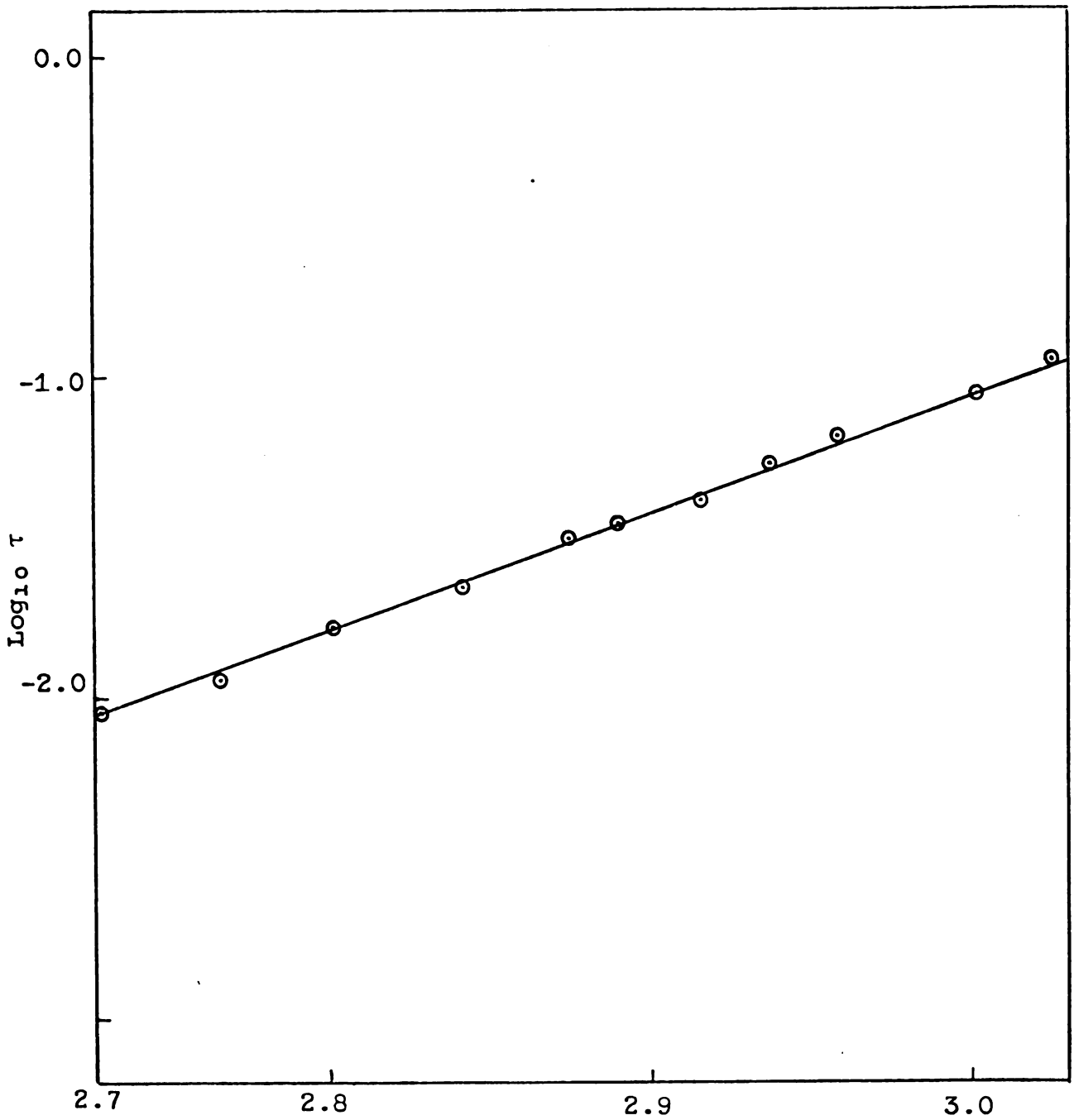

Figure 15. Plot of $\log_{10} \tau$ against $10^3/T^{\circ}K$ for $DCON(CH_3)_2$ in F_3CCOOH solution.

Table 11. Temperature dependence of the rate of internal rotation about the central C-N bond of $DCON(CH_3)_2$ in s-$C_2H_2Cl_4$** solution.

$10^3/T^oK$	p_A*	$\tau \times 10^2$ sec I.R.	$\tau \times 10^2$ sec P.S.	$\tau \times 10^2$ sec T.L.S.	Log τ*	FR* rad/sec
2.766	0.50263	10.613	4.574	18.7	-0.728	84.44
2.713	0.49697	9.371	4.153	11.768	-0.929	83.942
2.666	0.51163	7.877	4.153	7.9801	-1.098	84.236
2.632	0.50851	6.619	3.767	7.6506	-1.116	83.489
2.563	0.50138	3.507	2.999	3.5281	-1.452	86.138
2.53	0.49406	2.67	2.537	2.6257	-1.581	86.788
2.533	0.49988	2.502	2.397	2.4002	-1.62	88.8
2.501	0.50011	1.88	1.865	1.6349	-1.787	92.784
2.498	0.49845	2.01	1.98	1.8957	-1.722	89.559
2.470	0.49768			1.2292	-1.91	97.27
2.439	0.4996			0.69077	-2.161	105.31

Coalescence point = $10^3/T_c^oK \cong 2.48$

* Results from T.L.S.

** Approx. conc. of solute is 0.67 mole fraction.

Table 12. Thermodynamic and kinetic parameters for internal rotation about the central C-N bond of $DCON(CH_3)_2$ in S— $C_2H_2Cl_4$ solution.

Method	E_a kcal/mole	Log 2A	$\Delta F^{\ddagger}_{379.9^oK}$ kcal/mole
I.R.*	15.43	10.13	20.9
P.S.*	6.499	5.22	20.47
T.L.S.	18.96	12.14	21.01

*FR = 13.9 Hz.

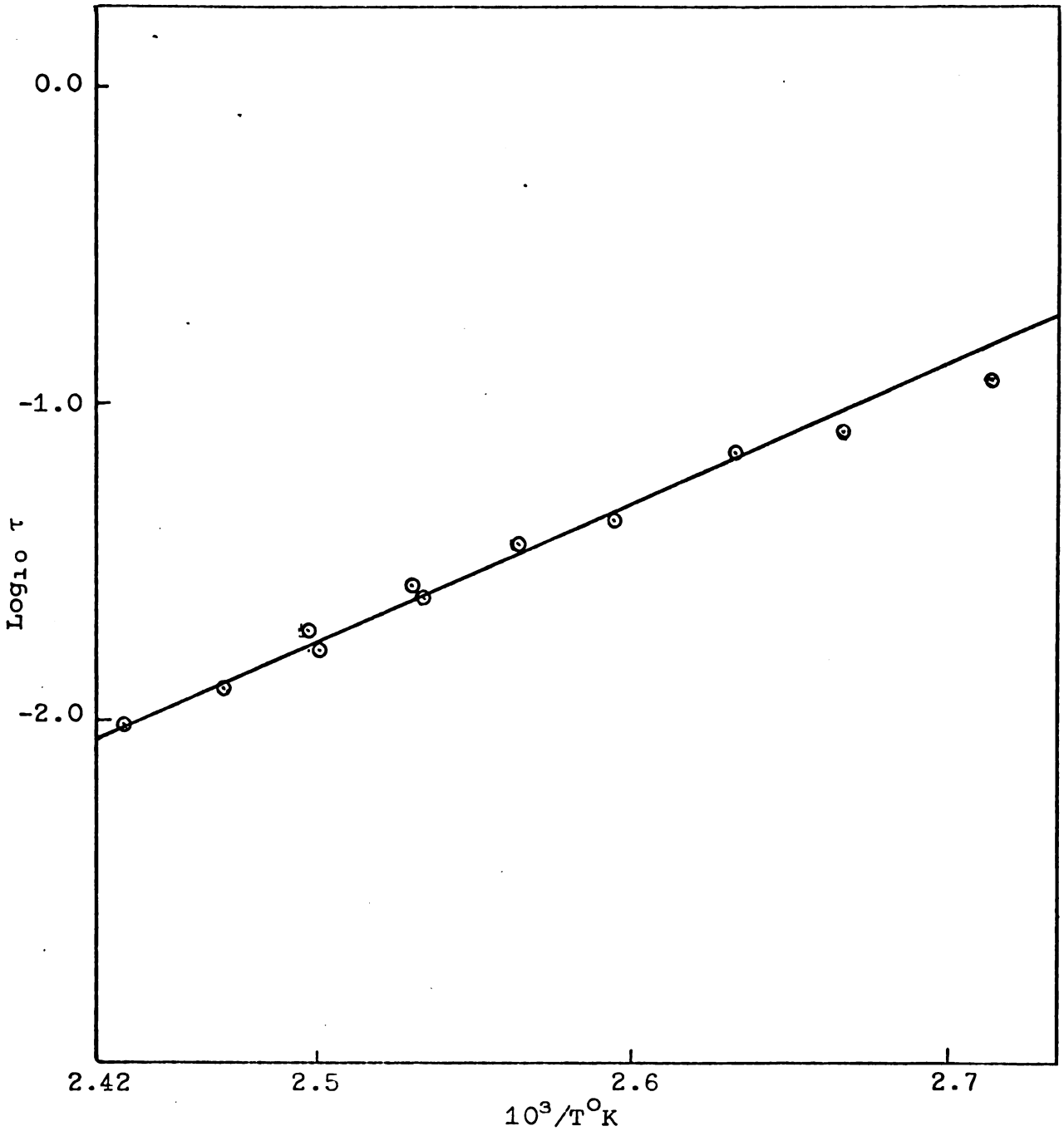

Figure 16. Plot of $\log_{10} \tau$ against $10^3/T^{\circ}K$ for ~0.67 mole fraction of $DCON(CH_3)_2$ in $C_2H_2Cl_4$ solution.

Table 13. Temperature dependence of the rate of internal rotation about the central C-N bond of $DCON(CH_3)_2$ in $C_6H_5C(CH_3)_3$.**

$10^3/T^oK$	p_A*	$\tau \times 10^2$ sec I.R.	$\tau \times 10^2$ sec P.S.	$\tau \times 10^2$ sec T.L.S.	Log τ*	FR* rad/sec
2.730	0.49368	10.51	11.49	22.256	-0.052	59.777
2.697	0.49988	8.582	8.717	11.924	-0.924	60.39
2.665	0.50469	7.106	8.165	10.977	-0.959	60.02
2.631	0.50702	5.512	6.018	6.7539	-1.17	60.886
2.596	0.50238	4.207	4.725	4.6392	-1.334	61.88
2.562	0.51107	3.149	3.406	2.9333	-1.533	65.569
2.545	0.50429	2.805	2.808	2.8717	-1.542	62.48
2.529	0.50361			2.4914	-1.604	61.83
2.512	0.50773			1.9265	-1.715	64.414
2.497	0.49832			1.4846	-1.828	69.276
2.465	0.49845			1.1446	-1.941	65.95

Coalescence point = $10^3/T_c^oK \cong 2.53$.

* Results from T.L.S.

** Approximate concentration of amide is 0.7 mole fraction.

Table 14. Thermodynamic and kinetic parameters for internal rotation about the central C-N bond of $DCON(CH_3)_2$ in $C_6H_5C(CH_3)_3$.

Method	E_a kcal/mole	Log 2A	$\Delta F^{\ddagger}_{380^oK}$ kcal/mole
I.R.*	14.56	9.657	20.76
P.S.*	14.76	9.719	20.83
T.L.A.	21.63	13.61	20.92

*FR = 9.7 Hz.

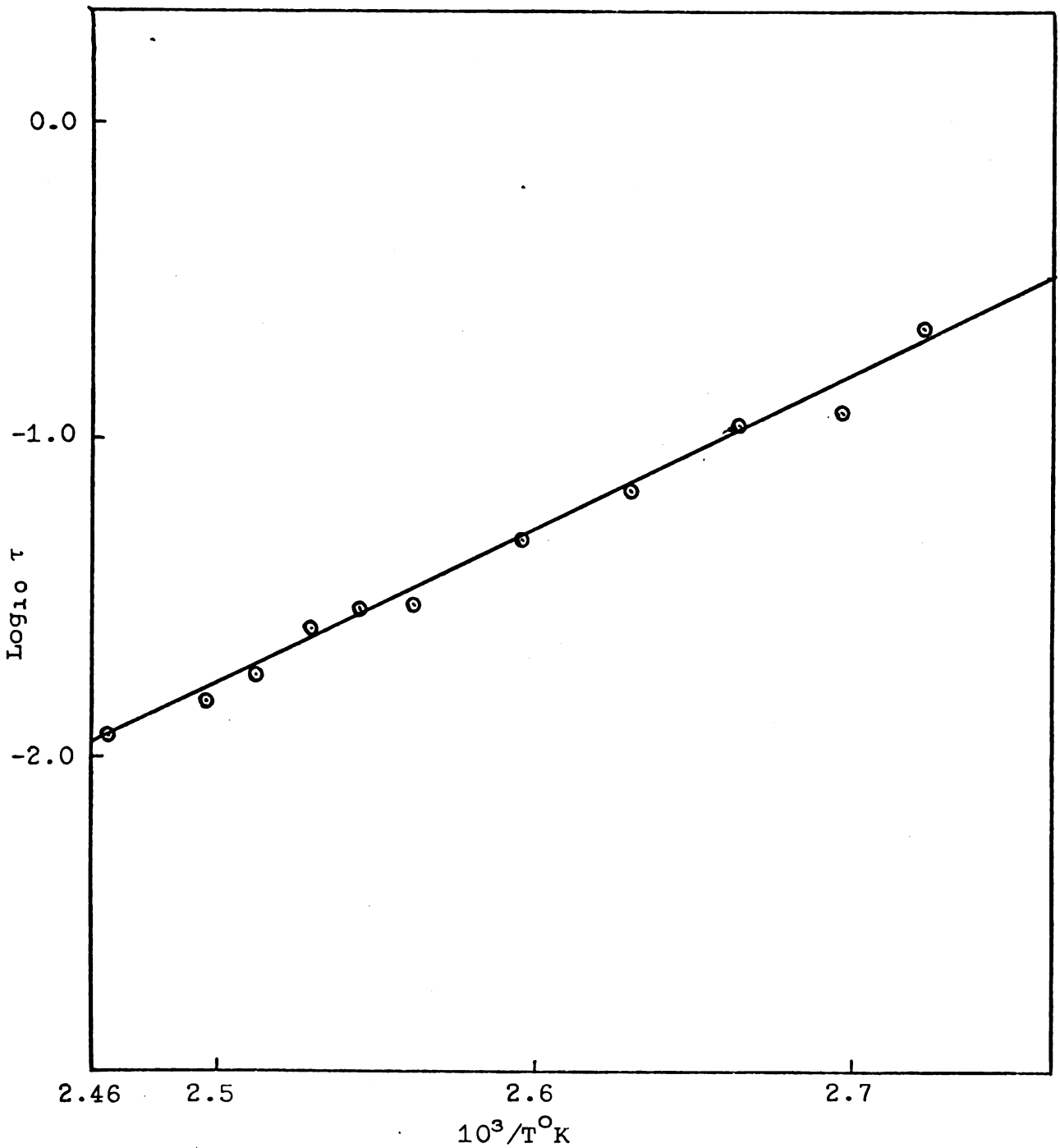

Figure 17. Plot of $\log_{10} \tau$ against $10^3/T^{\circ}K$ for $DCON(CH_3)_2$ in $C_6H_5C(CH_3)_3$ solution ($\sim$ 0.7 mole fraction).

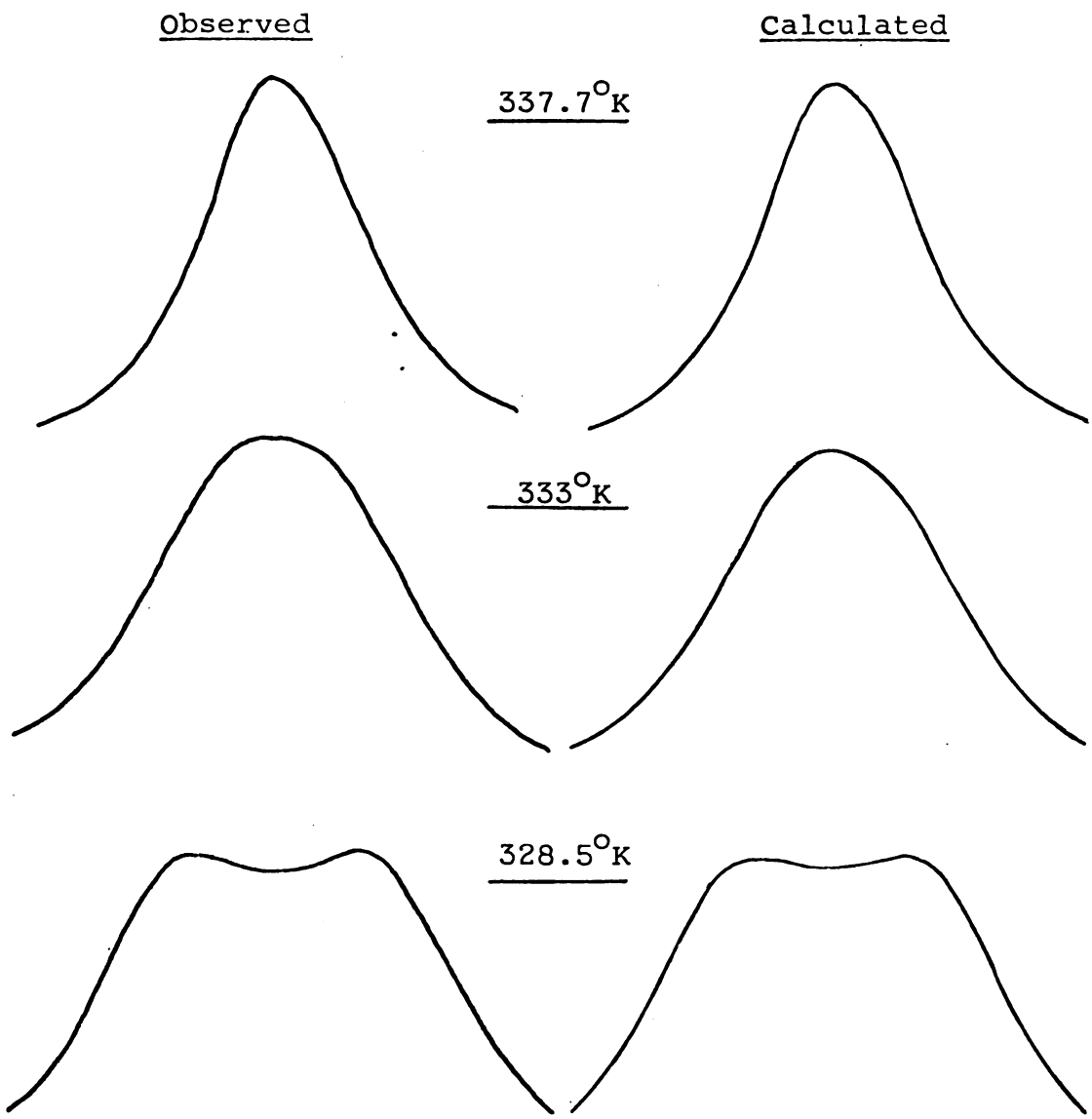

Figure 18. Temperature dependence of observed and calculated proton magnetic resonance spectra of $CH_3CON(CH_3)_2$.

Figure 18 cont'd.

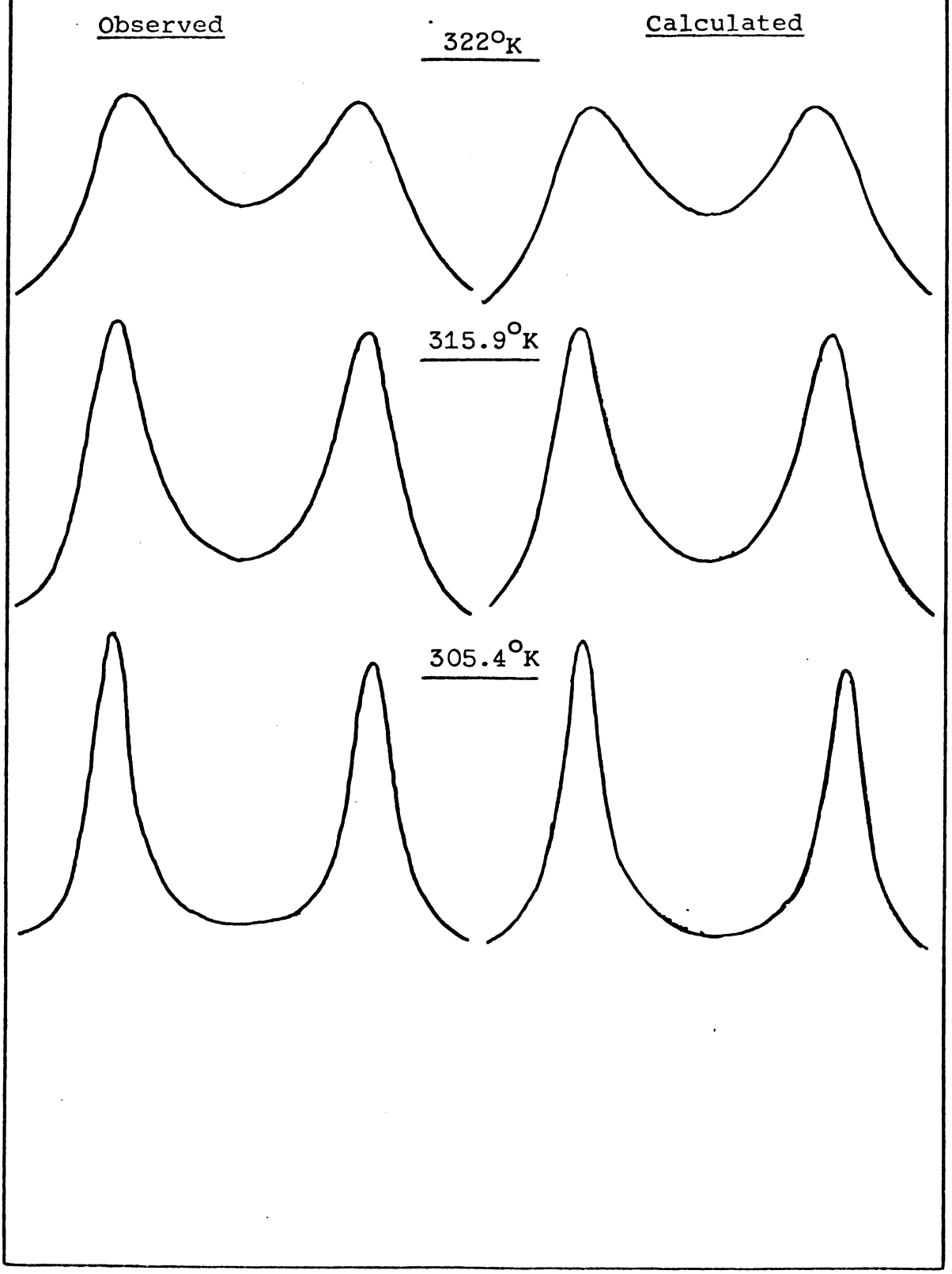

Table 15. Temperature dependence of the rate of internal rotation about the central C-N bond of $CH_3CON(CH_3)_2$.**

$10^3/T^oK$	p_A*	$\tau \times 10^2$ sec I.R.	$\tau \times 10^2$ sec P.S.	$\tau \times 10^2$ sec T.L.S.	$Log_{10}\ \tau$*	FR* rad/sec
3.273	0.49555	19.48	3.838	150.26	0.177	109.98
3.175	0.50874			649.25	0.8124	109.95
3.130	0.49270	9.583	7.037	24.488	-0.611	109.87
3.077	0.44370	7.977	6.103	10.167	-0.993	111.18
3.03	0.49169	5.399	4.998	8.2084	-1.086	109.92
2.785	0.49180	3.806	3.566	5.2434	-1.280	108.33
2.941	0.50112	2.559	2.62	2.8212	-1.550	108.97
2.899	0.50636	1.726	1.772	1.7881	-1.748	109.96
2.861	0.5024			1.2129	-1.916	113.65
2.857	0.51021			1.2169	-1.915	110.73
2.813	0.50168			0.71116	-2.148	118.16
2.778	0.49788			0.4122	-2.385	125.01
2.740	0.49794			0.2462	-2.609	134.45
2.703	0.49868			0.1897	-2.722	123.98

Coalescence point= $10^3/T_c^oK \cong 2.87$

* Results from T.L.S.

** TMS as internal reference.

Table 16. Thermodynamic and kinetic parameters for internal rotation about the central C-N bond of $CH_3CON(CH_3)_2$.**

Method	E_a kcal/mole	Log 2A	$\Delta F^{\ddagger}_{330^oK}$ kcal/mole
I.R.*	12.71	9.748	17.925
P.S.*	15.17	11.39	17.874
T.L.A.	22.56	16.06	18.199

*TMS as internal reference.
**FR = 17.2 Hz.

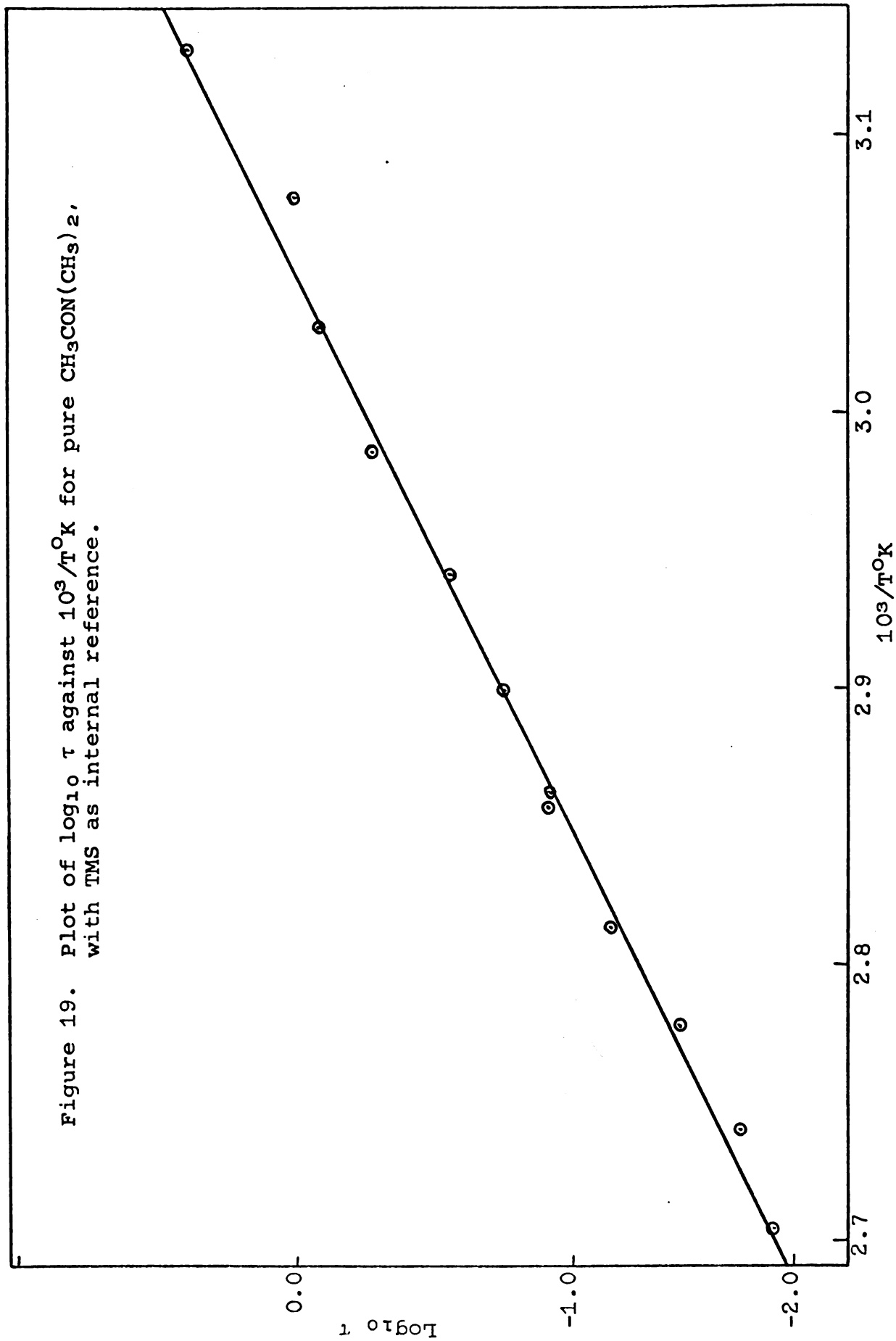

Figure 19. Plot of $\log_{10} \tau$ against $10^3/T^{\circ}K$ for pure $CH_3CON(CH_3)_2$, with TMS as internal reference.

Table 17. Temperature dependence of the rate of internal rotation about the central C-N bond of $CH_3CON(CH_3)_2$.**

$10^3/T^oK$	p_A*	$\tau \times 10^2$ sec I.R.	$\tau \times 10^2$ sec P.S.	$\tau \times 10^2$ sec T.L.S.	$Log_{10}\ \tau$*	FR* rad/sec
3.1787	0.50460			119.75	0.07829	
3.13	0.49386			0.456	-0.1775	
3.076	0.48874	8.643	5.216	21.308	-0.071	107.09
3.034	0.50314	6.304	4.099	10.004	-0.974	106.51
2.987	0.51889	4.113	3.719	4.2081	-1.376	110.22
2.947	0.49759	2.875	3.154	3.5855	-1.445	106.85
2.908	0.50372	2.028	1.914	2.0672	-1.685	107.14
2.866	0.50237			1.2327	-1.909	111.98
2.824	0.50069			0.71025	-2.149	118.28
2.784	0.50034			0.31955	-2.495	129.49
2.738	0.50006			0.18955	-2.722	126.88
2.704	0.50009			0.11234	-2.949	135.48

Coalescence point= $10^3/T^oK \cong 2.86$

* Result from T.L.S.

** HMDS as external reference.

Table 18. Thermodynamic and kinetic parameters for internal rotation about the central C-N bond of $CH_3CON(CH_3)_2$.**

Method	E_a kcal/mole	Log 2A	$\Delta F^{\ddagger}_{329.6}$ kcal/mole
I.R.*	17.29	12.69	18.0
P.S.*	10.55	8.367	17.73
T.L.A.	27.16	19.0	18.36

* FR = 17.2 Hz.

** HMDS as external reference.

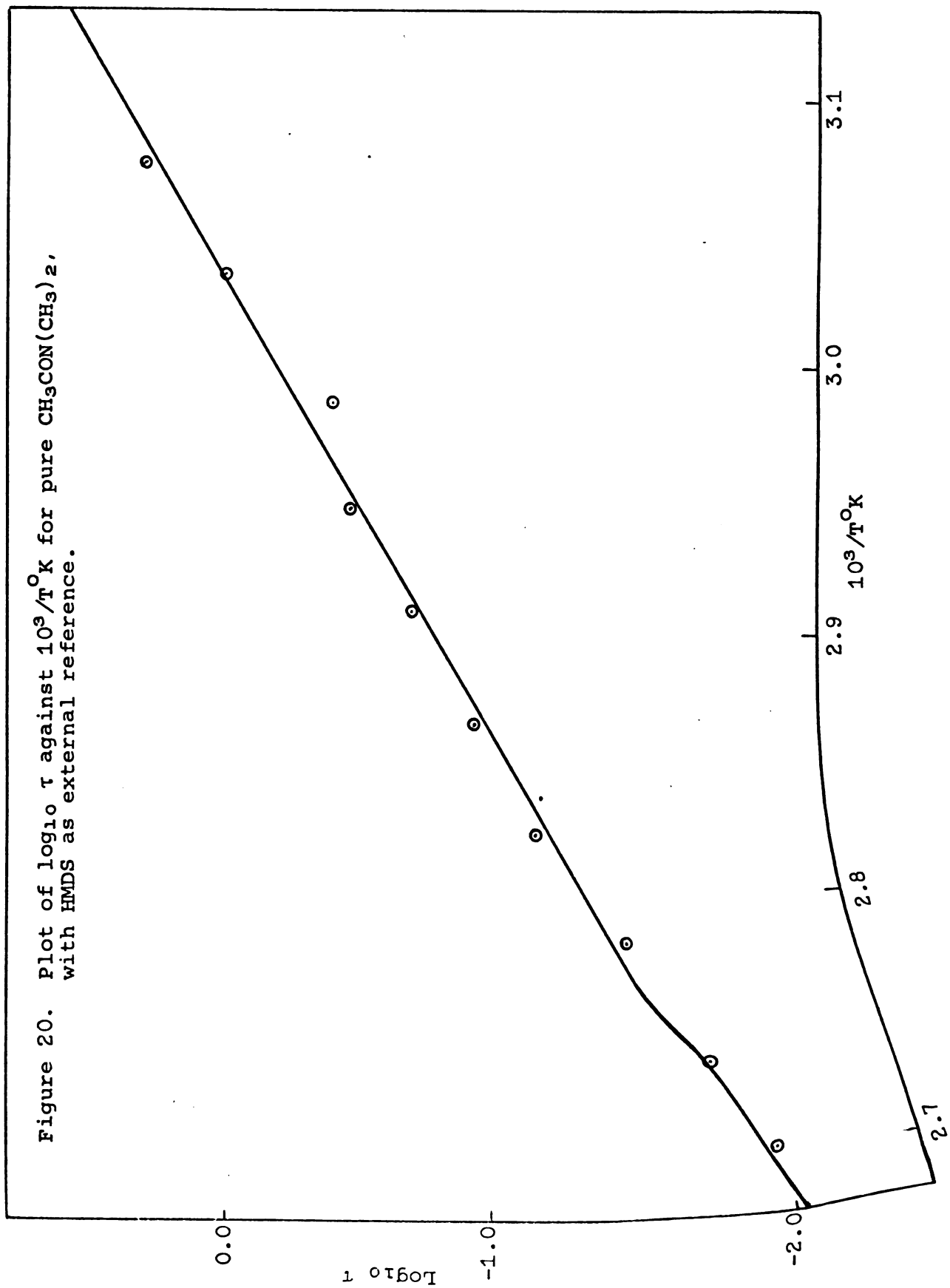

Figure 20. Plot of $\log_{10} \tau$ against $10^3/T^{\circ}K$ for pure $CH_3CON(CH_3)_2$, with HMDS as external reference.

Table 19. Temperature dependence of the rate of internal rotation about the central C-N bond of $CH_3CON(CH_3)_2$ in F_3CCOOH.

$10^3/T^oK$	p_A*	$\tau \times 10^2$ sec I.R.	$\tau \times 10^2$ sec P.S.	$\tau \times 10^2$ sec T.L.S.	$Log_{10}\ \tau$*	FR* rad/sec
3.432	0.48339	4.11	4.339	7.1562	-1.145	45.817
3.428	0.48895	6.08	7.195	6.9454	-1.158	47.026
3.39	0.51606	6.148	7.433	3.5972	-1.444	50.487
3.345	0.5074			3.1828	-1.497	47.151
3.316	0.46845			1.7025	-1.709	51.405
3.28	0.48979			1.1823	-1.927	52.009
3.246	0.4842			0.67956	-2.168	53.258
3.224	0.50059			0.53012	-2.276	55.05

Coalescence point = $10^3/T_c^oK \cong 3.25$

* Results from T.L.S.

Table 20. Thermodynamic and kinetic parameters for internal rotation about the central C-N bond of $CH_3CON(CH_3)_2$ in F_3CCOOH.

Method	E_a kcal/mole	Log 2A	$\Delta F^{\ddagger}_{295^oK}$ kcal/mole
I.R.*	18.24	14.91	16.033
P.S.*	24.23	19.33	16.144
T.L.A.	24.54	19.57	15.72

*FR = 6.9 Hz.

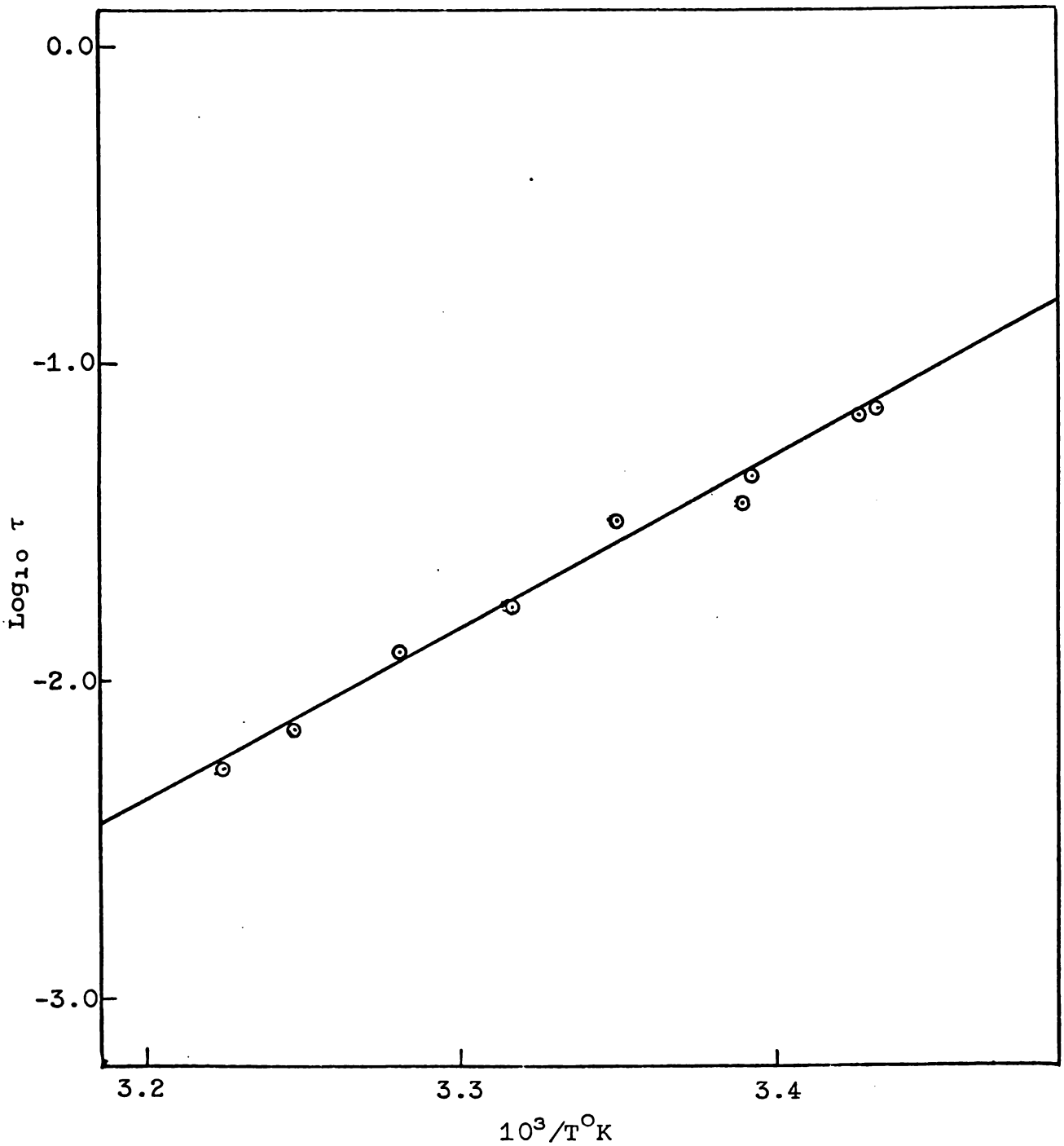

Figure 21. Plot of $\log_{10} \tau$ against $10^3/T^{\circ}K$ for $CH_3CON(CH_3)_2$ in F_3CCOOH solution.

Table 21. Temperature dependence of the rate of internal rotation about the central C-N bond of $C_2H_5CON(CH_3)_2$.

$10^3/T^oK$	p_A*	$\tau \times 10^2$ sec I.R.	$\tau \times 10^2$ sec P.S.	$\tau \times 10^2$ sec T.L.S.	$Log_{10}\tau$*	FR* rad/sec
3.274	0.50512			17.265	-0.783	89.339
3.165	0.49822	4.396	5.572	6.7491	-1.171	88.721
3.123	0.49842	3.266	3.984	3.6670	-1.436	91.1267
3.105	0.4978	2.2962	3.29	3.6158	-1.442	88.824
3.085	0.49908	2.5	2.69	2.84	-1.547	89.168
3.044	0.50067			1.8659	-1.729	92.183
3.021	0.49952			1.4942	-1.826	93.529
3.003	0.50094			1.1098	-1.826	98.126
2.961	0.48525			0.08684	-2.163	103.13

Coalescence point= $10^3/T_c^oK \cong 3.02$.

* Results from T.L.S.

Table 22. Thermodynamic and kinetic parameters for internal rotation about the central C-N bond of $C_2H_5CON(CH_3)_2$.

Method	E_a kcal/mole	Log_{10} 2A	$\Delta F^{\ddagger}_{324.5^oK}$ kcal/mole
I.R.*	13.65	10.85	17.17
P.S.*	17.83	13.61	17.12
T.L.A.	21.44	15.92	17.2

*FR = 13.9 Hz.

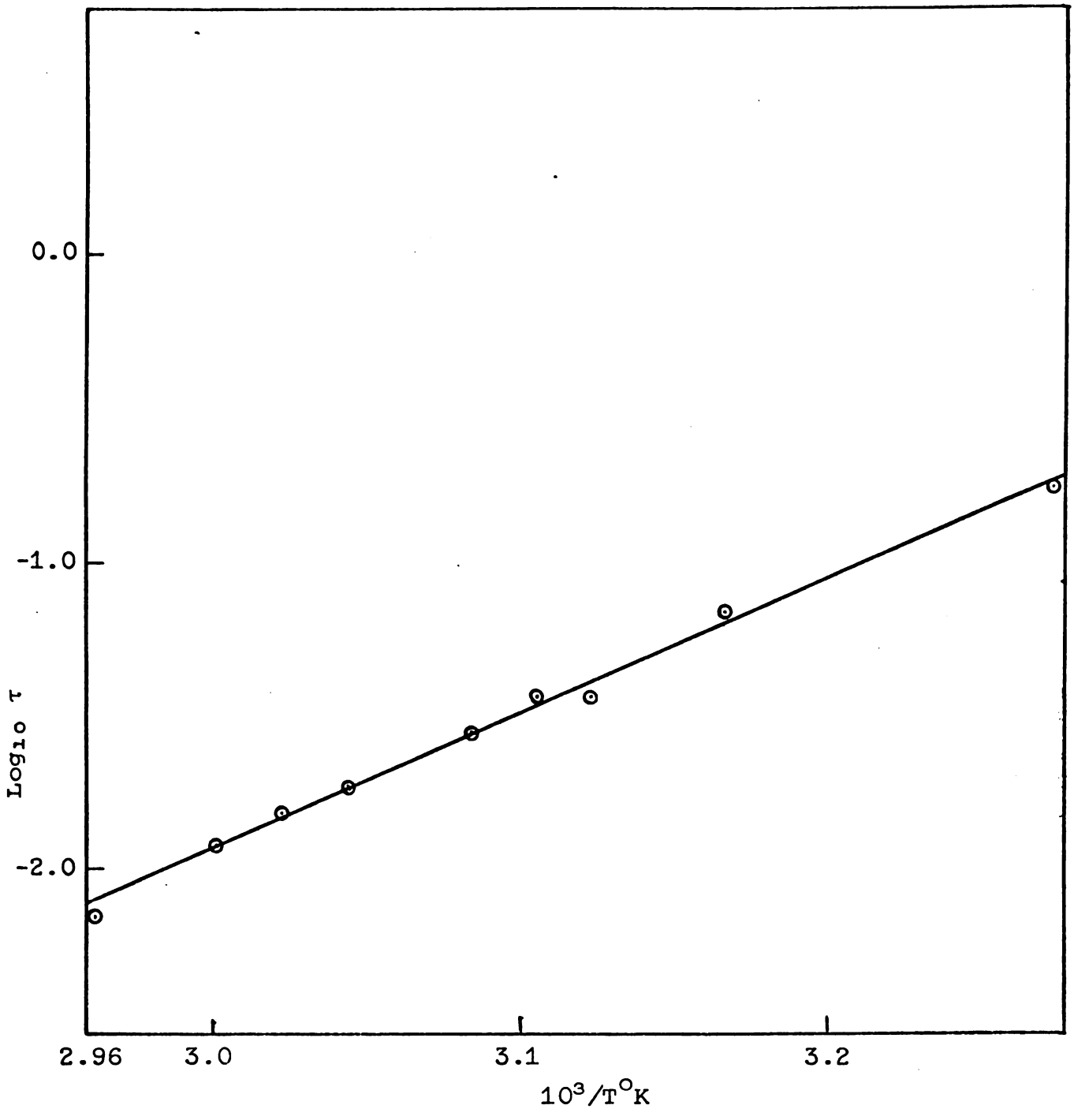

Figure 22. Plot of $\log_{10} \tau$ against $10^3/T^{\circ}K$ for pure $C_2H_5CON(CH_3)_2$.

Table 23. Temperature dependence of the rate of internal rotation about the central C-N bond of $CH_2=CHCON(CH_3)_2$.

$10^3/T^oK$	p_A*	$\tau \times 10^2$ sec I.R.	$\tau \times 10^2$ sec P.S.	$\tau \times 10^2$ sec T.L.S.	$Log_{10}\ \tau$*	FR* rad/sec.
3.469	0.50138	10.25	9.22	39.965	-0.398	95.949
3.354	0.49897	6.547	6.172	11.547	-0.938	95.046
3.277	0.4999	4.672	4.657	7.0901	-1.149	93.729
3.175	0.50256	2.589	2.667	2.9892	-1.524	94.424
3.137	0.50387	1.961	1.967	1.8637	-1.730	99.791
3.119	0.50092			1.5080	-1.822	103.49
3.105	0.50309			1.4916	-1.826	98.138
3.086	0.50985			1.2192	-1.914	100.03
3.055	0.50257			0.90529	-2.043	100.73

Coalescence point = $10^3/T^oK \cong 3.105$.

* Results from T.L.S.

Table 24. Thermodynamic and kinetic parameters for internal rotation about the central C-N bond of $CH_2{=}CHCON(CH_3)_2$.

Method	E_a kcal/mole	Log_{10} 2A	$\Delta F^{\ddagger}_{318.8}$ kcal/mole
I.R.*	9.845	8.43	16.65
P.S.*	9.092	7.901	16.66
T.L.S.	17.82	13.95	16.66

*FR = 15 Hz.

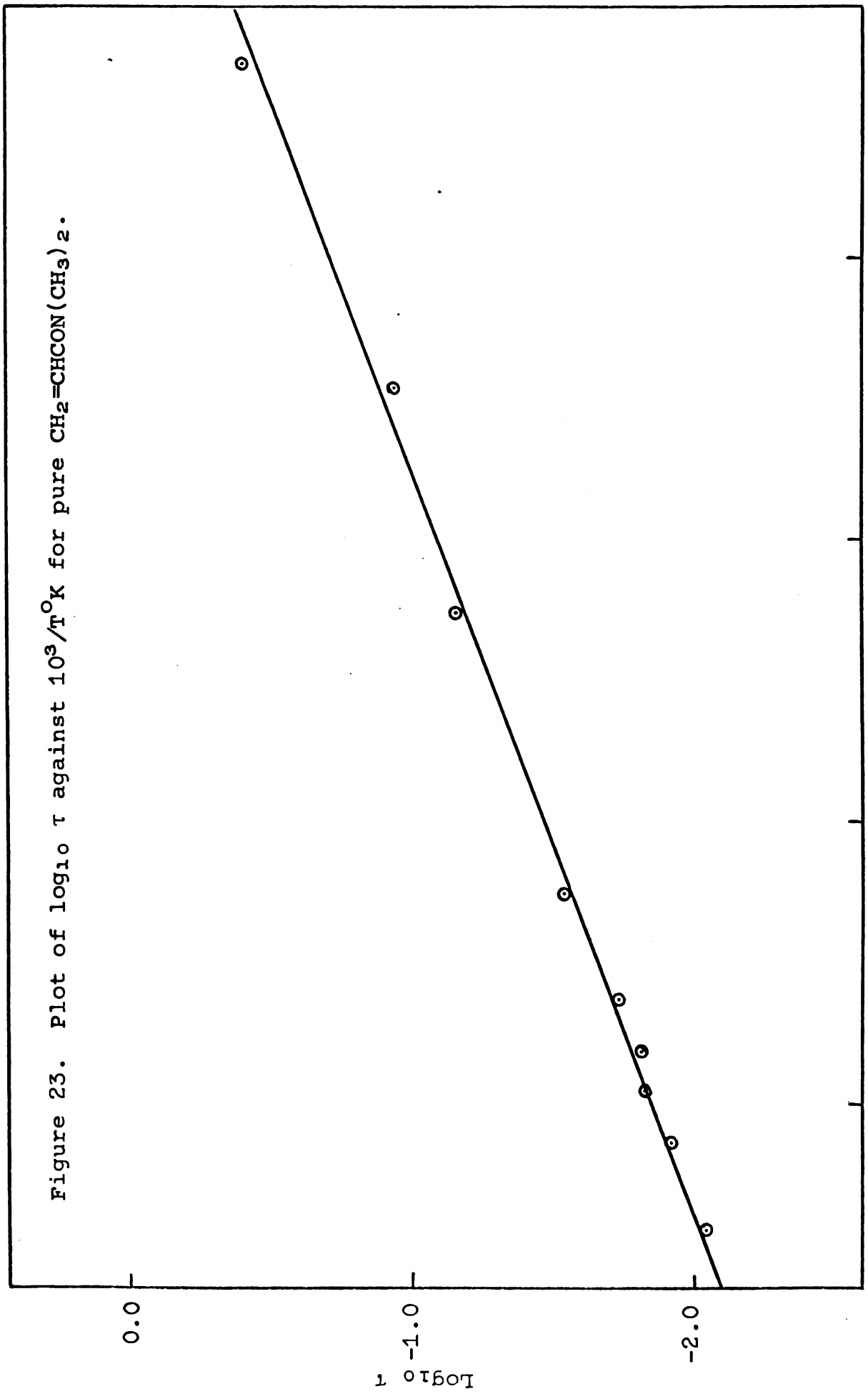

Figure 23. Plot of $\log_{10} \tau$ against $10^3/T^{\circ}K$ for pure $CH_2=CHCON(CH_3)_2$.

Table 25. Temperature dependence of the rate of internal rotation about the central C-N bond of $CCl_3CON(CH_3)_2$.**

$10^3/T^oK$	p_A*	$\tau \times 10^2$ sec I.R.	$\tau \times 10^2$ sec P.S.	$\tau \times 10^2$ sec T.L.S.	$Log_{10}\ \tau$*	FR* rad/sec
3.668	0.48593			112.92	0.05275	183.13
3.604	0.49070			14.056	-0.8521	180.90
3.535	0.47374	3.109	3.002	3.273	-1.478	184.22
3.472	0.50995	2.056	1.983	2.1322	-1.671	183.78
3.406	0.49961	1.235	1.232	1.2206	-1.913	183.22
3.345	0.50430			0.56421	-2.249	207.19
3.285	0.49433			0.32097	-2.494	204.68
3.228	0.50868			0.1462	-2.835	220.22
3.233	0.50765			0.14003	-2.836	227.63
3.179	0.50402			0.086133	-3.068	237.16
3.130	0.49828			0.038024	-3.420	253.78
3.08	0.49936			0.025634	-3.591	189.1

Coalescence point = $10^3/T_c^oK \cong 3.34$.

*Results from T.L.S.

**HMDS as external reference

Table 26. Thermodynamic and kinetic parameters for internal rotation about the central C-N bond of $CCl_3CON(CH_3)_2$.**

Method	E_a kcal/mole	Log_{10} 2A	$\Delta F^{\ddagger}_{293.6^oK}$ kcal/mole
I.R.*	14.21	12.49	15.02
P.S.*	13.71	12.13	15.02
T.L.A.	22.11	18.47	15.013

*FR = 28.6 Hz.

**HMDS as external reference.

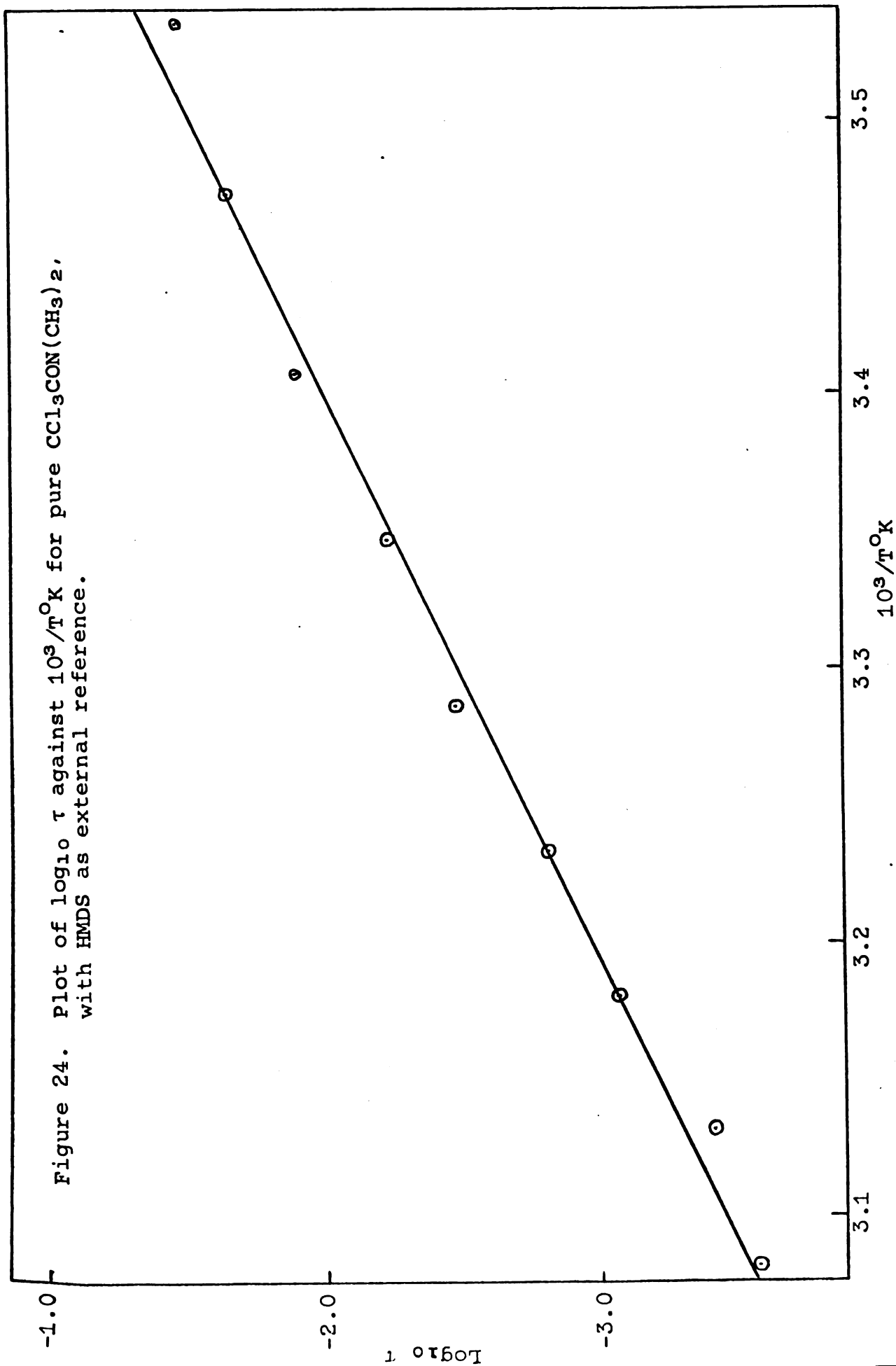

Figure 24. Plot of $\log_{10} \tau$ against $10^3/T^{\circ}K$ for pure $CCl_3CON(CH_3)_2$, with HMDS as external reference.

Table 27. Temperature dependence of the rate of internal rotation about the central C-N bond of $CCl_3CON(CH_3)_2$.**

$10^3/T^oK$	p_A*	$\tau \times 10^2$ sec I.R.	$\tau \times 10^2$ sec P.S.	$\tau \times 10^2$ sec T.L.S.	$Log_{10}\ \tau$*	FR* rad/sec
3.668	0.47986			182.78	0.2619	182.77
3.668	0.48405			72.236	-0.1412	182.97
3.597	0.49319			8.7065	-1.060	182.29
3.535	0.49615	3.518	3.162	4.5262	-1.344	181.09
3.495	0.49149	1.866	1.824	2.2626	-1.645	180.21
3.412	0.51305	1.174	1.193	1.1655	-1.933	186.14
3.339	0.52067			6.9764	-2.156	187.77
3.290	0.51191			0.32097	-2.494	204.8
3.234	0.51295			0.19031	-2.721	211.62
3.179	0.50537			0.080048	-3.065	242.35
3.128	0.50823			0.065823	-3.182	201.24
3.083	0.50287			0.02566	-3.591	197.85
3.034	0.49868			0.025581	-3.592	138.45

* Coalescence point = $10^3/T_c^oK \cong 3.34$.
** Results from T.L.S.
TMS as internal reference.

Table 28. Thermodynamic and kinetic parameters for internal rotation about the central C-N bond of $CCl_3CON(CH_3)_2$.**

Method	E_a kcal/mole	Log_{10} 2A	$\Delta F^{\ddagger}_{293.6^oK}$ kcal/mole
I.R.*	16.71	14.42	14.96
P.S.*	14.88	13.05	14.97
T.L.A.	21.07	17.66	14.96

*FR = 28.6 Hz.

**TMS as internal reference.

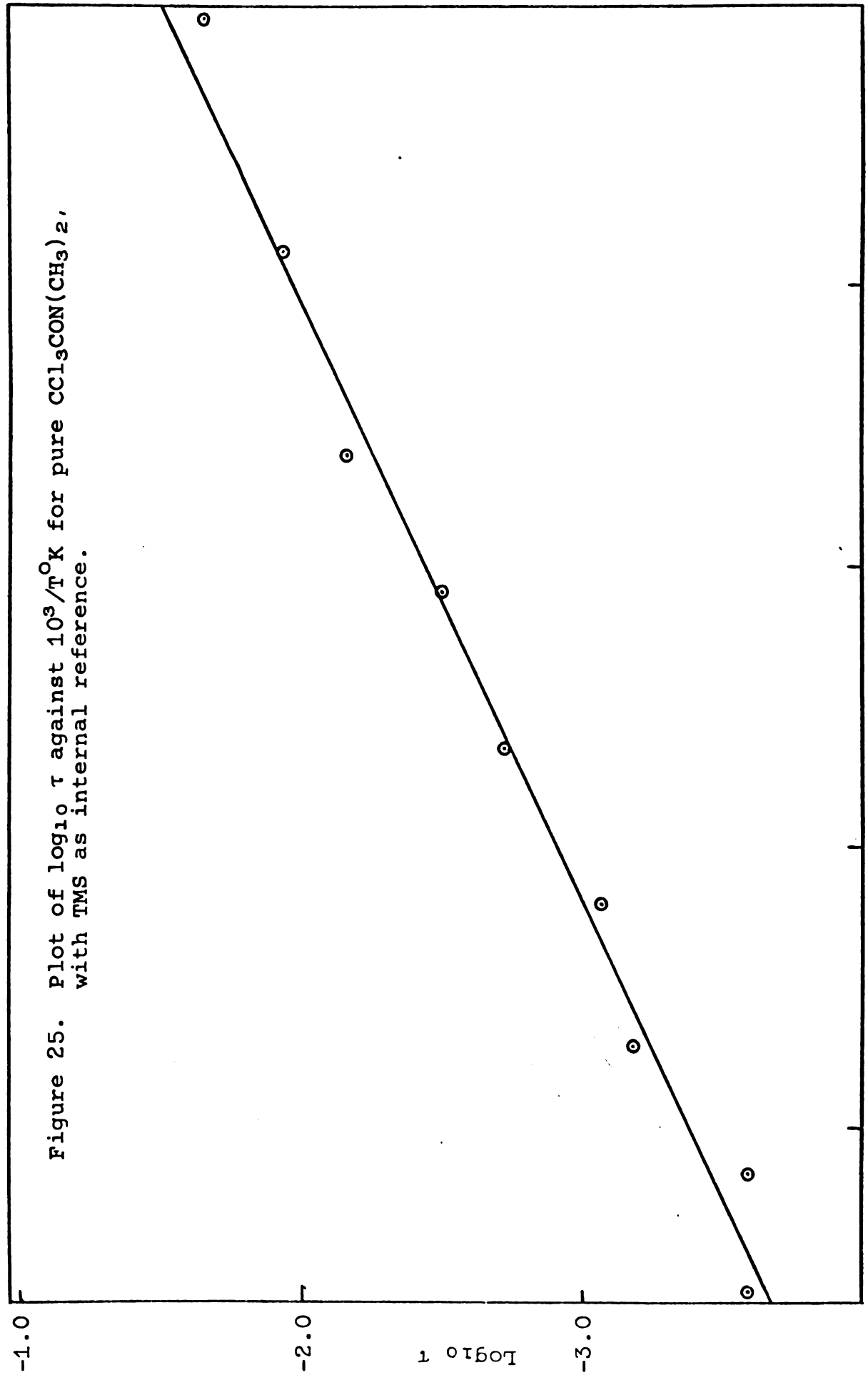

Figure 25. Plot of $\log_{10} \tau$ against $10^3/T^{\circ}K$ for pure $CCl_3CON(CH_3)_2$, with TMS as internal reference.

Table 29. Temperature dependence of the rate of internal rotation about the central C-N bond of $ClCON(CH_3)_2$.**

$10^3/T^oK$	p_A*	$Log_{10}\ \tau$*
3.456	0.55	0.10924
3.03	0.5018	0.380
3.181	0.424	-1.0044
3.135	0.5046	-1.250
3.110	0.5055	-1.325
3.070	0.502	-1.495
3.029	0.4829	-1.738
2.974	0.4925	-1.958

ΔE_a = 21.91 kcal/mole

Log_{10} 2A = 16.21

$\Delta F^{\ddagger}_{321.5^oK}$ = 17.36 kcal/mole

*Results from T.L.S.

**Not degassed, cyclohexane as external reference.

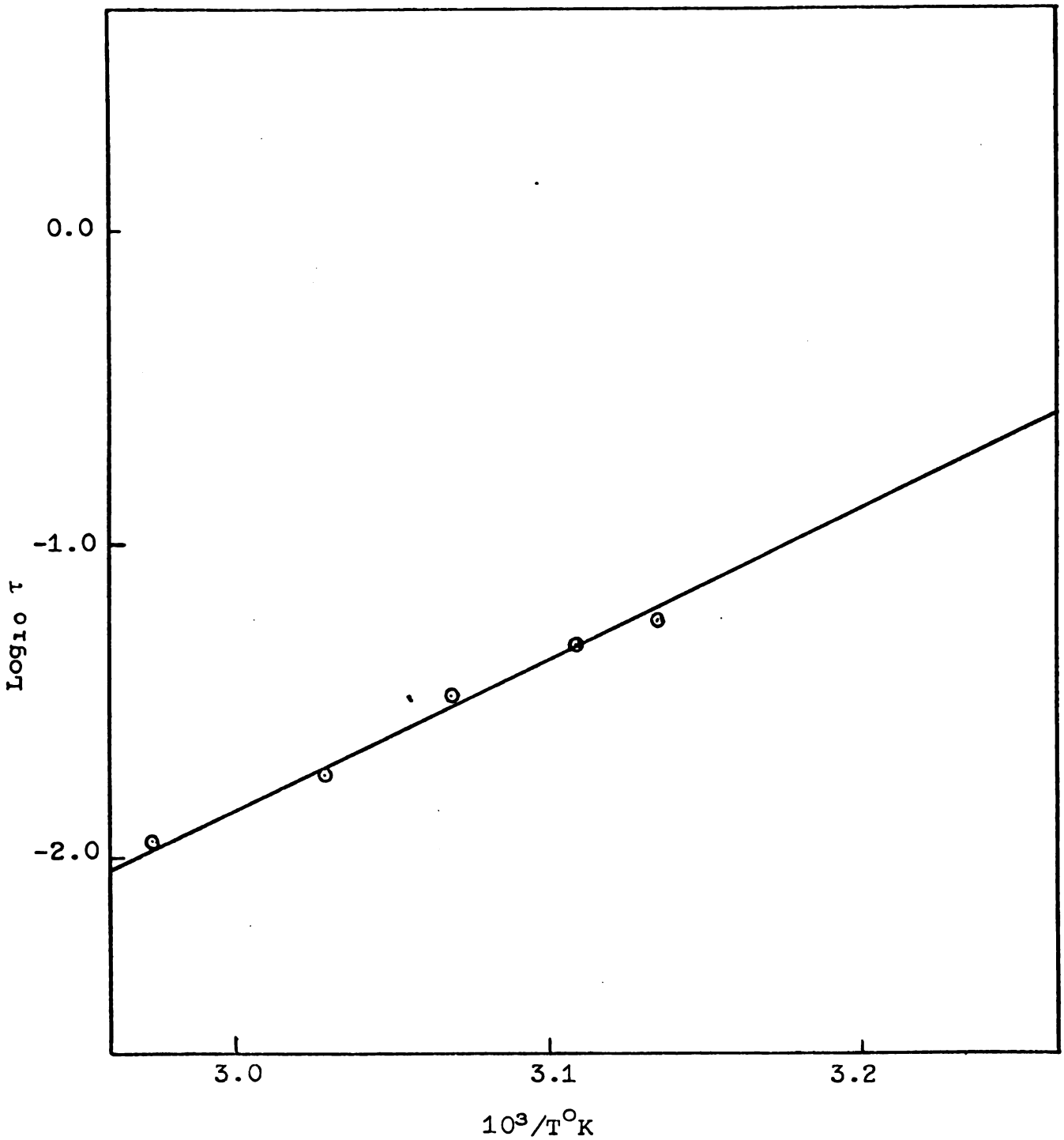

Figure 26. Plot of $\log_{10} \tau$ against $10^3/T^{\circ}K$ for pure $ClCON(CH_3)_2$, with cyclohexane as external reference.

Table 30. Temperature dependence of the rate of internal rotation about the central C-N bond of $ClCON(CH_3)_2$.**

$10^3/T^oK$	p_A*	$Log_{10}\ \tau$*
3.618	0.515	0.5
3.482	0.4829	0.172
3.315	0.4959	-0.616
3.274	0.509	-1.162
3.184	0.505	-1.168
3.125	0.509	-1.3401
3.096	0.495	-1.444
3.072	0.503	-1.535
3.015	0.508	-1.755

ΔE_a = 17.7 kcal/mole

Log_{10} 2A = 13.45

$\Delta F^{\ddagger}_{317.5^oK}$ = 18.17 kcal/mole

*Results from T.L.S.

**Saturated with O_2 and TMS as internal reference.

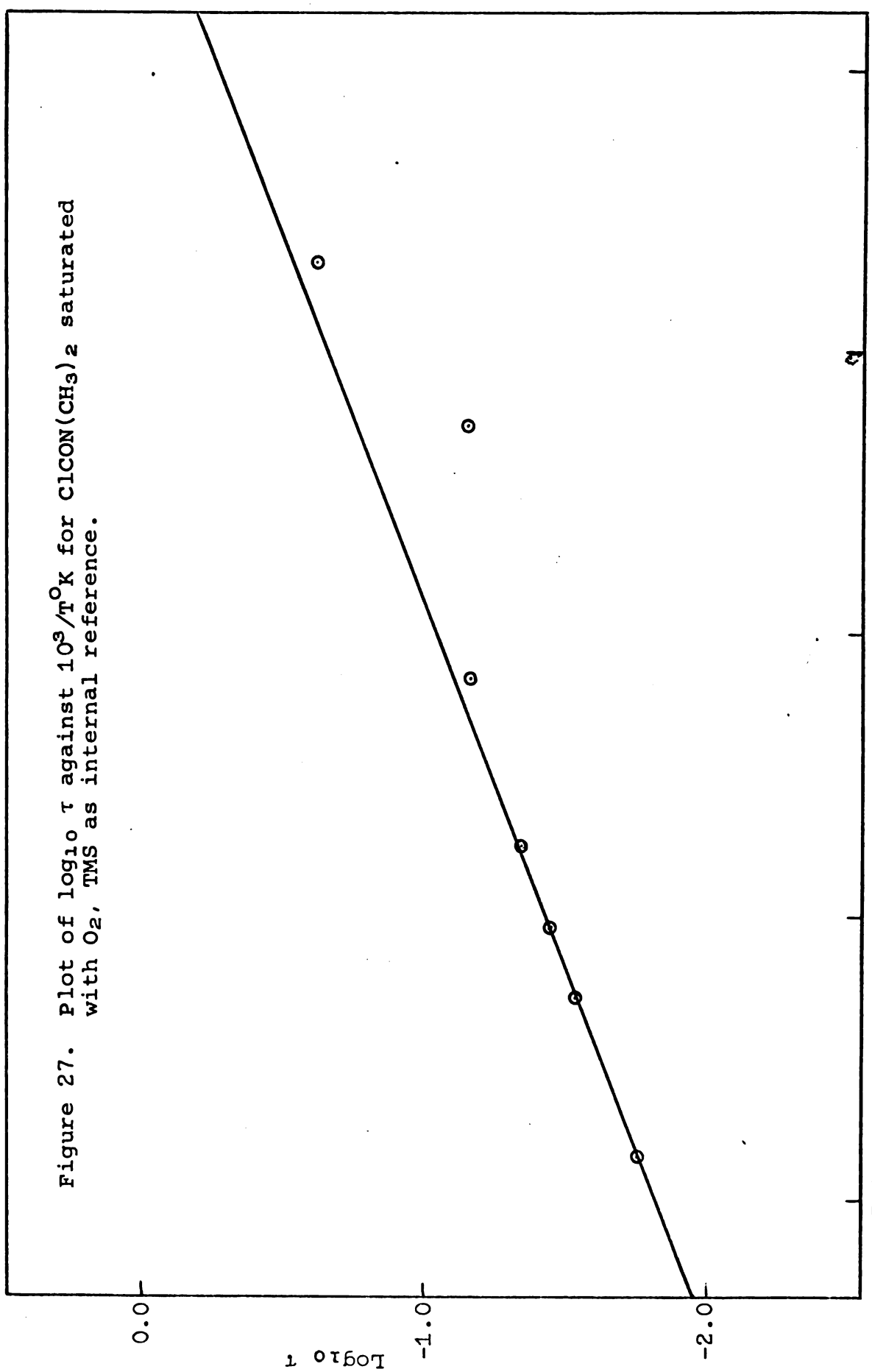

Figure 27. Plot of $\log_{10} \tau$ against $10^3/T^{\circ}K$ for $ClCON(CH_3)_2$ saturated with O_2, TMS as internal reference.

Table 31. Temperature dependence of the rate of internal rotation about the central C-N bond of $ClCON(CH_3)_2$.**

$10^3/T^oK$	p_A*	$Log_{10}\ \tau$*
3.618	0.4650	0.4623
3.422	0.4989	-0.1910
3.315	0.5006	-0.875
3.262	0.5095	-1.2479
3.184	0.5141	-1.277
3.125	0.5033	-1.438
3.096	0.4815	-1.541
3.072	0.5074	-1.64
3.02	0.5088	-1.751

E_a = 13.79 kcal/mole

Log 2A = 10.88

$\Delta F^{\ddagger}_{317.5^oK}$ = 17.79 kcal/mole

*Results from T.L.S.

**From K and K, not purified, not degassed, cyclohexane as internal reference.

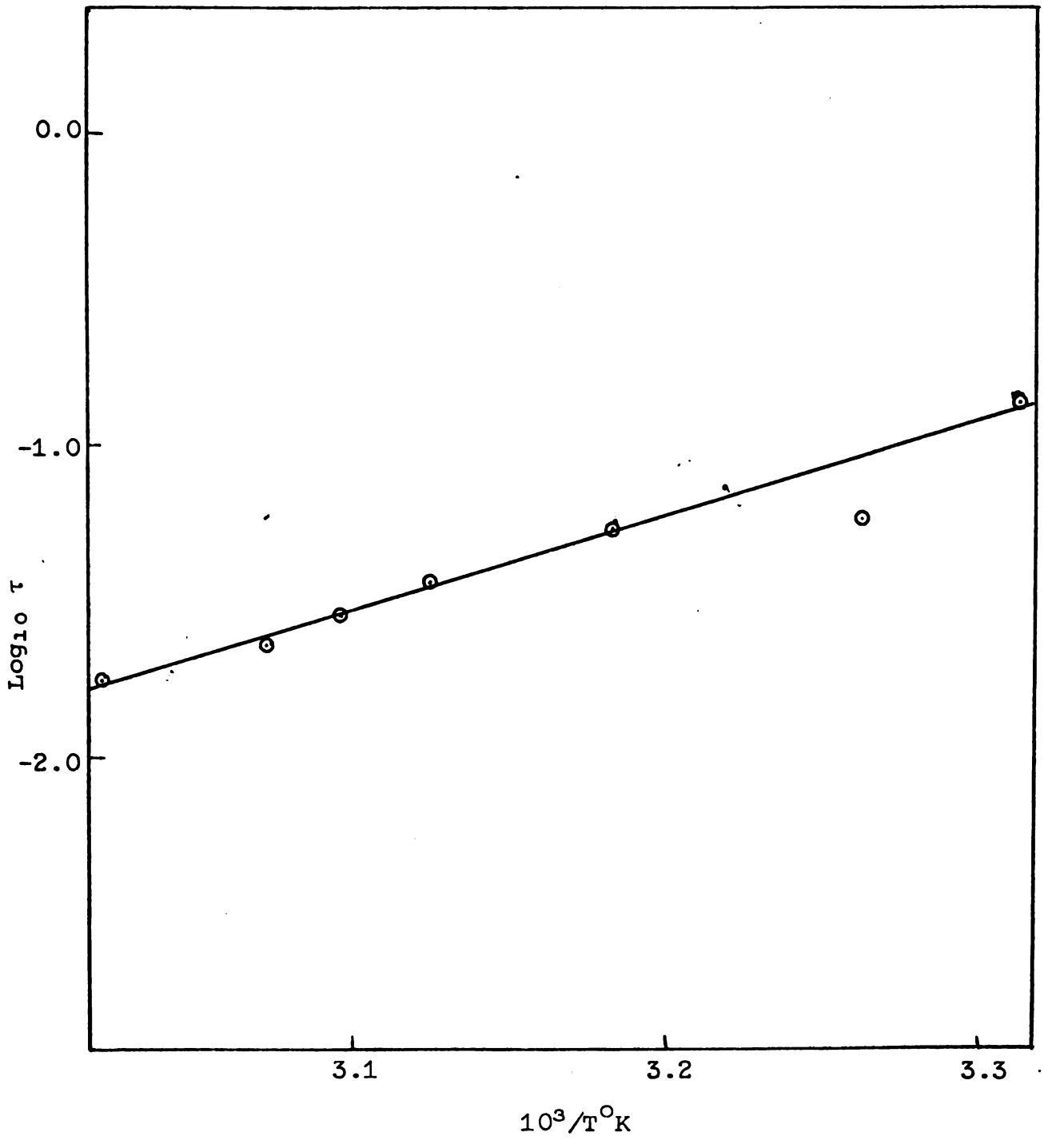

Figure 28. Plot of $\log_{10} \tau$ against $10^3/T^{\circ}K$ for not purified $ClCON(CH_3)_2$, not degassed, with HMDS as external reference.

Table 32. Temperature dependence of the rate of internal rotation about the central C-N bond of $ClCON(CH_3)_2$.**

$10^3/T^oK$	P_A*	$Log_{10}\ \tau$*
3.311	0.4930	-0.412
3.181	0.5034	-1.025
3.168	0.4952	-1.047
3.135	0.4947	-1.217
3.086	0.5180	-1.384

E_a = 20.02 kcal/mole

Log 2A = 14.93

$\Delta F^{\ddagger}_{314.5^oK}$ = 17.4 kcal/mole

*Results from T.L.S.

**Highly purified (V.P.C.), degassed, HMDS as external reference.

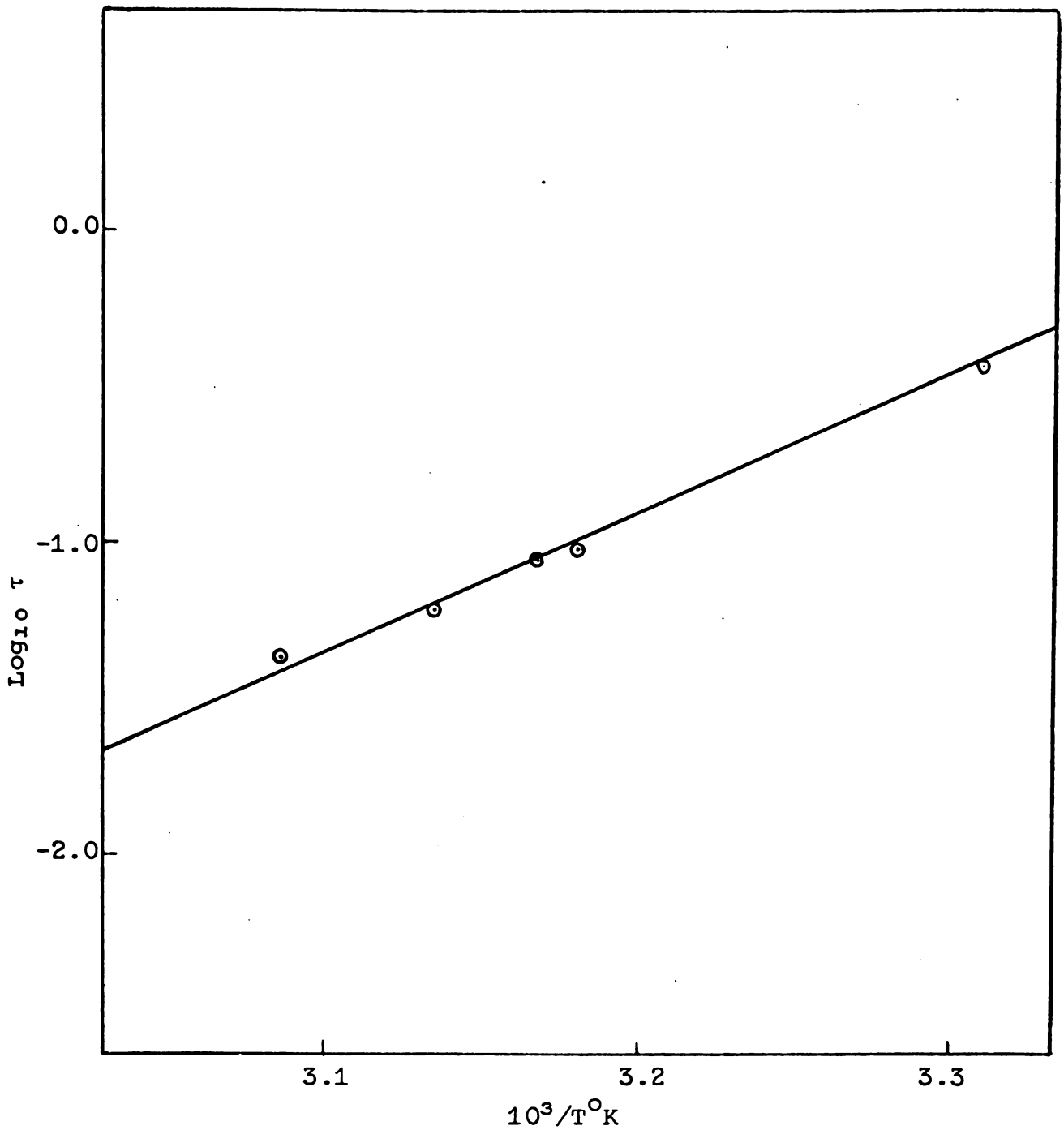

Figure 29. Plot of $\log_{10} \tau$ against $10^3/T^{\circ}K$ for highly purified $ClCON(CH_3)_2$, with HMDS as external reference.

Table 33. Temperature dependence of the rate of internal rotation about the central C-N bond of $ClCON(CH_3)_2$.**

$10^3/T^oK$	p_A*	$\tau \times 10^2$ sec I.R.	$\tau \times 10^2$ sec P.S.	$\tau \times 10^2$ sec T.L.S.	$Log_{10}\ \tau$*	FR* rad/sec
	0.51218			6156.000	5.209	67.405
3.417	0.49034			781	0.8927	66.691
3.382	0.50324			137.63	0.1387	67.410
3.342	0.50265	9.987	10.78	84.467	-0.07331	66.969
3.318	0.50321	8.598	9.652	46.758	-0.3301	66.517
3.286	0.50833	8.214	7.228	38.657	-0.4128	66.292
3.21	0.49774	5.763	5.829	9.3041	-1.0311	65.94
	0.51733			5.671	-1.246	
3.243	0.5044	5.944	4.339	13.582	-0.867	66.668
3.18	0.49038	4.146	3.831	6.1938	-1.208	62.8
3.16	0.49035	3.511	3.070	4.5508	-1.342	67.45
3.14	0.50103	2.937	2.580	3.697	-1.432	65.576
3.11	0.50966	2.490		3.0342	-1.518	65.3
3.091	0.51942			2.139	-1.67	68.8
3.072	0.51116			2.0837	-1.681	66.929
3.04	0.5062			1.2502	-1.903	69.463
3.021	0.51452			1.1499	-1.939	68.34
2.985	0.30316			0.88145	2.055	67.846

Coalescence point = $10^3/T^oK \cong 3.09$.
*Results from T.L.S.
**Highly purified, degassed, TMS internal reference.

Table 34. Thermodynamic and kinetic parameters for internal rotation about the central C-N bond of $ClCON(CH_3)_2$.**

Method	E_a kcal/mole	Log_{10} 2A	$\Delta F^{\ddagger}_{314.5^oK}$ kcal/mole
I.R.*	11.8	9.609	16.89
P.S.*	12.5	10.08	16.84
T.L.S.	21.36	16.06	17.14

*FR = 11 Hz.

**Highly purified, degassed, TMS internal reference.

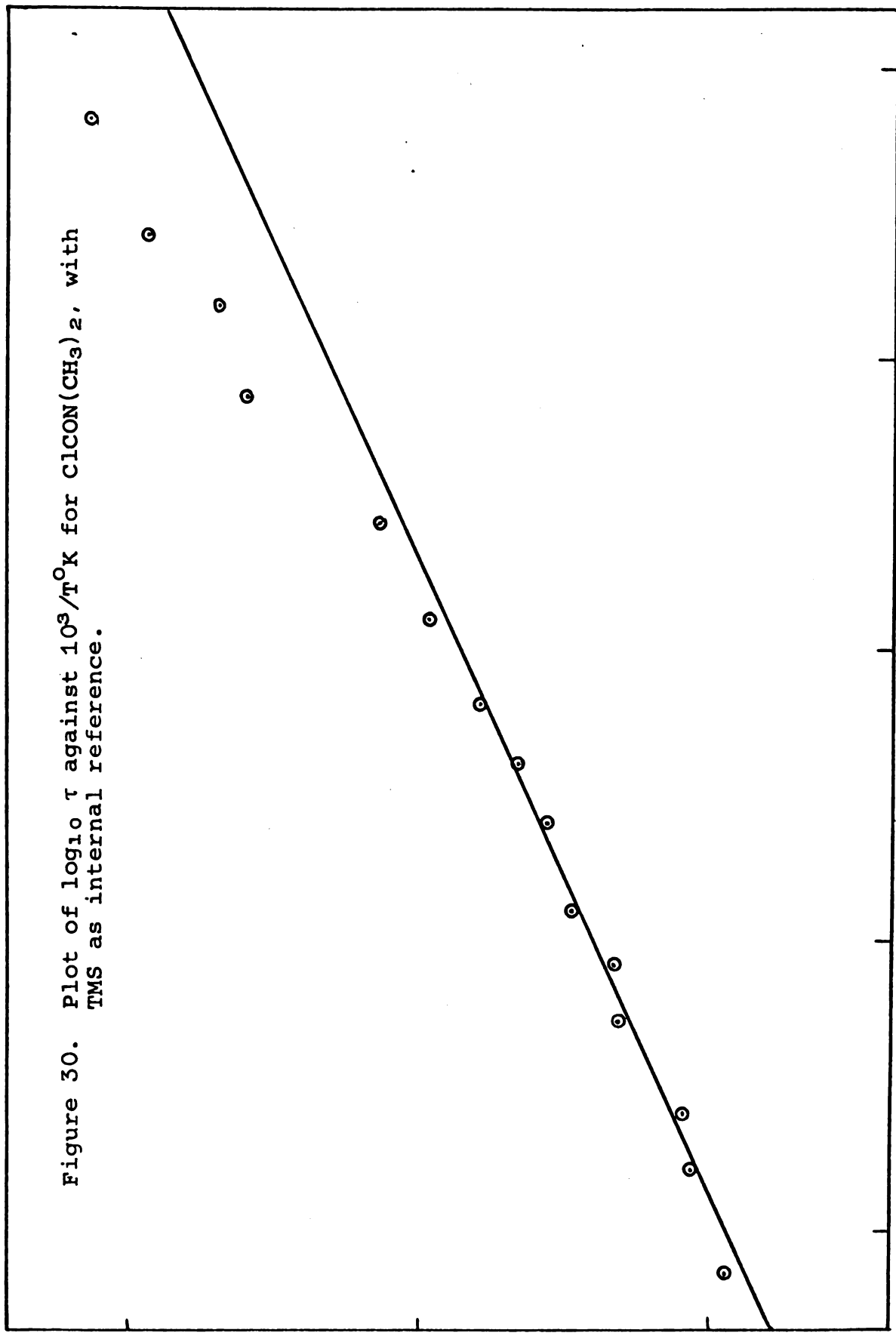

Figure 30. Plot of $\log_{10} \tau$ against $10^3/T^{\circ}K$ for $ClCON(CH_3)_2$, with TMS as internal reference.

Table 35. Temperature dependence of the rate of internal rotation about the central C-N bond of $ClCON(CH_3)_2$.**

$10^3/T^oK$	p_A*	$\tau \times 10^2$sec I.R.	$\tau \times 10^2$ sec P.S.	$\tau \times 10^2$ sec T.L.S.	$Log_{10}\ \tau$*	FR* rad/sec
3.441	0.50337			283.44	0.4525	
3.417	0.42066			357.75	0.5536	
3.382	0.48895			120.84	0.08222	
3.343	0.48826	11.26	8.822	45.728	-0.340	69.22
3.318	0.49963	9.1	8.822	30.914	-0.510	69.57
3.286	0.50553	8.87	8.822	27.091	-0.507	69.315
3.243	0.50196	5.226	5.465	10.302	-0.987	69.889
3.210	0.49957	6.646	7.657	10.551	-0.977	68.297
3.180	0.50705	4.285	4.420	5.8457	-1.233	68.608
3.160	0.50671	3.147	3.642	4.6762	-1.330	68.505
3.140	0.51489	2.953	3.094	3.027	-1.519	71.924
3.091	0.51370			2.0672	-1.685	71.588
3.110	0.50754	2.529	2.558	2.9134	-1.536	68.481
3.072	0.50763			2.0357	-1.691	67.655
3.040	0.49661			1.1823	-1.927	72.821
3.021	0.49743			0.88593	-2.053	79.009
2.970	0.49740			0.67783	-2.109	76.447

*Coalescence point = $10^3/T^oK \cong 3.09$.
**Results from T.L.S.
External reference HMDS.

Table 36. Thermodynamic and kinetic parameters for internal rotation about the central C-N bond of $ClCON(CH_3)_2$.**

Method	E_a kcal/mole	Log_{10} 2A	$\Delta F^{\ddagger}_{314.5^oK}$ kcal/mole
I.R.*	12.9	10.37	16.9
P.S.*	11.24	9.19	16.93
T.L.S.	23.16	17.32	17.1

*FR = 11 Hz.

**HMDS as external reference.

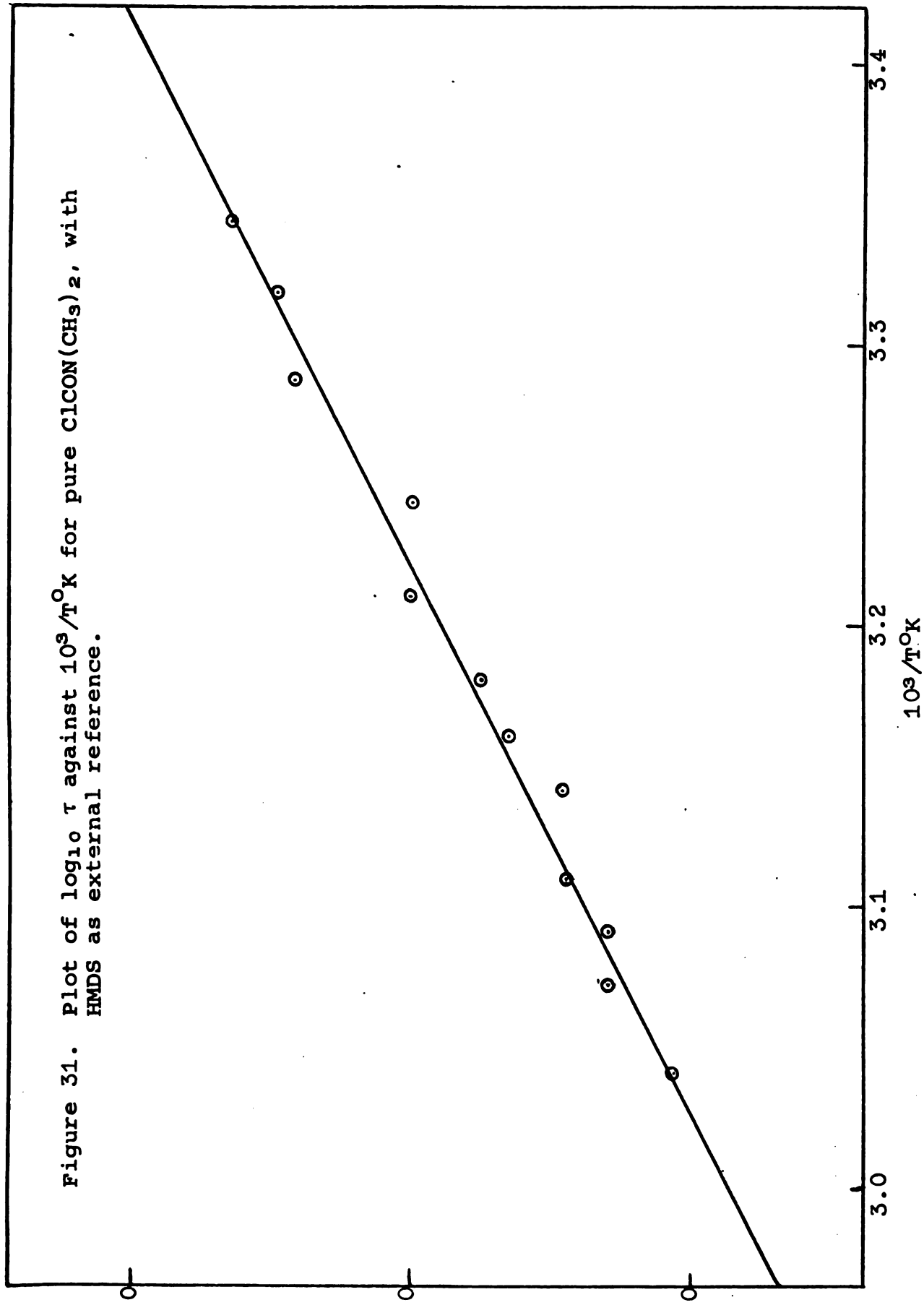

Figure 31. Plot of $\log_{10} \tau$ against $10^3/T^{\circ}K$ for pure $ClCON(CH_3)_2$, with HMDS as external reference.

N-Methyl-N-ethylacetamide

This compound was studied by T.L.S. and the calculated results are tabulated in Table 37 and plotted as $\log_{10} \tau$ against $10^3/T^{\circ}K$ in Figure 32.

N-Methyl-N-n-butylacetamide

The internal rotation of this compound was studied by T.L.S. and the results are tabulated in Table 38 and plotted as $\log_{10} \tau$ against $10^3/T^{\circ}K$ in Figure 33.

N-Methyl-N-cyclohexylacetamide

The results from T.L.S. of this compound are tabulated in Table 39 and plotted as $\log_{10} \tau$ against $10^3/T^{\circ}K$ in Figure 35.

N-Methyl-N-isopropylacetamide

The results from T.L.S. of this compound are tabulated in Table 40 and plotted as $\log_{10} \tau$ against $10^3/T^{\circ}K$ in Figure 38.

N-Methyl-N-benzylformamide

The results from T.L.S. of this compound are tabulated in Tables 41 and 42, and plotted as $\log_{10} \tau$ against $10^3/T^{\circ}K$ in Figures 39 and 40.

Table 37. Temperature dependence of the rate of internal rotation about the central C-N bond of $CH_3CON(CH_3)C_2H_5$.

$10^3/T^oK$	p_A*	$K=\frac{p_A}{p_B}$*	$Log_{10}\ \tau$*	FR* rad/sec
3.070	0.49937	0.998	-1.192	100.48
3.042	0.50694	1.028	-1.303	100.56
3.014	0.50514	1.021	-1.447	100.33
3.002	0.52473	1.104	-1.532	100.28
2.987	0.50171	1.007	-1.602	101.89
2.960	0.51488	1.061	-1.716	100.05
2.957	0.50476	1.019	-1.710	98.477
2.940	0.51352	1.056	-1.818	103.39
2.934	0.50882	1.036	-1.835	106.32
2.905	0.49797	0.9919	-2.033	116.97
2.900	0.50667	1.003	-2.033	112.31
2.880	0.49253	0.971	-2.463	117.19
2.865	0.49292	0.972	-2.168	105.29

Coalescence point = $10^3/T_c^oK \cong 2.9$.

*Results from T.L.S.

E_a = 22.85 kcal/mole

Log 2A = 16.53

$\Delta F^{\ddagger}_{338.2^oK}$ = 17.7 kcal/mole

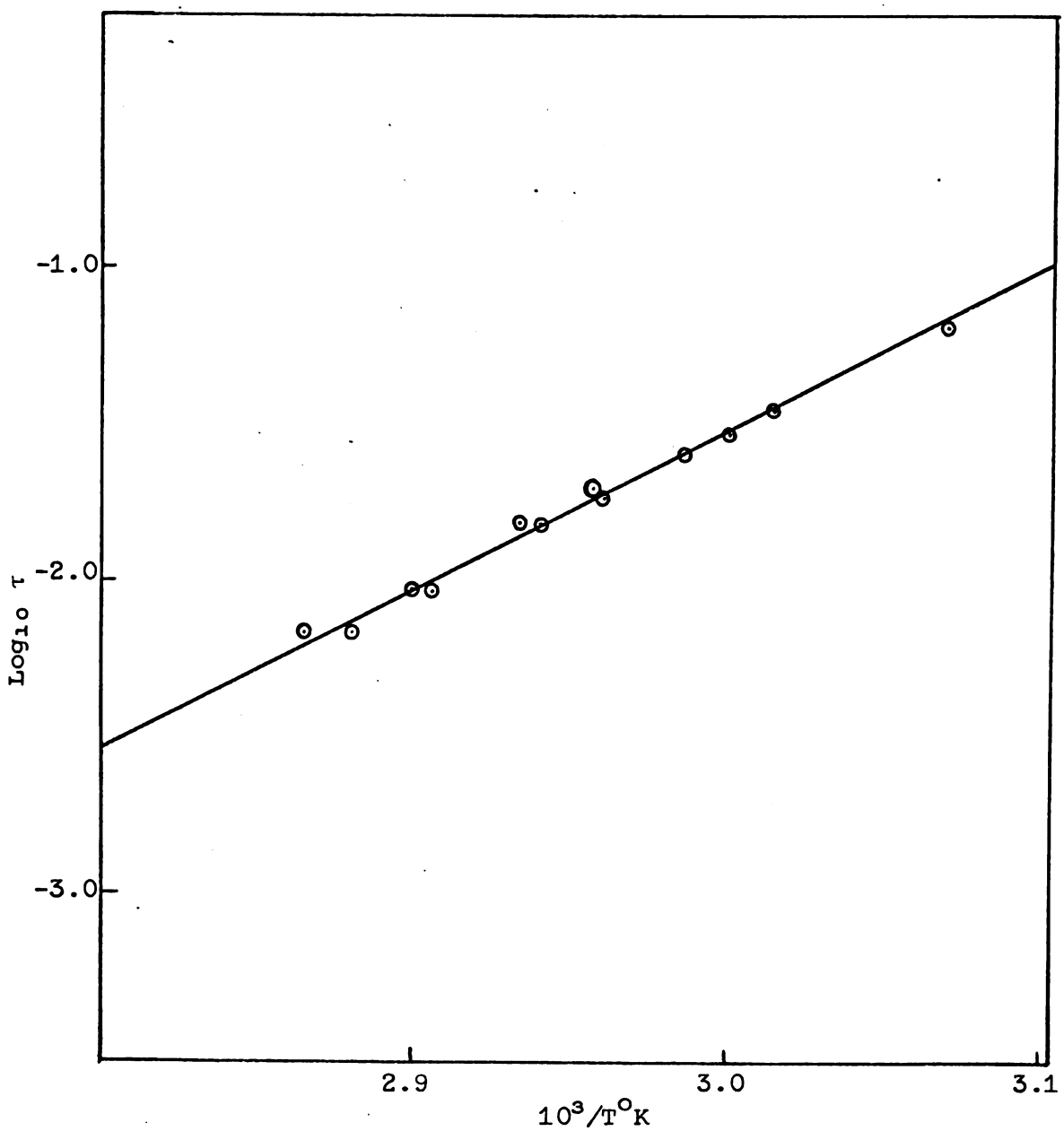

Figure 32. Plot of $\log_{10} \tau$ against $10^3/T^{\circ}K$ for pure $CH_3CON(CH_3)C_2H_5$.

Table 38. Temperature dependence of the rate of internal rotation about the central C-N bond of $CH_3CON(CH_3)C_4H_9$.

$10^3/T^oK$	p_A*	$K = \frac{p_A}{p_B}$	Log τ*	FR* rad/sec
2.996	0.53854	1.17	-1.537	95.693
2.994	0.53501	1.15	-1.528	92.0
2.960	0.53737	1.16	-1.725	99.04
2.957	0.52949	1.125	-1.699	93.39
2.931	0.53245	1.139	-1.857	98.677
2.919	0.53535	1.15	-1.903	98.867
2.988	0.53682	1.159	-2.037	105.54
2.880	0.53343	1.143	-2.158	105.28
2.870	0.53331	1.14	-2.158	102.11

E_a = 24.2 kcal/mole

Log 2A = 17.39

$\Delta F^{\ddagger}_{342.6^oK}$ = 17.64 kcal/mole

Coalescence point = $10^3/T^o_cK \cong 2.93$.

*Results obtained from T.L.S.

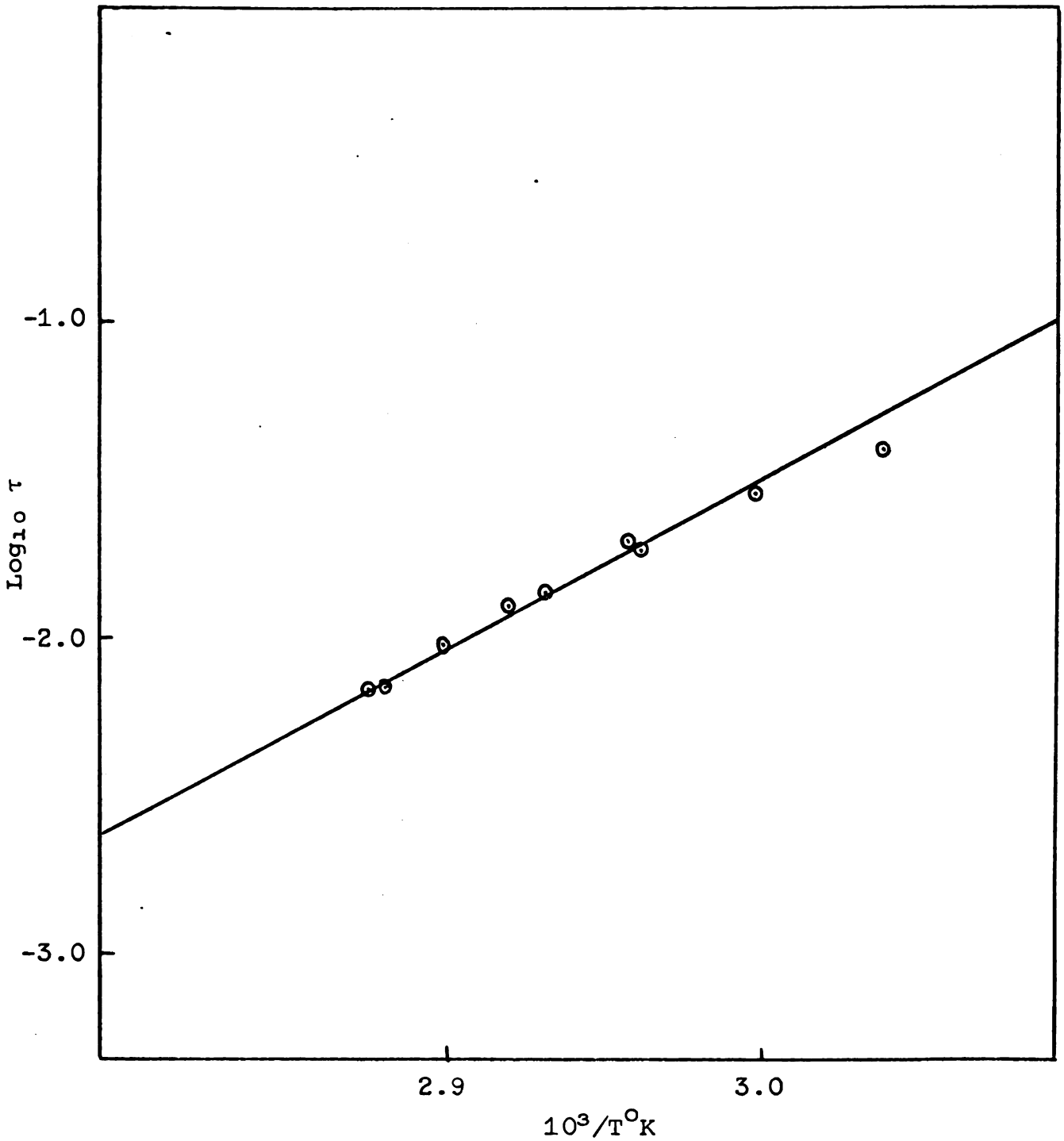

Figure 33. Plot of $\log_{10} \tau$ against $10^3/T^{\circ}K$ for pure $CH_3CON(CH_3)C_4H_9$.

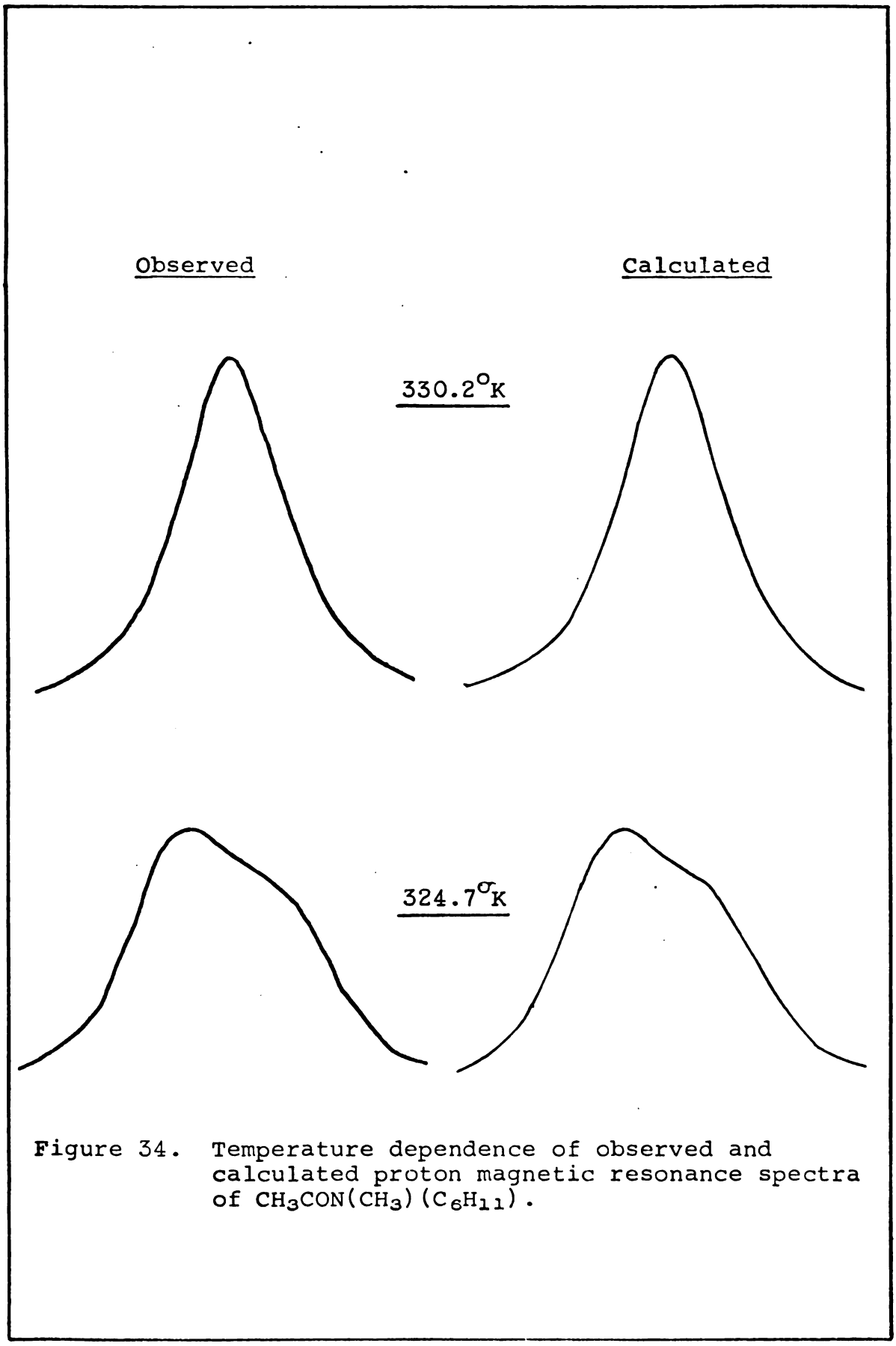

Figure 34. Temperature dependence of observed and calculated proton magnetic resonance spectra of $CH_3CON(CH_3)(C_6H_{11})$.

Figure 34 cont'd.

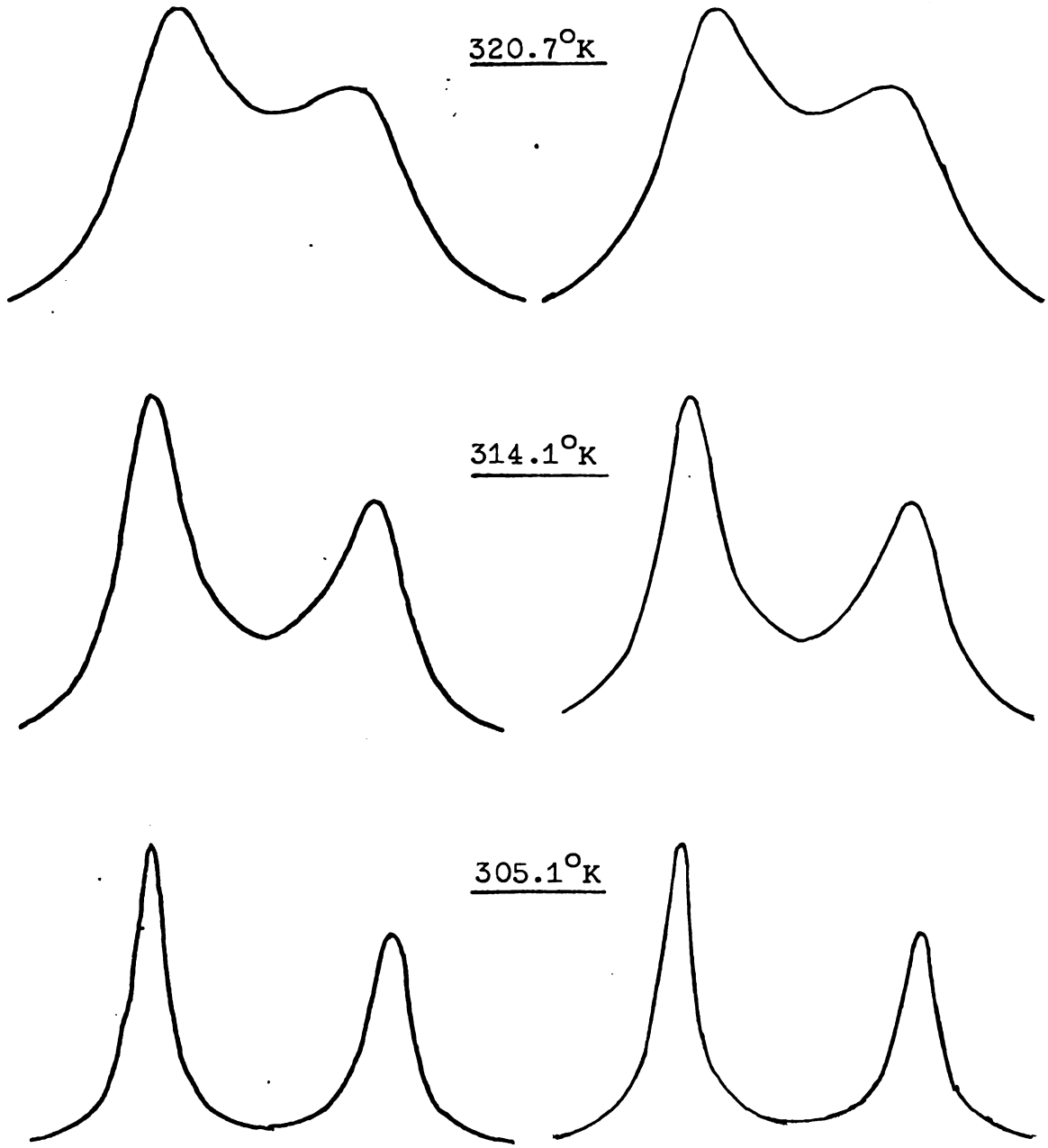

Table 39. Temperature dependence of the rate of internal rotation about the central C-N bond of $CH_3CON(CH_3)c\text{-}C_6H_{11}$.

$10^3/T^oK$	p_A*	$K = \frac{p_A^*}{p_B}$	Log τ*	FR* rad/sec
3.277	0.54209	1.184	-0.519	70.506
3.184	0.55304	1.237	-1.208	70.081
3.14	0.53812	1.165	-1.401	69.62
3.118	0.53740	1.162	-1.525	72.112
3.107	0.53542	1.15	-1.544	70.261
3.102	0.5059	1.023	-1.678	80.555
3.08	0.52832	1.12	-1.696	73.38
3.06	0.50537	1.02	-1.83	76.633
3.029	0.49833	0.993	-1.952	72.543

E_a = 26.2 kcal/mole

Log 2A = 19.38

$\Delta F^{\ddagger}_{321.9^oK}$ = 17.06 kcal/mole

Coalescence point = $10^3/T_c^oK \cong 3.07$.

*Results from T.L.S.

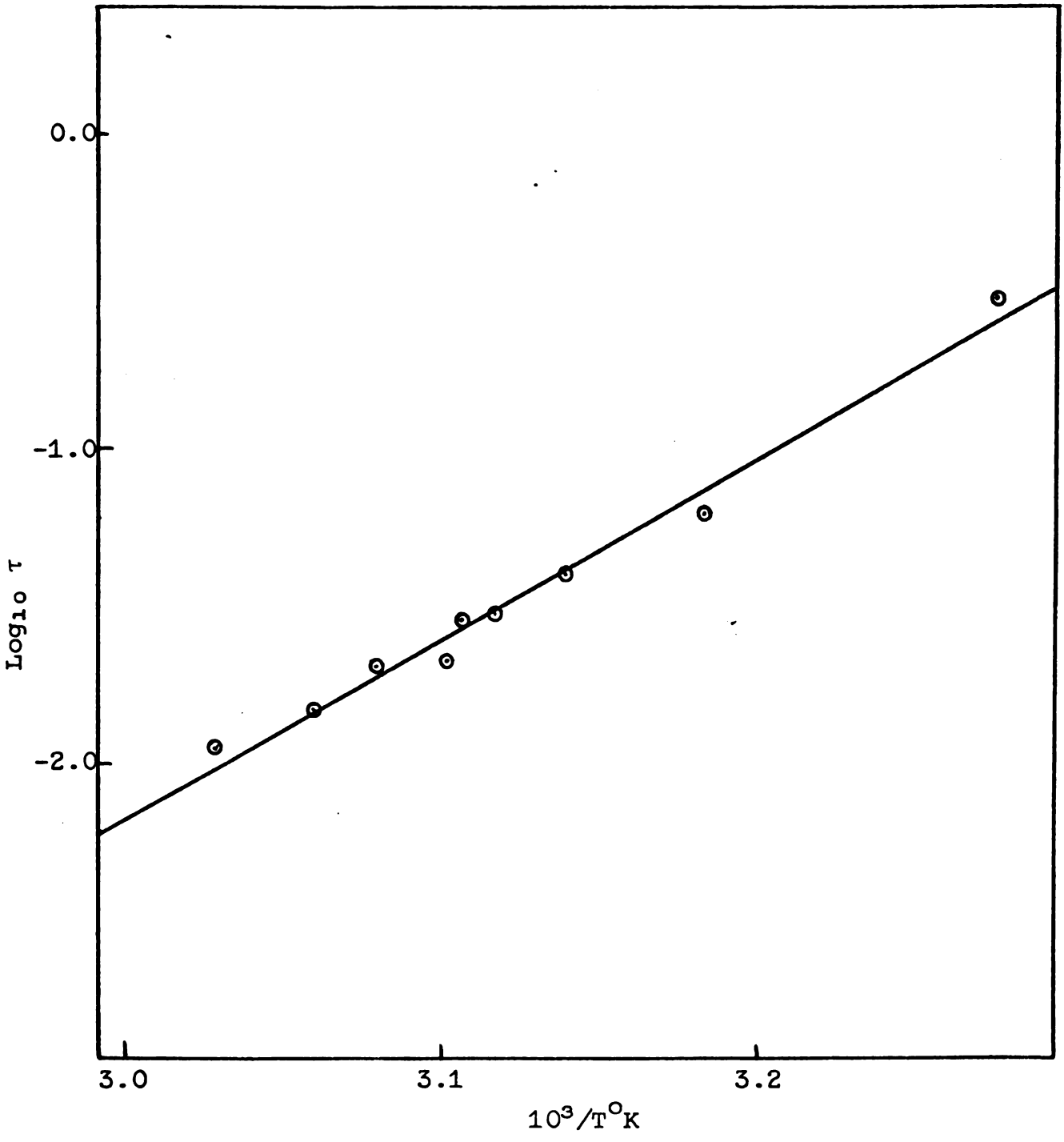

Figure 35. Plot of $\log_{10} \tau$ against $10^3/T^{\circ}K$ for pure $CH_3CON(CH_3)C_6H_{11}$.

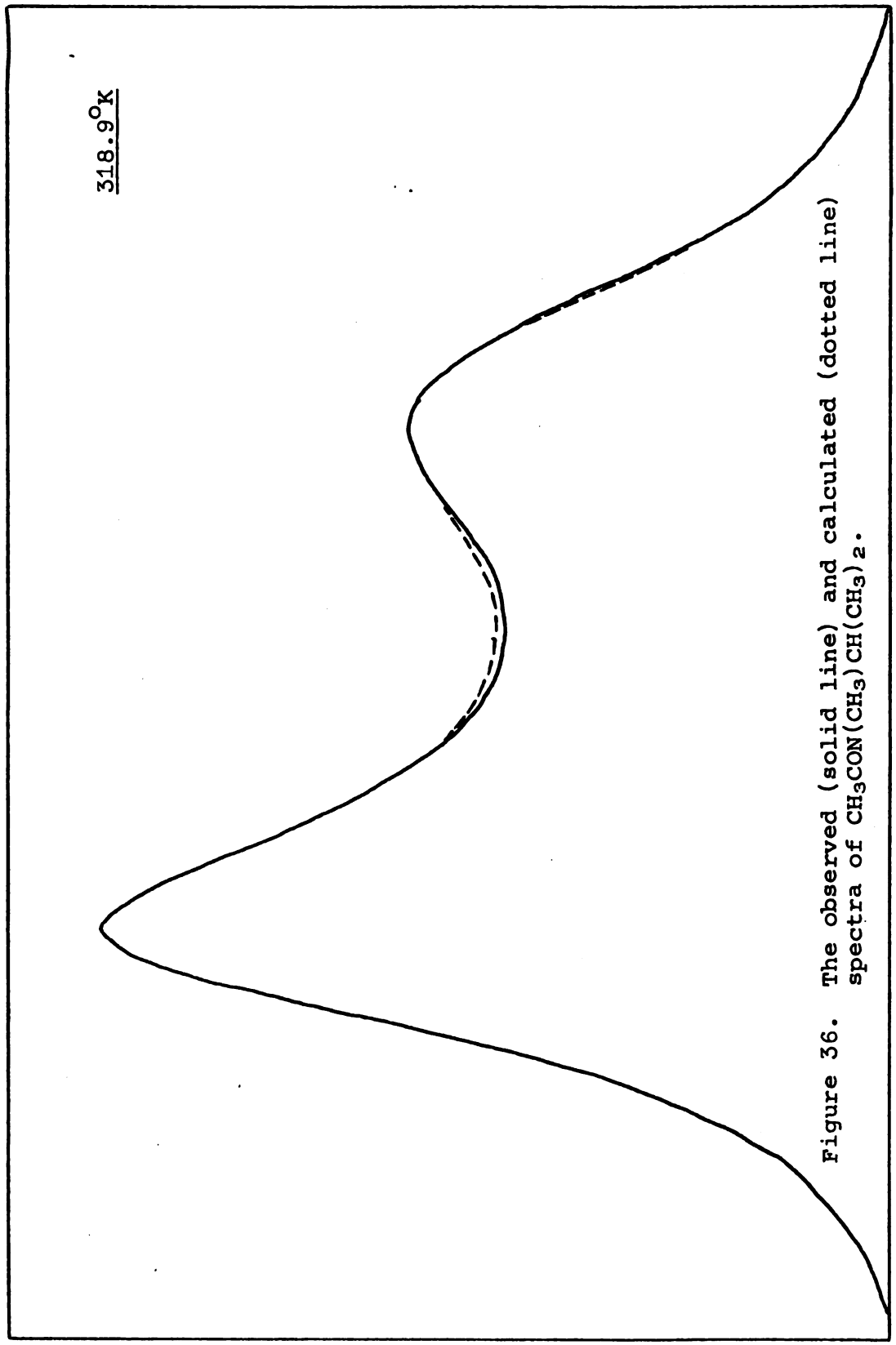

Figure 36. The observed (solid line) and calculated (dotted line) spectra of $CH_3CON(CH_3)CH(CH_3)_2$.

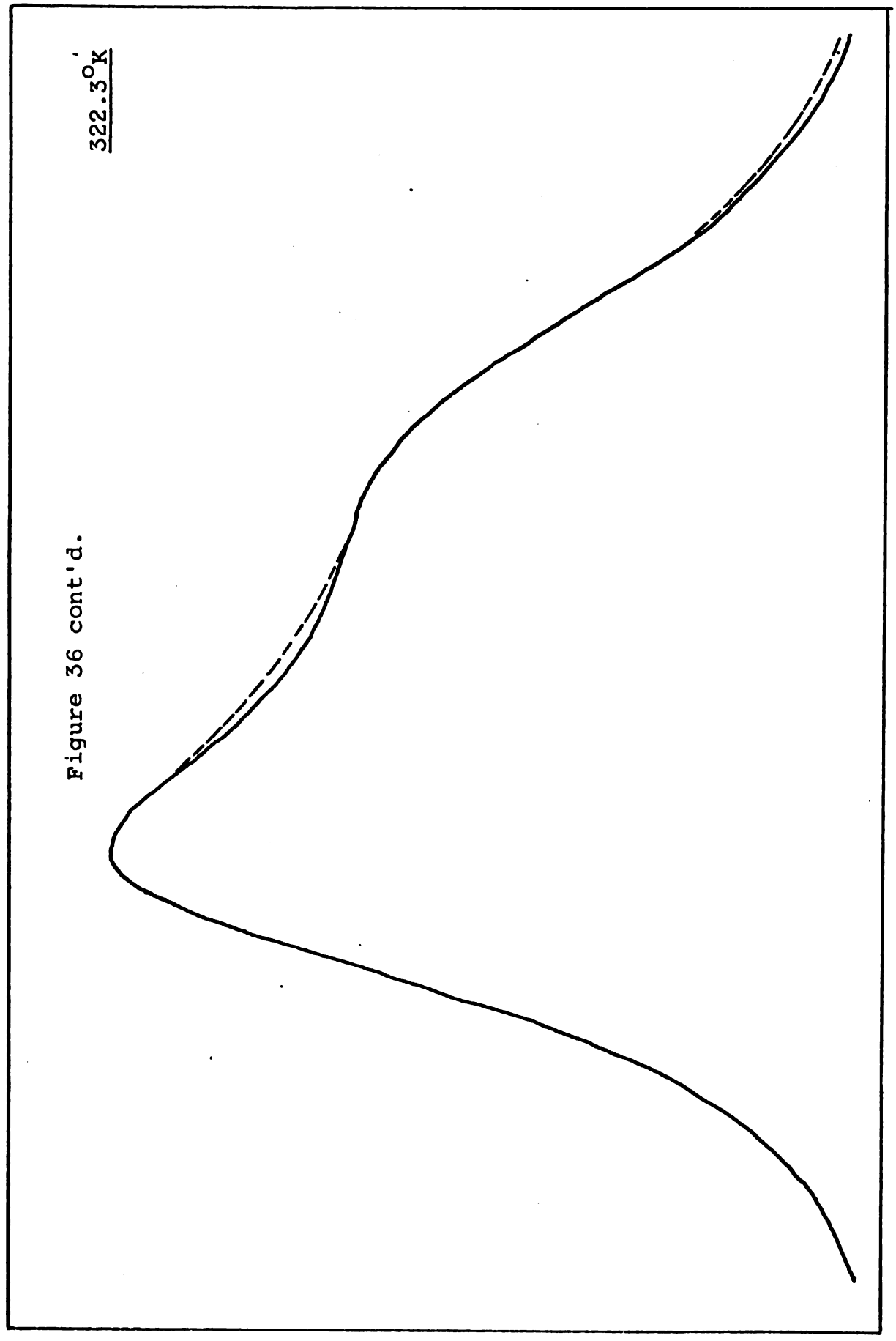

Figure 36 cont'd.

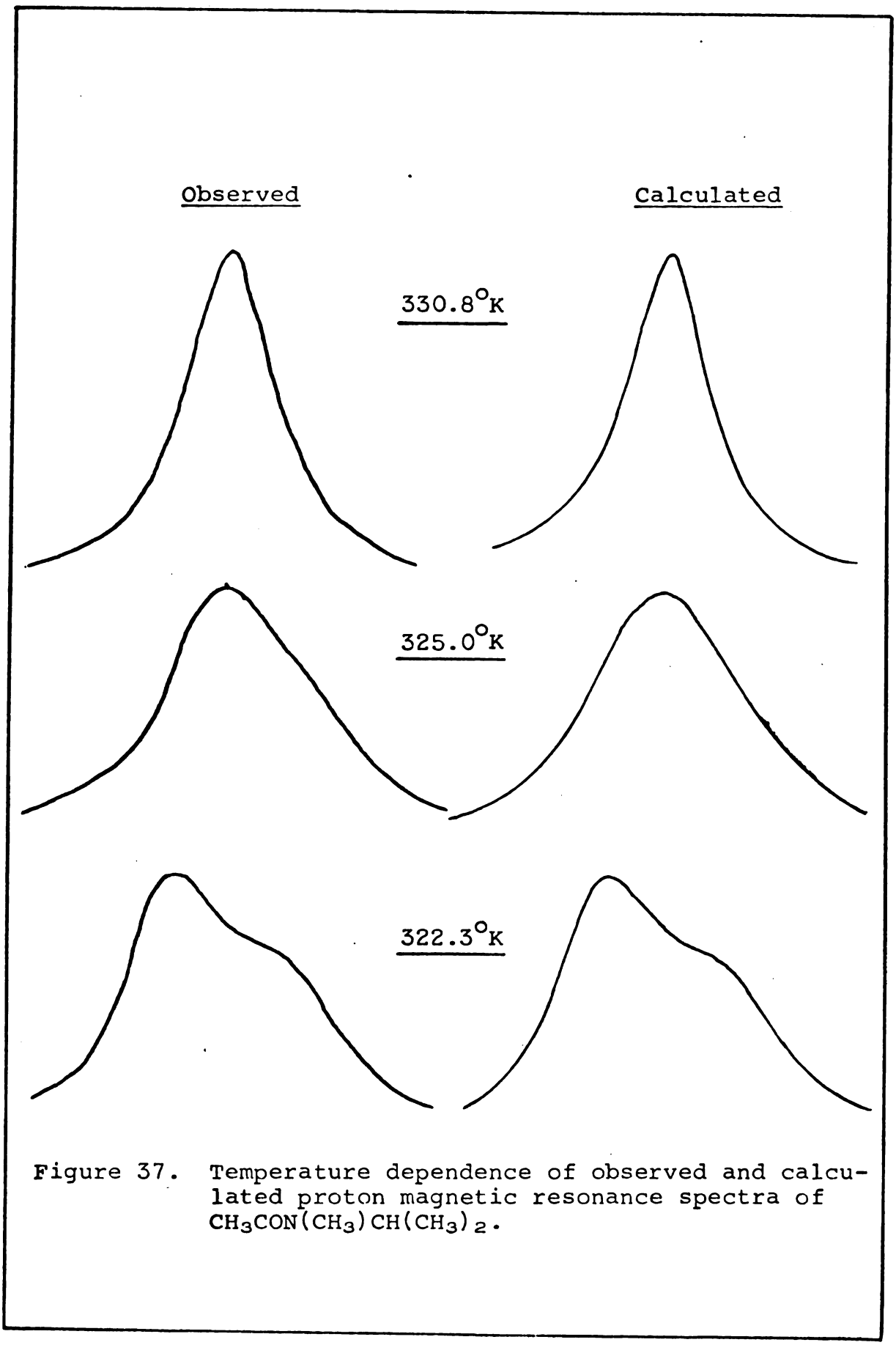

Figure 37. Temperature dependence of observed and calculated proton magnetic resonance spectra of $CH_3CON(CH_3)CH(CH_3)_2$.

Figure 37 cont'd.

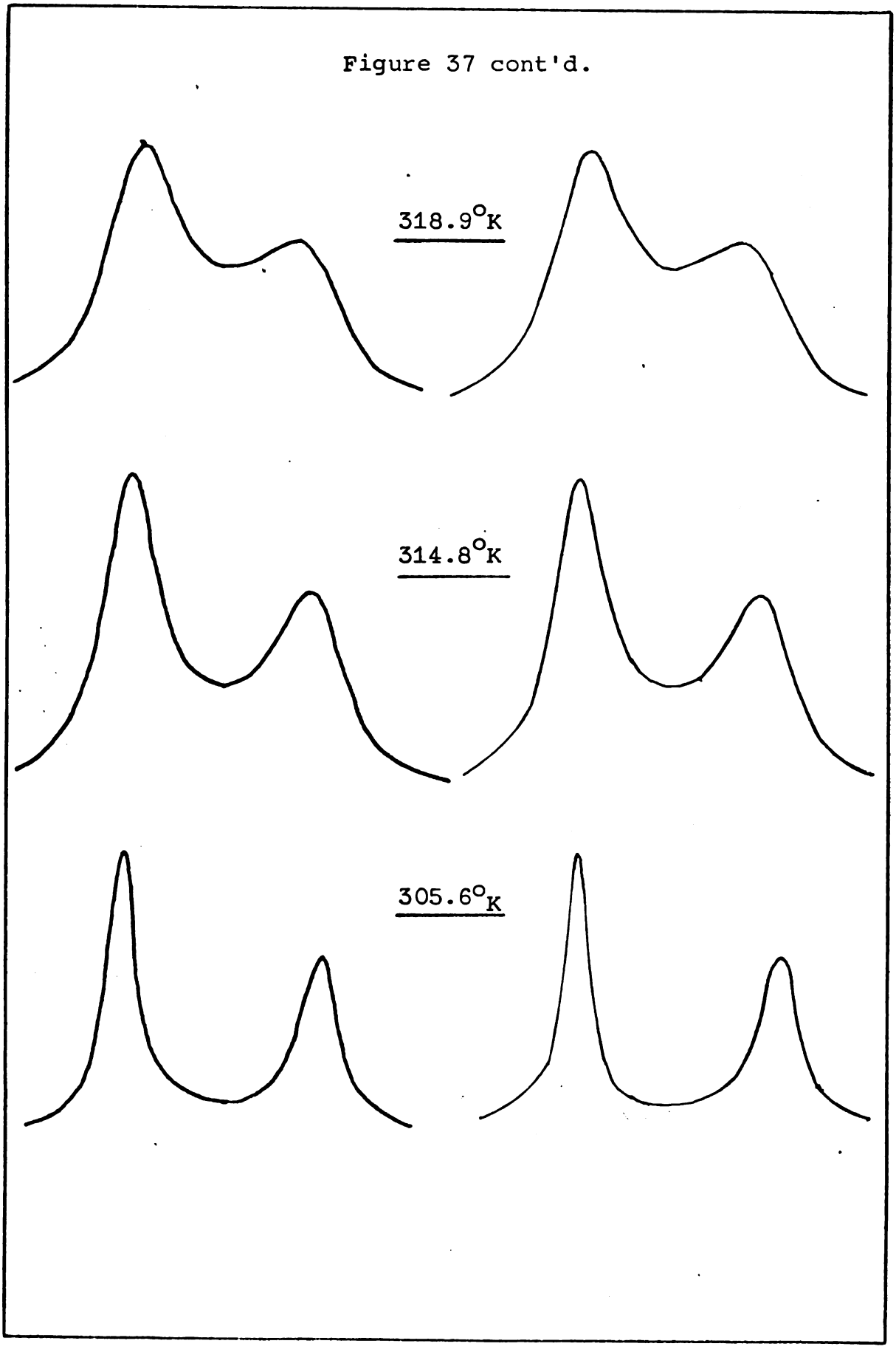

Table 40. Temperature dependence of the rate of internal rotation about the central C-N bond of $CH_3CON(CH_3)CH(CH_3)_2$.

$10^3/T^oK$	p_A^*	$K = \frac{p_A}{p_B}$	Log τ^*	FR* rad/sec
3.27	0.52148	1.089	-0.608	72.864
3.17	0.5534	1.239	-1.269	70.445
3.15	0.56307	1.289	-1.394	72.140
3.13	0.56352	1.29	-1.493	72.593
3.11	0.56439	1.296	-1.572	72.868
3.10	0.546	1.203	-1.68	76.465
3.07	0.5284	1.12	-1.819	78.295
3.06	0.526	1.11	-1.908	78.130
3.02	0.53	1.13	-2.062	72.507

E_a = 26.77 kcal/mole

Log_{10} 2A = 19.81

$\Delta F^{\ddagger}_{321.5^oK}$ = 17 kcal/mole

Coalescence point = $10^3/T_c^oK \cong 3.1$.

*Results from T.L.S.

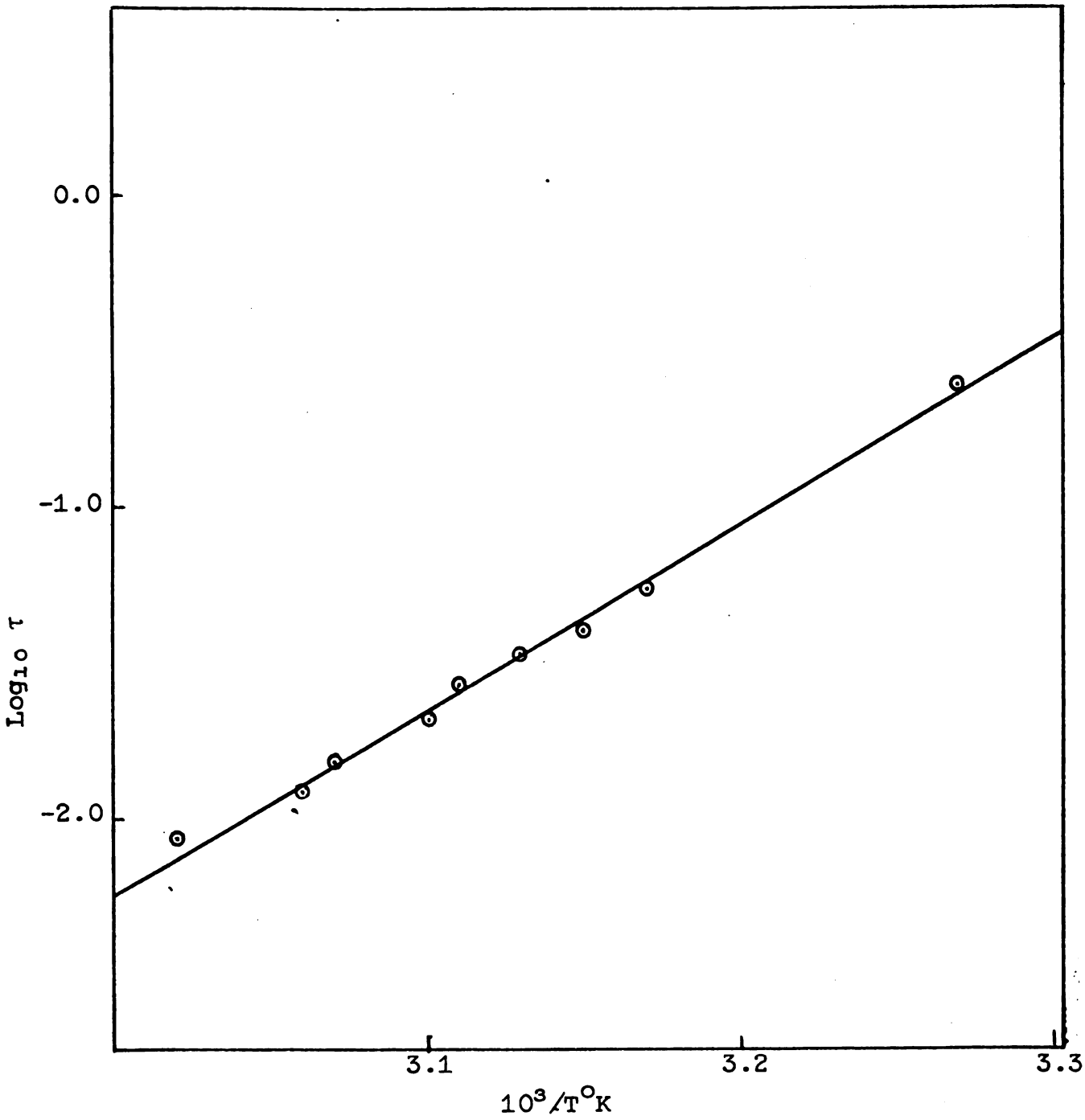

Figure 38. Plot of $\log_{10} \tau$ against $10^3/T^oK$ for pure $CH_3CON(CH_3)CH(CH_3)_2$.

Table 41. Temperature dependence of the rate of internal rotation about the central C–N bond of $HCON(CH_3)CH_2C_6H_5$.***

$10^3/T^oK$	p_A*	$K = \frac{p_A}{p_B}$	Log τ**	Log τ*	FR* rad/sec
2.660	0.45464	0.8336	-1.127	-1.126	123.68
2.631	0.46424	0.8665	-1.185	-1.185	127.28
2.617	0.46065	0.854	-1.318	-1.318	124.45
2.595	0.45165	0.843	-1.324	-1.324	123.56
2.563	0.46894	0.883	-1.546	-1.546	125.88
2.537	0.44872	0.814	-1.64	-1.640	123.39
2.511	0.45936	0.85	-1.823	-1.823	130.46
2.481	0.46796	0.88	-1.912	-1.912	125.31
2.446	0.49468	0.9789	-2.165	-2.164	135.22

E_a = 23.24 kcal/mole

Log 2A = 14.57

$\Delta F^{\ddagger}_{394.5^oK}$ = 20.88 kcal/mole

Coalescence point = $10^3/T_c^oK \cong 2.48$.

*Results from T.L.S.

**Superposition technique is used and J_1 and J_2 are assumed to be 0.4 cps and 0.6 cps.

***T.L.S. on the benzyl – doublet.

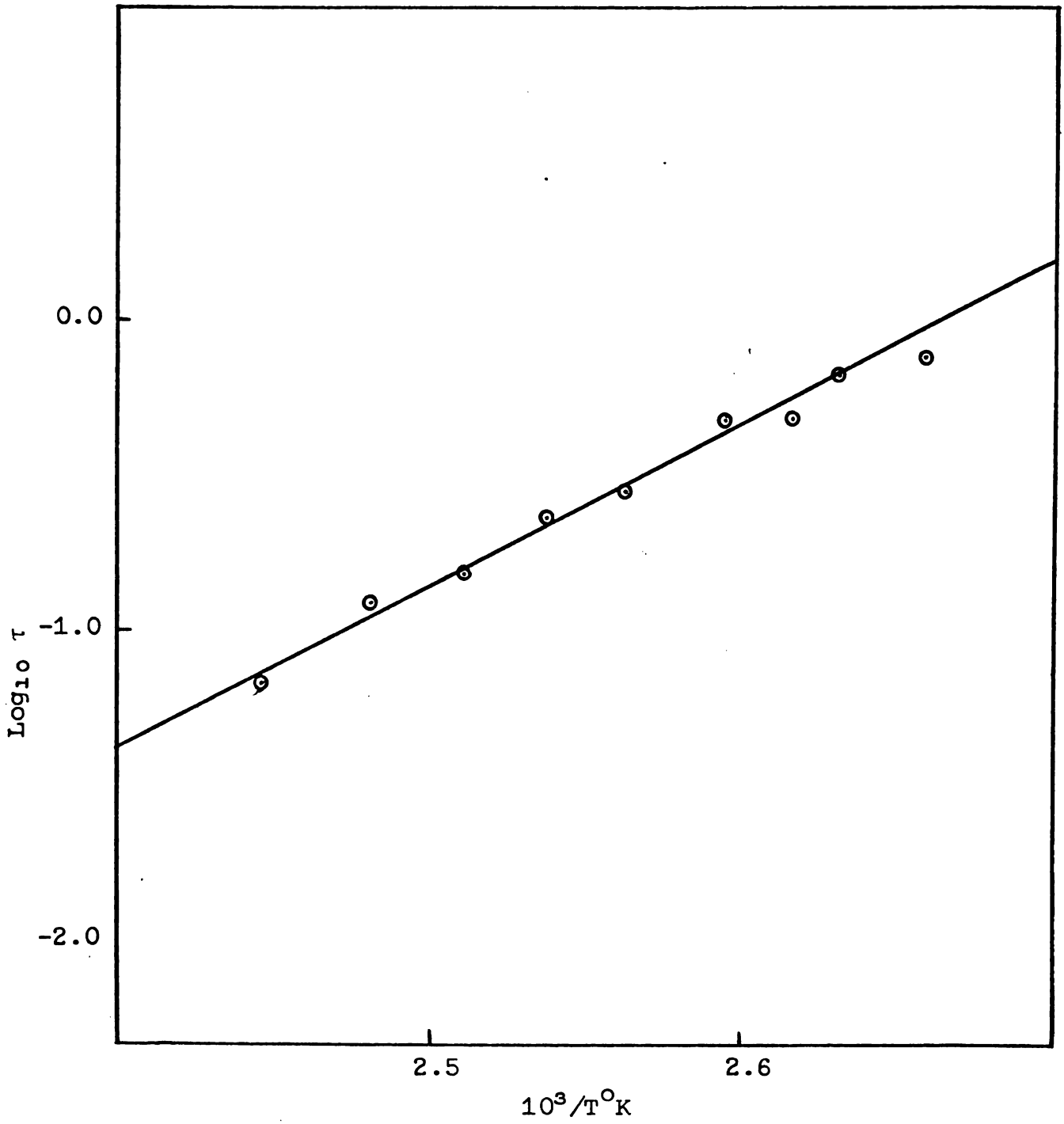

Figure 39. Plot of $\log_{10} \tau$ against $10^3/T^{\circ}K$ for pure $HCON(CH_3)CH_2C_6H_5$ (from benzyl protons).

Table 42. Temperature dependence of the rate of internal rotation about the central C-N bond of $HCON(CH_3)CH_2C_6H_5$.***

$10^3/T^oK$	p_A*	$K = \frac{p_A}{p_B}$	$Log_{10}\ \tau$*	FR * rad/sec
2.660	0.54595	1.2024	-1.003	110.69
2.631	0.52486	1.1046	-1.262	111.47
2.617	0.57939	1.3468	-1.301	115.41
2.595	0.52920	1.124	-1.381	110.4
2.563	0.58639	1.418	-1.596	115.1
2.537	0.55102	1.227	-1.753	117.35
2.511	0.20404	0.25	-1.766	165.37
2.481	0.51246	1.0511	-2.023	124.89
2.446	0.49656	0.9863	-2.162	123.03

E_a = 22.87 kcal/mole

Log_{10} 2A = 14.41

$\Delta F^{\ddagger}_{394.2^oK}$ = 20.68 kcal/mole

Coalescence point = $10^3/T^o_cK \cong 2.48$.

*Results from T.L.S.

***T.L.S. on the formyl doublet.

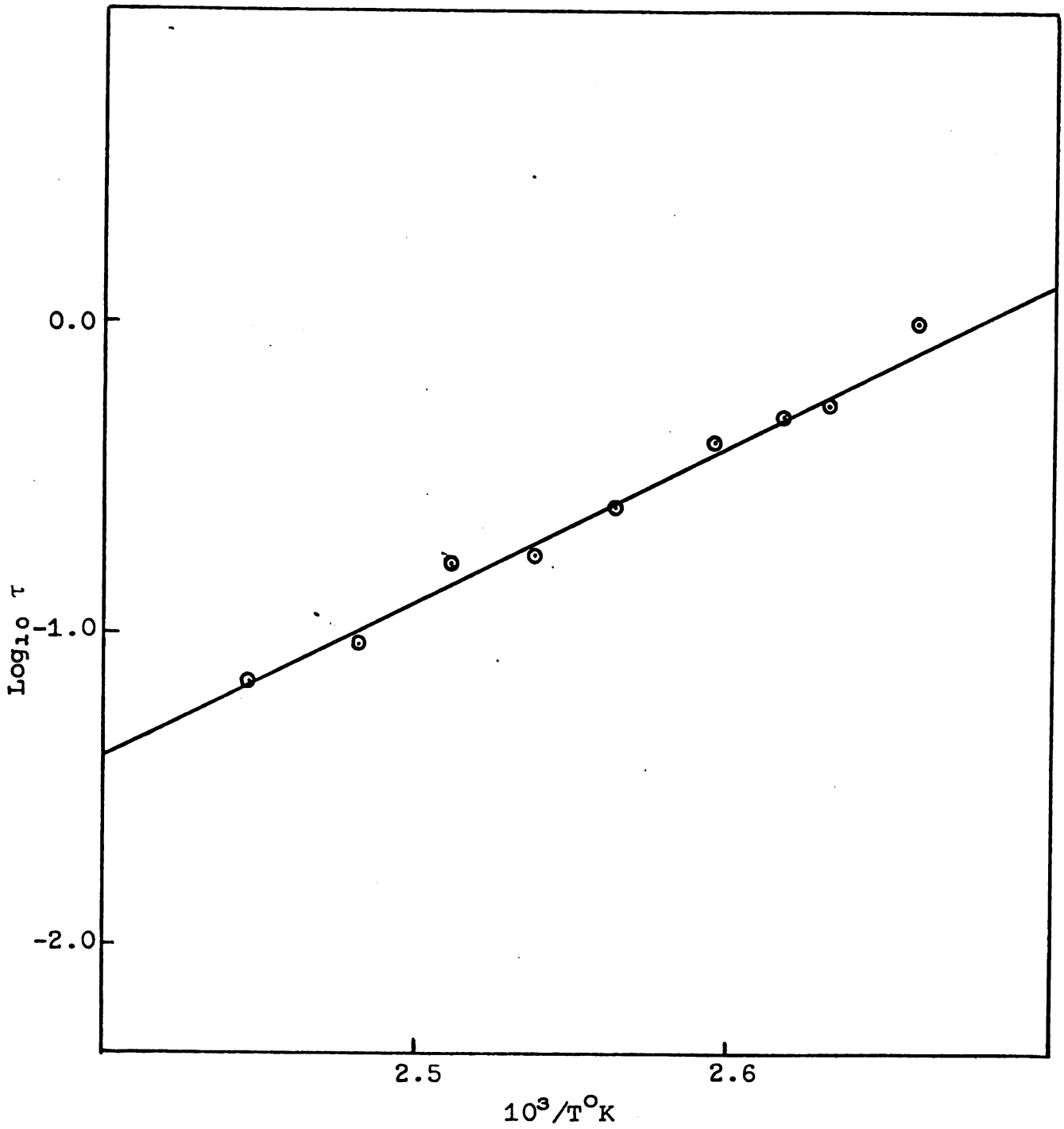

Figure 40. Plot of $\log_{10} \tau$ against $10^3/T^oK$ for pure $HCON(CH_3)CH_2C_6H_5$ (from the formyl doublet).

DISCUSSION

Methods for Obtaining Rate Data from NMR Spectra

The values reported in this thesis for the energy barriers hindering internal rotation in substituted amides have been obtained using three different methods for analyzing the NMR data. These are the peak-separation method, the intensity-ratio method and the method of total line-shape analysis. These methods will now be discussed from the viewpoint of selecting the most practical procedure for applications to chemical problems.

Method I--The Intensity-Ratio Method

This method is based on the measurement of the ratio of maximum to central minimum intensities in a partially coalesced doublet. Any factors which produce errors in this ratio will reduce the accuracy of the results. These factors include spin-coupling in the case where it is small enough to broaden the lines but not sufficiently large to give higher multiplets. In molecules such as DMF this introduces an important error and must be taken into account in the calculations or eliminated. A second error may arise

from overlap of the components of the doublet if the chemical shift between them is not large compared to the line width. This can be corrected for in the calculations (4), but makes it difficult to measure energy barriers when the chemical shift is less than about 5 Hz. The most important error in this method arises from the inhomogeneous broadening of the lines when the static magnetic field varies over the sample volume and, particularly, when the field inhomogeneities change during a given series of measurements. Even though care is taken to tune the spectrometer for maximum field homogeneity at each temperature the line widths in the absence of exchange are limited by this factor and it varies from one measurement to another. Line broadening from this source decreases the maxima and builds up the minima giving intensity ratios which are too small. A systematic error is thereby introduced into the rate constants and the energy barriers. It is this factor which is primarily responsible for the energy barriers being too low when determined by the IR method. A final difficulty is that the intensity ratio can only be determined with precision from the temperature where exchange broadening first causes the doublet components to overlap, up to the coalescence temperature. This range is scarcely large enough for the accurate determination of energy barriers.

Method II--The Peak-Separation Method

This method requires the precise measurement of the apparent chemical shift between doublet components at various temperatures. It is more difficult to make this measurement precisely than it is to measure the intensity ratio, particularly near the coalescence point where the peaks are broad and flat, and it is subject to the same disadvantages as the former method. When the chemical shift in the absence of exchange is small, overlap must be considered. Gutowsky and Holm (3), who originally applied this method to the study of energy barriers in DMF and DMA, at a spectrometer frequency of 17.735 Mhz, suggested that going to higher spectrometer frequencies would reduce the overlap error. The temperature range accessible by this method is unusually small because in the region of slow exchange the peak separation changes only very slowly as the rate of rotation changes while in the region near the coalescence point the errors in the measurement are large. Woodbrey (50) has discussed the dependence of the peak separation on rate of exchange. The peak-separation method is the easiest but the least effective one to use in practice.

The disadvantages of these first two methods and their range of effectiveness have been discussed by Fryer et al. (14). They developed a system for combining several techniques, using data points obtained by each only in the temperature range where that method gives best results.

In this way they obtained plots of rate constant vs temperature covering a wide range of temperature with reasonable precision.

Method III--Total Line-Shape Analysis

The only generally satisfactory method for extracting kinetic results from NMR data is to compare the actual line shape observed with spectra calculated using various combinations of the NMR parameters. To obtain the best values of these parameters some curve fitting procedure is required and the digital computer is the only rapid way to achieve this. It has been shown in this work that, for exchange between two sites, the parameters required are: (1) the chemical shift FR in the absence of exchange, which may itself depend on temperature; (2) the relative populations of protons at sites A and B, p_A and p_B; (3) the individual line widths in the absence of exchange $1/T_{2_A}$ and $1/T_{2_B}$; and (4) the rate constant for the exchange process $1/2\tau$.

The chemical shift in the absence of exchange FR has been assumed constant over the entire temperature range employed in most previous studies. However, it has been recently shown (23) that it often does change with temperature. It should, therefore, be introduced into the line-shape analysis as an adjustable parameter to be determined at each temperature. The curve fitting procedure used in this work has provided the values of FR shown in the final

column of each of the above tables. It is seen that they tend to decrease with increasing temperature until about the coalescence temperature when this trend seems to stop and even reverse. At low temperatures the amides are highly associated (69) and these changes in FR must result partly from the changes in degree of association with temperature.

The population factors p_A, p_B should be exactly 0.5 for symmetrically substituted amides but the computer may select a slightly different value since the experimental lines are not always completely symmetrical. For the unsymmetrical amides p_A may take values other than 0.5, but should approach 0.5 with increase in temperature. In practice this factor changes only slightly with temperature and Gutowsky was able to use the constant value of $p_A = 0.54$ over the entire temperature range covered in his investigation of N-methyl-N-benzylformamide (23) without introducing appreciable error into the rate constants. In this work the program NMRFIT provides values of p_A, p_B at each temperature.

The line widths $1/T_{2_A}$ and $1/T_{2_B}$ should be equal for the symmetrically substituted amides and at low temperatures should be about equal to the line width for the reference. As the temperature increases and exchange broadening becomes important the "natural" line widths become relatively unimportant and the computer tends to select very small values for these parameters. These values have no particular significance and the rate constants are not appreciably altered

if these values are fixed throughout at the values they have in the absence of exchange.

Errors in the Measurement of Rotational Barriers

Values reported for the rotational barriers in a given amide have varied widely. Thus for N,N-dimethylformamide values from 7 to 28.2 kcal/mole have been reported (Table 1), with frequency factors ranging from 10^3 to 10^{17}. Woodbrey investigated in detail the random errors in these parameters as determined by NMR and showed that the 90% confidence limits for values of E_a were usually within ± 1 kcal/mole of the reported values. The large deviations from one laboratory to another, and even within the same laboratory when measurements are made under different conditions (Table 2), must come from important systematic errors.

Fryer, Conti and Franconi (14) attempted to determine the reasons for great variations observed. They considered particularly the effects of field inhomogeneities and gradients (which lead to non-Lorentzian line shapes) and the systematic errors associated with the methods for analyzing NMR data. In this work we have considered the possible effects of impurities, of dissolved oxygen, of the standard used (external or internal) and of the number of data points taken and the temperature range covered. The results for a study of N,N-dimethylcarbamolychloride are shown in Table 44. In each case the field has been optimized

at each temperature, using the 100 MHz instrument, and the total line-shape method for analyzing the data has been used.

It is seen at once that impurities lower the rotational barrier markedly. Even with purified samples the line broadening from dissolved (paramagnetic) air may be significant as shown by the fact that a sample saturated with oxygen gas gave a much lower barrier (17.7 kcal/mole) than that obtained under optimum conditions (21.4 kcal/mole).

The use of an external reference appears to lead to systematic errors which produce values of the rotational barrier which are too high. Since spinning sidebands become more significant with the arrangement used for external referencing the intensity distribution is altered and this result is not unreasonable. The most reliable values for DMCC appear to be E_a = 21.4 kcal/mole and log A = 16.1 obtained with internal TMS reference. It may similarly be noted that the use of external HMDS reference for DMA gave a value of E_a larger by 4.5 kcal/mole than that obtained with internal TMS. The lower value is preferred in each case since the best values reported from other laboratories for DMCC and DMA are 16.9 and 20.6, respectively (Table 1).

Although the values reported here for the rotational barriers in the N,N-dimethylamides agree fairly well with the most recent numbers from the literature and differences are still well beyond the rather small statistical errors (about ± 0.3 kcal/mole) computed by probability theory in

the usual manner. The conclusion must be that all the important factors determining these values have not been isolated and fully taken into account yet. The present values (Tables 43, 44, and 45) represent the results of reducing all the known systematic errors to a minimum.

One possible source of the differences between the present results and those reported in the literature is the unknown effect of the internal reference material which must be used in our work to provide a stable lock signal. A rather large amount of reference (0.2-0.3 mole fraction) must be used and a solvent effect on the barrier is quite possible. Use of an external reference gives less reliable results because of spinning problems. Use of an external lock requires (in our laboratory) going to a spectrometer frequency of 60 MHz where the chemical shift is smaller and the errors correspondingly larger. For this reason we have no completely reliable data on the amides with which to compare our internally referenced samples. Most other authors have used internal TMS in unspecified amount so similar observations hold. The spin-echo measurements are, however, made with pure materials as are all our externally referenced measurements.

It has frequently been noted by investigators in this field (16) that values of $\Delta F^{\ddagger}$ obtained in various laboratories tend to agree quite well; the disagreement is in the values of E_a and log A. For this reason we should

Table 43. Thermodynamic and kinetic parameters for internal rotation about the central C-N bond of some N,N-dimethylamides. [a]

Compound	Solvent	Reference [d]	Number of Data Points [c]	E_a kcal/mole	Log_{10} 2A	$\Delta F^{\ddagger}$	$\Delta H^{\ddagger}$	$\Delta S^{\ddagger}$ e.u.	$T^{\circ}K$	Best Literature Values [f]
$HCON(CH_3)_2$ [e]	--	I-TBB	9	24.2	15.1	21.0	23.4	6.4	375.9	22.0,26.0
$DCON(CH_3)_2$	--	I-TMS	13	27.1	16.7	21.2	26.5	15.4	373.8	22.0,27.4
$DCON(CH_3)_2$	S-$C_2H_2Cl_4$ [b]	I-HMDS	11	19.0	12.1	21.0	18.2	-7.4	379.9	--
$DCON(CH_3)_2$	TBB [b]	I-TBB	11	21.6	13.6	20.9	20.9	-0.1	380.0	(22.0)
DMF-d-H^+	CF_3COOH	I-HMDS	12	16.8	12.1	18.5	16.1	-7.0	337.9	24.0,26.5
$CH_3CON(CH_3)_2$	--	I-TMS	14	22.6	16.1	18.2	21.9	11.2	330.0	23.0
$CH_3CON(CH_3)_2$	--	E-TMS	12	27.1	19.0	18.4	26.5	24.7	329.6	--
DMA-H^+	CF_3COOH	I-HMDS	8	24.5	19.6	15.7	24.0	27.9	295.0	--
$C_2H_5CON(CH_3)_2$	--	I-HMDS	9	21.4	15.9	17.2	20.8	11.1	324.5	21.0
$CH_2=CHCON(CH_3)_2$	--	I-HMDS	9	17.8	14.0	16.7	17.2	1.5	318.8	6.8
$Cl_3CCON(CH_3)_2$	--	E-HMDS	12	22.1	18.5	15.0	21.5	22.2	293.6	--
$Cl_3CCON(CH_3)_2$	--	I-TMS	13	21.1	17.7	15.0	20.5	18.9	293.6	17.0,14.6
$ClCON(CH_3)_2$	--	I-TMS	18	21.4	16.1	17.1	20.7	11.4	314.5	16.9

[a] Values of E_a, $\Delta F^{\ddagger}$, $\Delta H^{\ddagger}$, are in kcal/mole.

[b] Mole fraction amide is about 0.6.

[c] Reference was internal (I) or external (E) and reference materials were hexamethyldisiloxane (HMDS), t-butylbenzene (TBB) or tetramethylsilane (TMS).

[e] The value E_a=23.5kcal/mole is obtained neglecting overlap; the value 24.2 kcal/mole was obtained after making the correction for overlap.

[f] See Table 1.

Table 44. Effect of various factors on the rotational energy barriers in N,N-dimethylcarbamoylchloride (DMCC).[a]

Comments	Reference	N.D.P.[b]	E_a	Log 2A	$\Delta F^{\ddagger}$	$T^{o}K$
Not purified, not degassed	I-c-C_6H_{12}	9	13.8	10.9	17.8	317.5
Purified, not degassed	E-c-C_6H_{12}	8	21.9	16.2	17.4	321.5
Purified, saturated with O_2	I-TMS	9	17.7	13.5	18.2	317.5
Purified and degassed	E-HMDS	5	20.0	14.9	17.4	314.5
Purified and degassed	E-HMDS	17	23.1	17.3	17.1	314.5
Purified and degassed	I-TMS	18	21.4	16.1	17.1	314.5

[a] Values of E_a, $\Delta F^{\ddagger}$, $\Delta H^{\ddagger}$ are in kcal/mole.

[b] NDP = Number of data points.

Table 45. Thermodynamic and kinetic parameters for internal rotation about the central C-N bond of some unsymmetrically N,N-disubstituted amides.

Compound	Reference	NDP	E_a kcal/ mole	Log 2A	$\Delta F^{\ddagger}$	$\Delta H^{\ddagger}$	$\Delta S^{\ddagger}$ e.u.	$T^{o}K$
$CH_3CON(CH_3)C_2H_5$	I-HMDS	13	22.9	16.5	17.7	22.2	13.2	338.2
$CH_3CON(CH_3)$-n-C_4H_9	I-HMDS	10	24.2	17.4	17.6	23.2	17.2	342.6
$CH_3CON(CH_3)$-c-C_6H_{11}	I-HMDS	9	26.2	19.4	17.1	25.6	26.4	321.9
$CH_3CON(CH_3)$-i-C_3H_7	I-HMDS	9	26.8	19.8	17.0	26.1	28.4	321.5
$HCON(CH_3)(CH_2\phi)$[a]	I-TBB	9	23.2	14.6	20.9	22.5	4.0	394.5
$HCON(CH_3)(CH_2\phi)$[b]	I-TBB	9	22.9	14.4	20.7	22.1	3.6	394.5

[a]Results from benzyl proton doublet

[b]Results from formyl proton doublet.

particularly stress the interpretation of the $\Delta F^{\ddagger}$ values when discussing substituent effects. Our values of $\Delta F^{\ddagger}$ almost always agree ± 0.2 kcal/mole with the best literature values.

The values of E_a obtained by the computerized versions of the peak-separation method and the intensity-ratio method are included in the tables of data for the various compounds. These values are consistently lower than those obtained by total line-shape analysis. Since they are less reliable than the latter they will not be used in the discussion.

Rotational Barriers in Symmetrically Substituted Amides

The energy barriers for internal rotation about the C-N bond in the disubstituted amides are much higher than those for internal rotations in ethane, amines, alcohols and ketones, all of which have values about 3 kcal/mole (37). The extra height of the barrier for internal rotation about the C-N bond in amides is believed to result from large partial double bond character in the C-N bond. There is a variety of evidence that

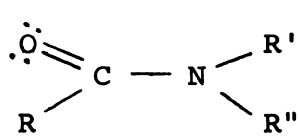

I'

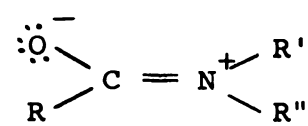

II'

structures I' and II' contribute about equally to the resonance hybrid (97,99). However, there has not been enough data of sufficient reliability to evaluate the effect of substituents R, R', R" on the rotational barrier despite the many articles which have appeared on the subject (see HISTORICAL BACKGROUND). Since the substituent effects should lead to a better understanding of the origin of the barrier an attempt has been made to obtain more precise values for a series of N,N-dimethylamides. The results are summarized in Table 1.

The value obtained here for the rotational barrier in DMF (24.2 kcal/mole) is close to the mean of the best two values available in the literature and there now appears to be reasonable agreement that this value is in the range 24 ± 2 kcal/mole. The higher value (27.4 kcal/mole) obtained with DMF-d_1 and internal TMS may reflect the difficulty of using this standard for the measurements at higher temperature since it is volatile and boils out of the solution causing the internal-lock signal to be erratic; the higher value is, therefore, considered less reliable. Any isotope effect should be small and less than the uncertainties in our values for the barriers. The value for DMF-d_1 will be free of any error from overlap effects but the DMF result has been corrected for overlap so any residual error from this source should be small. A careful spin-echo study of DMF-d_1 has yielded a value E_a = 22 kcal/mole (93)

and the less reliable study of Franconi et al. (14), made by a combination of approximate methods, a value E_a = 27.4 kcal/mole.

The value of 22.6 kcal/mole found here for the rotational barrier in N,N-dimethylacetamide is close to the best value in the literature, 23.0 kcal/mole. Neuman and Jonas (17) have reported 19.6 kcal/mole for DMA-d_3 but this difference may represent a true isotope effect, at least in part. They suggest that the decreased electronegativity and hyperconjugation plus the smaller effective size of CD_3 relative to CH_3 could lead to a decrease in $\Delta F^{\ddagger}$ in the deuterated compound. However, our best value for $\Delta F^{\ddagger}$ (18.2) in DMA is identical with theirs in DMA-d_3 so no isotope effect on $\Delta F^{\ddagger}$ has been established.

Three factors may be of particular importance in determining the size of the rotational barriers. (1) Increasing steric size of the substituent group might be expected to lower the barrier as a result of relief of steric strain in proceeding from the planar ground state to the rotational transition state in symmetrically substituted amides. (2) Increasing resonance donation of charge (by hyperconjugation in this case) should also lower the barrier since cross-conjugation would tend to compete with the principal resonance which provides the large partial double-bond character. Thus, contributions of structures such as III would reduce the partial double-bond character of the

central C-N bond and so the barrier. (3) Increasing inductive donation of charge from the group X will tend to

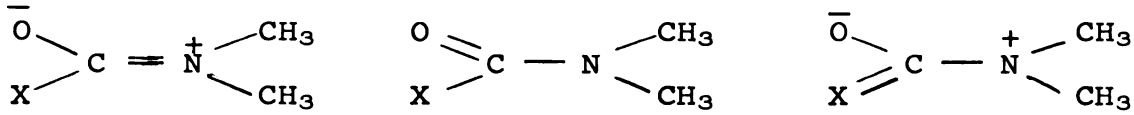

I II III

favor form II and reduce the barrier. Neuman and Jonas (17) have shown that these ideas are in semi-quantitative agreement with experiment by correlating $\Delta F^{\ddagger}$ with the substituent constants σ^* and E_S which measure polar effect and combined steric size and resonance effect, respectively.

Finally, in comparing values of E_a or $\Delta F^{\ddagger}$ in different compounds possible solvent effects must be borne in mind. Even in going from one pure amide to another differences in size and shape of the molecules, and in dielectric constants of the liquids, may alter rotational energy barriers. Further effects from internal reference materials used in the NMR studies are probable.

A significant decrease is observed in both $\Delta F^{\ddagger}$ and E_a on going from DMF ($\Delta F^{\ddagger}$ = 21.0, E_a = 24.2) to DMA ($\Delta F^{\ddagger}$ = 18.2, E_a = 22.6). Substitution of hydrogen by methyl will both increase the size of the group and its ability to donate electrons inductively and both these factors should lower the rotational barrier. Hyperconjugation may also be significant through the contribution of additional structures of type III', which also would reduce the barrier.

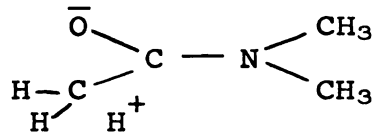

III'

A further decrease in E_a and $\Delta F^{\ddagger}$ is observed in going from DMA to N,N-dimethylpropionamide and can be attributed to both the increase in steric size of the group and in the inductive donation of charge when the methyl group is replaced by ethyl group.

It was suggested by Rogers and Woodbrey (4) that substituents in which cross conjugation with carbonyl oxygen would be important should lead to decreased double-bond character in the central C-N bond and lower barriers. The results for N,N-dimethylacrylamide (E_a = 17.8, $\Delta F^{\ddagger}$ = 16.7) and N,N-dimethylcarbamoylchloride (E_a = 21.4, $\Delta F^{\ddagger}$ = 17.1) bear out this hypothesis, although the effects are not large.

In the case of N,N-dimethyltrichloroacetamide the rotational barrier (E_a = 22.1 kcal/mole) is very close to DMA but $\Delta F^{\ddagger}$ is 3.2 kcal/mole lower. The trichloromethyl group is much more polar than methyl which would tend to increase the barrier but the larger size should oppose this and evidently is the more important factor since a net decrease is observed.

The limited data available on substituent effects in N,N-dimethylamides indicates that the polar effect of the group is of relatively small importance since even the most polar groups (CF_3, CCl_3) lead to rotational barriers not

greatly different from DMA. Steric effects appear to be more important since all the compounds studied have lower rotational barriers than DMF. Resonance effects are perhaps most important since a substantial drop in the barrier occurs when groups capable of conjugating with the carbonyl group are introduced (ϕ, CH_2=CH-, Cl). Much more research will be required to evaluate the influence of each of these factors.

The rotational energy barriers for DMF and DMA in trifluoroacetic acid solution, where the principal species are expected to be DMF-H^+ and DMA-H^+, have been measured. The values for DMF-H^+ ($\Delta F^{\ddagger}$ = 18.5, E_a = 16.8) are surprisingly low since previous investigators have reported much higher values for DMF-H^+. One might expect a higher barrier than in DMF itself since protonation on the oxygen atom

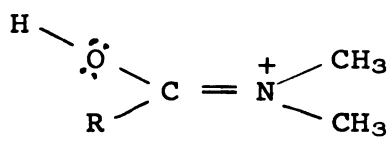

IV

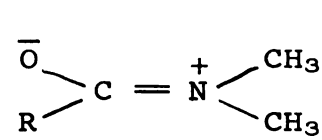

I

occurs and the contribution of resonance structure IV should be more important for the cation, where there is no separation of charge, than the corresponding structure (I) would be for DMF where there is a large separation of charge. It may be noted that although their absolute values are higher than ours, Conti and von Philipsborn (18) did observe a <u>decrease</u> of 3.4 kcal/mole in E_a and of 2 kcal/mole in $\Delta F^{\ddagger}$

on going from DMF-d to DMF-d-H^+. It may be that steric strain is greater in the protonated species thus destabilizing the ground state and lowering the rotational barrier. The expected increase in barrier on protonation does occur with DMA, however. Here E_a(24.5 kcal/mole) has increased 1.9 kcal/mole going from DMA to DMA-H^+ although $\Delta F^{\ddagger}$ has decreased by 2.5 kcal/mole. It was not possible to make precise measurements of the cations in 100% sulfuric acid because of the high viscosity; Franconi and Fraenkel (10) reported such measurements for DMF-H^+ but found that exchange protolysis was the dominant process with DMA.

Solvent Effects on Rotational Barriers in Amides

The effect of added solvent on the rotational barrier in DMF has been investigated by studying solutions of DMF-d_1 in S-tetrachloroethane and in t-butylbenzene. Choosing E_a = 24.2 as the best value for the barrier in DMF, and neglecting any deuterium isotope effect, the rotational barrier is lowered by 2.6 kcal/mole in going from the pure material (containing, however, t-butylbenzene as an internal reference) to a solution with about 0.4 mole fraction S-$C_2H_2Cl_4$. Since the dielectric constant of S-tetrachloroethane (8.2) is considerably lower than that of pure DMF (37.8 at 25°C) the polar ground state of the amide molecule should be destabilized relative to the less polar transition

state and the barrier lowered as is observed. Similarly, going from DMF containing only enough t-butylbenzene to maintain a lock signal to DMF containing about 40 mole percent solvent has lowered the barrier from 24.2 to 21.6 kcal/mole. Neuman et al. (16), however, found a slight increase for the rotational barrier for DMCC on dilution in carbon tetrachloride (but a decrease in $\Delta F^{\ddagger}$ of 0.5 kcal/mole). Our results indicate that both E_a and $\Delta F^{\ddagger}$ are lowered on dilution in a solvent of dielectric constant lower than that of the pure amide.

It should be noted that any solvent (other than an amide solvent) will tend to break up the structure believed to be present in these liquids. The structure arises from two factors--hydrogen bonding between two or more coplanar amide molecules and van der Waals forces between the planar molecules which tend to stack with their planes parallel. Both these factors will tend to increase the energy necessary for rotation of the $-N(CH_3)_2$ group. There will be a tendency then for solvent molecules of other types to lower the rotational barriers by breaking up this structure.

If the hypothesis is correct that solvents of higher dielectric constant stabilize the ground state more than the excited state, then solvents of dielectric constant higher than the pure amides should increase the barrier. This appears to be true since Neuman and Young (12) report a value of E_a = 26.3 kcal/mole for a 10 mole percent solution

of DMF in formamide and a value of E_a = 24.7 for a 10 mole percent solution of DMA in formamide and the dielectric constant of formamide (ε = 109.5 at 25°C) is higher than that of DMF (ε = 37.8) or DMA (ε = 37.9). Neuman and Jonas (17) also find that the value of E_a for DMA is 1 kcal/mole higher in 9.5 mole percent dimethylsulfoxide (ε = 48.9) than for the pure liquid. Unfortunately, no other data for solvent effects on rotational barriers have been reported using total line-shape analysis and the precision of the older work is in doubt.

Rotational Barriers in Unsymmetrically N,N-Disubstituted Amides

A number of older measurements made by the peak separation method (Table 3) have been reported for unsymmetrically N,N-disubstituted amides. However, these are subject to considerable uncertainty and the only reliable values, derived from total line-shape analyses, are those for the barriers in N-methyl-N-benzylformamide (23) and N-acetyl-N-methyl-2,4,6-trinitroaniline (24). In this investigation N-methyl-N-benzylformamide was studied to permit comparison with the work of Gutowsky, and rotational barriers for four N-methyl-N-alkylamides not previously studied have been obtained by the total line-shape analysis method.

In the case of N-methyl-N-benzylformamide the formyl proton is a doublet which coalesces at higher temperatures and the methylene protons of the benzyl group are a chemically

shifted doublet which also coalesces on heating so both can be used to evaluate rotational energy barriers. The values so derived, E_a = 23.2 kcal/mole from benzyl protons and E_a = 22.9 kcal/mole from formyl protons, may be compared with the values E_a = 25.0 kcal/mole (benzyl) and E_a = 22.7 kcal/mole (formyl) obtained by Gutowsky et al. (23). The agreement is good and, in the case of the $\Delta F^{\ddagger}$ values, is excellent. They also determined E_a by a direct equilibration method and obtained a value of 20 ± 3 kcal/mole. Our values agree better with each other than do those of Gutowsky perhaps because we corrected for spin coupling between the formyl and benzyl protons. This was done by estimating the cis and trans couplings and superposing two doublets separated by $(J_1 + J_2)/2$. Although the fine structure is not resolved the line broadening from the spin-coupling will introduce errors into the rate constants unless corrected for. The corrections are small (see Table 41).

In the series of substituted acetamides studied here (V-VIII) the rotational energy barriers are, respectively,

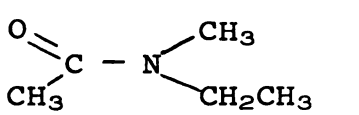

V

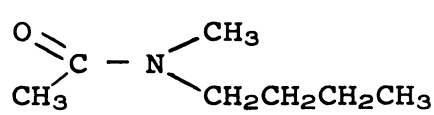

VI

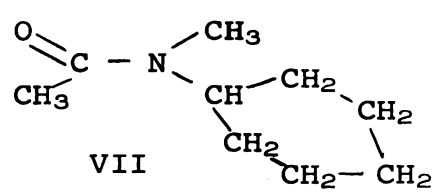

VII

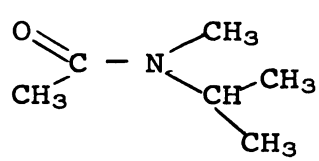

VIII

22.9 kcal/mole, 24.2 kcal/mole, 26.2 kcal/mole and 26.8 kcal/mole. This order roughly follows the order of increasing size of the groups. The steric substituent constants E_S (98) for C_2H_5, n-C_4H_9, c-C_6H_{11} and i-C_3H_7 are, respectively, -0.07, -0.39, -0.79 and -0.47, with cyclohexyl out of line. However, if the values of $\Delta F^{\ddagger}$ are compared then the order is exactly that that of the E_S constants ($\Delta F^{\ddagger}$ = 17.7, 17.6, 17.1 and 17.0 for V-VIII, respectively). However, the barriers would not be expected to increase with increasing size of substituent, but rather to decrease because the steric strain would be relieved in the rotational transition state. It therefore appears that the increasing electron donating powers of the groups must be the dominant effect. The σ^* constants for C_2H_5, n-C_4H_9, c-C_6H_{11} and i-C_3H_7 are -0.100, -0.130, -0.150 and -0.190, respectively. Electron donating substituents on nitrogen could increase the rotational barrier by stabilizing the polar structures of type II which are responsible for the partial double-bond character of the central C-N bond. A more electronegative substituent such as 2,4,6-trinitrophenyl should then lower the value of E_a and Weil et al. (24) report E_a = 19.7 kcal/mole for N-methyl-N-acetyl-2,4,6-trinitroaniline.

The spectra of N-methyl-N-n-butyltrimethylacetamide, N-methyl-N-α-naphthylacetamide, and N-methyl-N-phenylacetamide were also studied, but only one N-methyl resonance peak

was observed for each amide. It could be that: (1) the rate of rotation about the central C-N bond is very fast ($1/\tau \approx 2\pi(\nu_A - \nu_B)$) and only an average of the two N-methyl resonance peaks is observed, (2) the two N-methyl resonance peaks have the same chemical shift, or (3) only one isomer is present. The first possibility is not likely, because all three amides have been studied in the temperature range of -20°C to 65°C, and there is no evidence for two rotational isomers, The second possibility is also improbable, because all the other disubstituted amides did give two distinctive N-methyl resonance peaks, so the chance for these three amides to all accidentally have equal chemical shifts for cis and trans methyl groups is very small. The explanation for the observed single N-methyl resonance peak then must be that there is one dominant isomer, and the steric effects of the bulky substituent group slow the internal rotation about the central C-N bond in these amides. These amides may not be planar in the ground state as a result of steric interactions.

An inspection of the tables containing the activation parameters obtained from different methods indicates that the values of energy barriers and of log A have tended to increase when increasing care has been taken in conducting the experiments and in analyzing the experimental spectra. In several cases, the frequency factors are larger than the usually accepted value for unimolecular reactions,

$6 \times 10^{12} sec^{-1}$ at $300^{o}K$. However, this is not unexpected. From transition state theory the discrepancy reflects an entropy increase in going from the normal amide to the transition state. The large values of $\Delta S^{\ddagger}$ observed may be rationalized in the following way. Amide molecules are known to be approximately planar, hence in the ground state the resonance structure II is favored. The transition state for the internal rotation process is non-planar, and its electronic structure will be better represented by structure I. In the ground state an amide molecule tends to dimerize with another amide molecule to form a rigid configuration such as X.

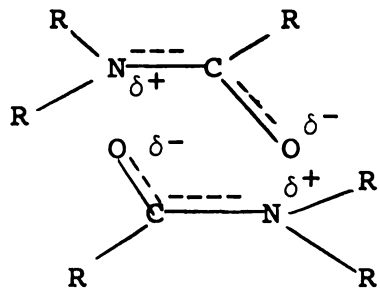

X

Comparing the configuration of the more polar ground state with the less polar activated state it can be seen that in the activated state the amide molecule has less constraint, or more degrees of freedom than in ground state, consequently a positive activation entropy is expected in going from ground state to the activated state. There may even be an additional positive contribution to $\Delta S^{\ddagger}$ because of

desolvation, since it should be more difficult to solvate the non-planar transition state. The high values of the frequency factors for internal rotation about the central C-N bond in amide molecules are thus reasonable.

SUMMARY

(1) Two approximate methods, the intensity-ratio and peak-separation methods for determining rate constants from NMR data, have been evaluated and shown to lead to systematically low values for rotational energy barriers in amides.

(2) A total line-shape analysis method has been developed for obtaining rate constants from NMR data over a wide temperature range. It fits the experimental curve to a "best" set of NMR parameters by a least-squares method and performs all computations and curve plotting using the CDC-3600 computer.

(3) A study has been made of the effects of such factors as sample purity, dissolved oxygen and method of NMR referencing on the rotational barrier of N,N-dimethyl-carbamoylchloride.

(4) The barriers hindering internal rotation in a series of substituted N,N-dimethylamides have been obtained by the total line-shape analysis method and compared with previous values. Substituent effects have been discussed.

(5) The effect of solvents on the rotational barrier in N-N-dimethylformamide has been studied.

(6) The barriers hindering rotation in a series of unsymmetrically N,N-disubstituted amides have been determined by the NMR method and the factors affecting the rotational barriers discussed.

BIBLIOGRAPHY

BIBLIOGRAPHY

1. L. Pauling, "The Nature of the Chemical Bond," p. 207. Cornell Univ. Press, Ithaca, N. Y., 1948.

2. W. D. Phillips, J. Chem. Phys., 23, 1363 (1955).

3. H. S. Gutowsky and C. H. Holm, J. Chem. Phys., 25, 1228 (1956).

4. M. T. Rogers and J. C. Woodbrey, J. Phys. Chem., 66, 540 (1962).

5. J. C. Woodbrey and M. T. Rogers, J. Am. Chem. Soc., 84, 13 (1962).

6. A. Allerhand and H. S. Gutowsky, J. Chem. Phys., 41, 2115 (1964).

7. H. S. Gutowsky and D. W. McCall, J. Chem. Phys., 21, 270 (1953).

8. W. D. Phillips, Annals N. Y. Acad. Sci., 70, 817 (1958).

9. A. Lowenstein and S. Meiboom, J. Chem. Phys., 27, 630 (1957).

10. G. Fraenkel, and C. Franconi, J. Am. Chem. Soc., 82, 4478 (1960).

11. R. J. Gillespie and T. Birchall, Can. J. Chem., 41, 148 (1963).

12. R. C. Neuman Jr., and L. B. Young, J. Phys. Chem., 69, 2570 (1965).

13. K. H. Abramson, P. T. Inglefield, E. Krakower and L. W. Reeves, Can. J. Chem., 44, 1685 (1966).

14. C. W. Fryer, F. Conti, and C. Franconi, Ric. Sci., 35 (II-A), 788 (1965).

15. A. A. Allerhand and H. S. Gutowsky, J. Am. Chem. Soc., 88, 3185 (1966).

16. R. C. Neuman Jr., D. N. Roark, and V. Jonas, J. Am. Chem. Soc., 89, 3412 (1967).

17. R. C. Neuman Jr., and Violet Jonas, J. Am. Chem. Soc., 90, 1970 (1968).

18. F. Conti, and W. von Phillipsborn, Helv. Chem. Acta., 50, 603 (1967).

19. C. Franconi, Z. Electrochem., 65, 645 (1961).

20. A. Mannschreck, Tetrahedron Lett., 19, 1341 (1965).

21. A. Mannschreck, A. Mattheus, and G. Rissman, J. Mol. Spectry., 23, 15 (1967).

22. D. G. Gehring, W. A. Mosher and G. S. Reddy, J. Org. Chem., 31, 3436 (1966).

23. H. S. Gutowsky, J. Jonas, and T. H. Siddall, J. Am. Chem. Soc., 89, 4300 (1967).

24. J. A. Weil, A. Blum, A. H. Heiss and J. K. Kinnaird, J. Chem. Phys., 46, 3132 (1966).

25. N. Bloembergen, E. M. Purcell, and R. V. Pound, Phys. Rev., 73, 679 (1948).

26. F. Bloch, W. W. Hansen, and M. Packard, Phys. Rev., 70, 460 (1946).

27. J. A. Pople, Disc. Faraday Soc., 34, 7 (1962).

28. J. A. Pople, Proc. Roy. Soc. A., 239, 54 (1957).

29. J. W. Emsley, J. Feeney, and L. H. Sutcliffe, "High Resolution NMR Spectroscopy," p. 839, Pergamon Press, 1965.

30. P. G. Maslov, J. Phys. Chem., 72, 1414 (1968).

31. K. J. Packer, J. Chem. Soc., 960 (1963).

32. A. D. Buckingham, T. Schaeffer, and W. G. Schneider, J. Chem. Phys., 32, 1227 (1960).

33. J. C. Schug, J. Phys. Chem., 70, 1816 (1966).

34. T. W. Marshall and J. A. Pople, Mol. Phys., 1, 199 (1958).

35. B. B. Howard, B. Linder, and M. T. Emerson, J. Chem. Phys., 36, 485 (1962).

36. M. Takeda, and E. O. Stejskal, J. Am. Chem. Soc., 82, 25 (1960).

37. C. C. Lin, and J. D. Swalen, Rev. Mod. Phys., 31, 841.

38. H. S. Gutowsky and D. W. McCall, Phys. Rev., 82, 748 (1951).

39. N. F. Ramsey and E. M. Purcell, Phys. Rev., 85, 143 (1952).

40. N. F. Ramsey, Phy. Rev., 91, 303 (1953).

41. J. A. Pople and D. P. Santry, Mol. Phys., 8, 1 (1964).

42. D. M. Grant, Ann. Rev. Phys. Chem., 15, 489 (1964).

43. W. A. Anderson, Phys. Rev., 102, 151 (1965).

44. J. D. Baldeschwieler, and E. W. Randall, Chem. Revs., 63, 81 (1963).

45. J. N. Shoolery, Disc. Faraday Soc., 34, 104 (1962).

46. A. L. Bloom, and J. N. Shoolery, Phys. Rev., 97, 1261 (1955).

47. D. W. Turner, J. Chem. Soc., 847 (1962).

48. R. Freeman and D. H. Whiffen, Mol. Phys., 4, 321 (1961).

50. J. C. Woodbrey, Ph. D. Thesis, M. S. U., 1960.

51. J. Jonas, A. Allerhand and H. S. Gutowsky, J. Phys. Chem., 42, 3396 (1965).

52. F. A. Bovey, E. W. Anderson, F. P. Hood and R. L. Kornegay, J. Chem. Phys., 40, 3099 (1964).

53. T. Nakagawa, Bull. Chem. Soc. Jap., 39, 1006 (1966).

54. H. S. Gutowsky, and P. A. Temussi, J. Am. Chem. Soc., 89, 4358 (1967).

55. M. Saunders, private communication to C. S. Johnson, "Advances in Magnetic Resonance," 1, 33 (1966).

56. F. A. L. Anet and A. J. R. Bourn, J. Am. Chem. Soc., 89, 760 (1967).

57. J. Kaplan, J. Chem. Phys., 28, 278 (1958).

58. S. Alexander, J. Chem. Phys., 37, 967 (1962).

59. S. Alexander, ibid., 974 (1962).

60. C. H. Sederholm, and R. A. Newmark, J. Chem. Phys., 43, 602 (1965).

61. R. J. Kurland, M. B. Ruben, and W. B. Wise, J. Chem. Phys., 40, 2426 (1964).

62. M. Oki, H. Iwamura, and N. Hayakawa, Bull. Chem. Soc. Japan, 37, 1865 (1964).

63. J. Heidberg, J. Weil, G. A. Janusonis, and J. Anderson, J. Chem. Phys., 41, 1033 (1964).

64. K. J. Laidler, "Chemical Kinetics," p. 65, McGraw-Hill, New York, N. Y., 1965.

65. S. W. Benson, "The Fundamentals of Chemical Kinetics," pp. 66-7, McGraw-Hill, New York, N. Y., 1960.

66. A. A. Frost and R. G. Pearson, "Kinetics and Mechanisms," 2nd ed., p. 99, John Wiley and Sons, New York, N. Y., 1961.

67. J. V. Hatton and R. E. Richards, Mol. Phys., 3, 253 (1960).

68. J. V. Hatton and R. E. Richards, Mol. Phys., 5, 139 (1962).

69. A. G. Whittaker and S. Siegel, J. Chem. Phys., 42, 3320 (1956); ibid., 43, 1575 (1965).

70. P. T. Narasimhan, and M. T. Rogers, J. Chem. Phys., 63, 1388 (1959).

71. A. A. Bothner-By and R. E. Glick, J. Chem. Phys., 25, 362 (1956).

72. A. A. Bothner-By, J. Mol. Spectry., 5, 52 (1960).

73. H. J. Bernstein and K. Frei, J. Chem. Phys., 37, 1891 (1962).

74. D. N. Glen, and H. D. Mak., Anal. Chem., 38, 1964 (1966).

75. R. Duerst, and A. Merbach, Rev. Sci. Instr., 36 (12), 1896 (1965).

76. H. D. Young, "Statistical Treatment of Experimental Data," John Wiley and Sons, New York, N. Y., 1962.

77. W. E. Deming, "Statistical Adjustment of Data," ibid., 1943.

78. W. J. Younder, "Statistical Methods for Chemists," John Wiley and Sons, New York, N. Y., 1951.

79. K. A. Anderson and R. L. Snow, J. Chem. Educ., 44, 756 (1967).

80. J. D. Rynbrandt, Personal communication, M.S.U.

81. DuPont, DMF Recovery and Purification Bulletin.

82. DuPont, DMAC Recovery and Purification Bulletin.

83. J. W. Bruhl, Z. Physik. Chem., 22, 388 (1897).

84. J. G. Erickson, J. Am. Chem. Soc., 74, 6281 (1952).

85. J. R. Ruhoff and E. E. Reid, J. Am. Chem. Soc., 59, 401 (1937).

86. A. W. Titherley, J. Am. Chem. Soc., 79, 391 (1901).

87. A. Skita and H. Rolfes, Ber., 53, 1249 (1920).

88. J. V. Braun, F. Jostes and H. Wagner, Ber., 61, 148 (1928).

89. L. A. LaPlanche, Ph. D. Thesis, M.S.U., 1965.

90. B. Sunners, L. Piette and W. G. Schneider, Can. J. Chem., 38, 681 (1960).

91. H. Eyring, T. Ree, D. M. Grant, and R. C. Hirst, Z. Elektrochem., 64, 146 (1960).

92. A. Kessler, Angew. Chem. Intern. Ed. Engl., 7, 228 (1968).

93. L. Reeves, Private communication.

94. G. Isaksson and J. Sandstrom, Acta. Chem. Scand., 21, 1605 (1967).

95. R. M. Hammaker and B. A. Gugler, J. Mol. Spectry., 17, 356 (1965).

96. C. Franconi, Scienza e Tecnica, N.S. Vol. IV, 183 (1960).

97. R. J. Kurland, J. Chem. Phys., 23, 2202 (1955).

98. J. E. Leffler and E. Grunwald, "Rates and Equilibria of Organic Reactions," p. 228, 1963, John Wiley and Sons, Inc., New York.

99. R. J. Kurland and E. B. Wilson Jr., J. Chem. Phys., 27, 585 (1957).

APPENDICES

APPENDIX I

NMRFIT

Description of variables:

P(1) is the τ value or the inverse of twice the rate constant.
P(2) is the population fraction of the lower field component of the doublet.
P(3) is the position of the center of the doublet.
P(4) is the peak separation of the doublet in the absence of exchange.
P(5) is the half width at half height of the lower field component in the absence of exchange.
P(6) is the half width at half height of the higher field component in the absence of exchange.
N is the number of experimental points.
COMPOUND identifies the spectrum.
X(I) is the experimental frequency reading.
Y(4,I) is the experimental intensity at X(I).
Y(3,I) is the calculated intensity at X(I).
Y(6,I) is Y(4,I)-Y(3,I), at X(I).
Y(5,I) is the calculated intensity of the first doublet.
Y(2,I) is the calculated intensity of the second doublet, which is to be superimposed onto the first doublet.
B is the intensity adjustment constant.
C(I), I=1 to 6, are the initial adjustment increments.
TR is the number of times the program passed through a given point in SIZE.
TRY is the desired number of trials.

Flow Chart for
NMRFIT

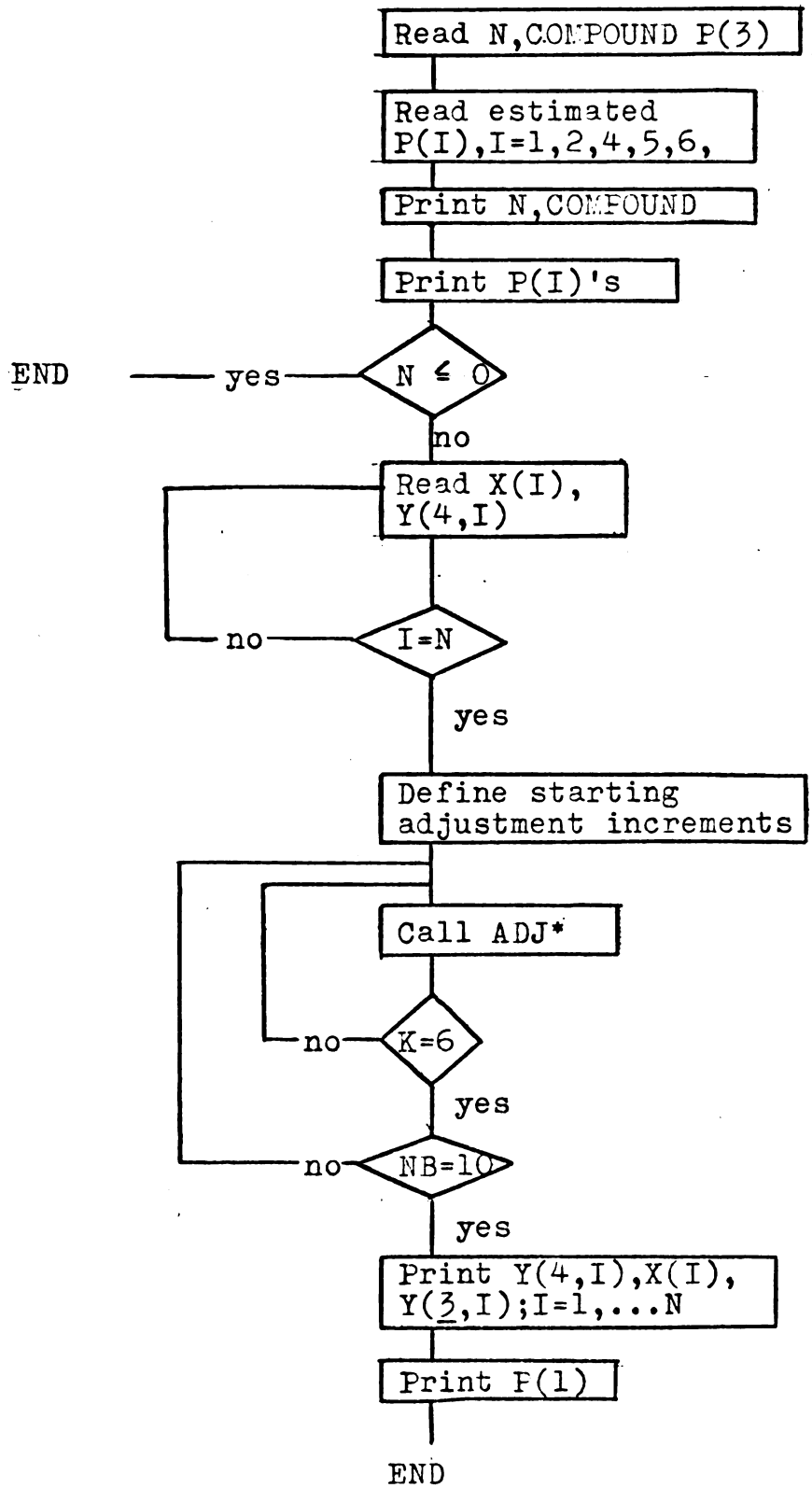

Flow Chart of ADJ*

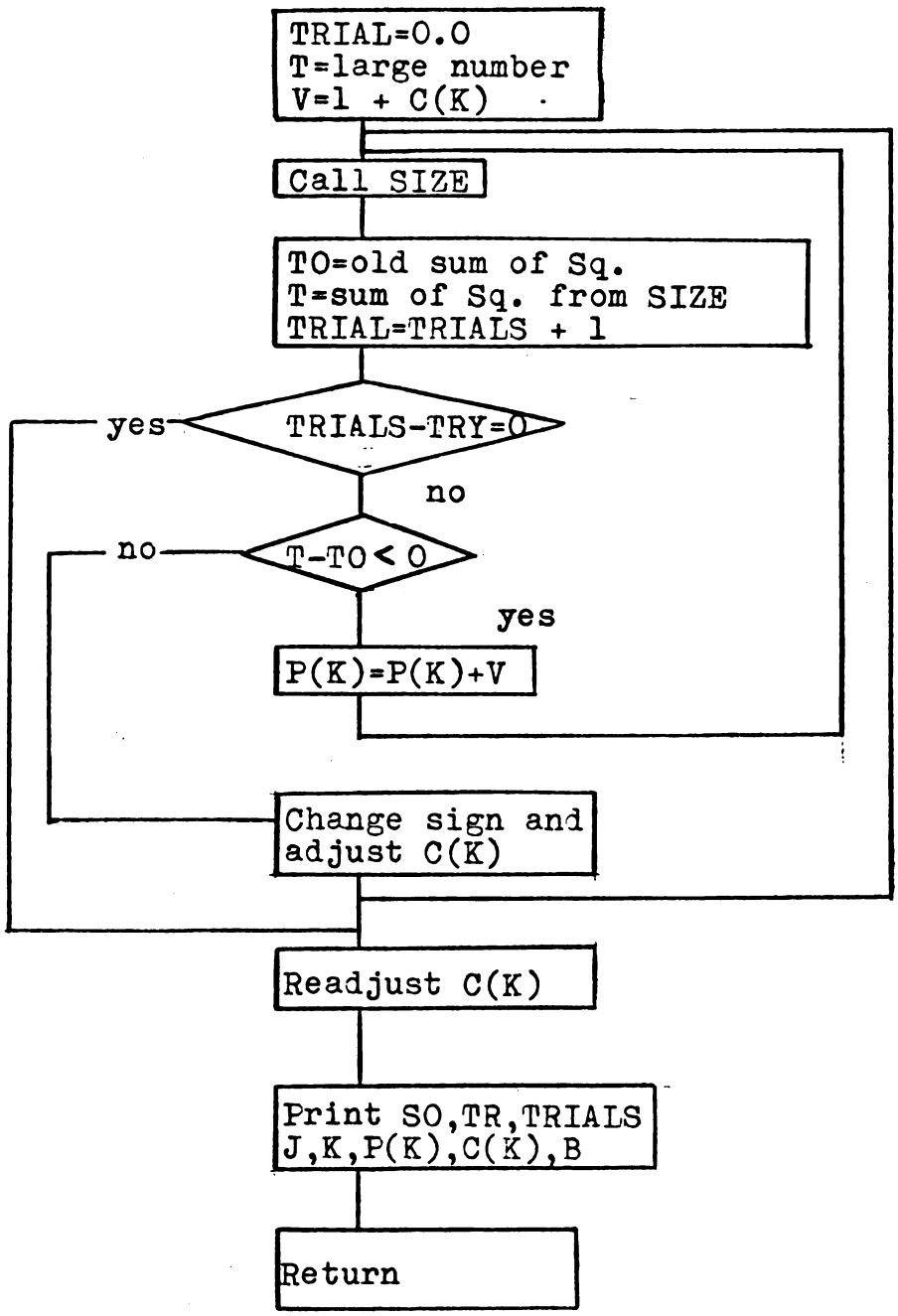

* Ref.80

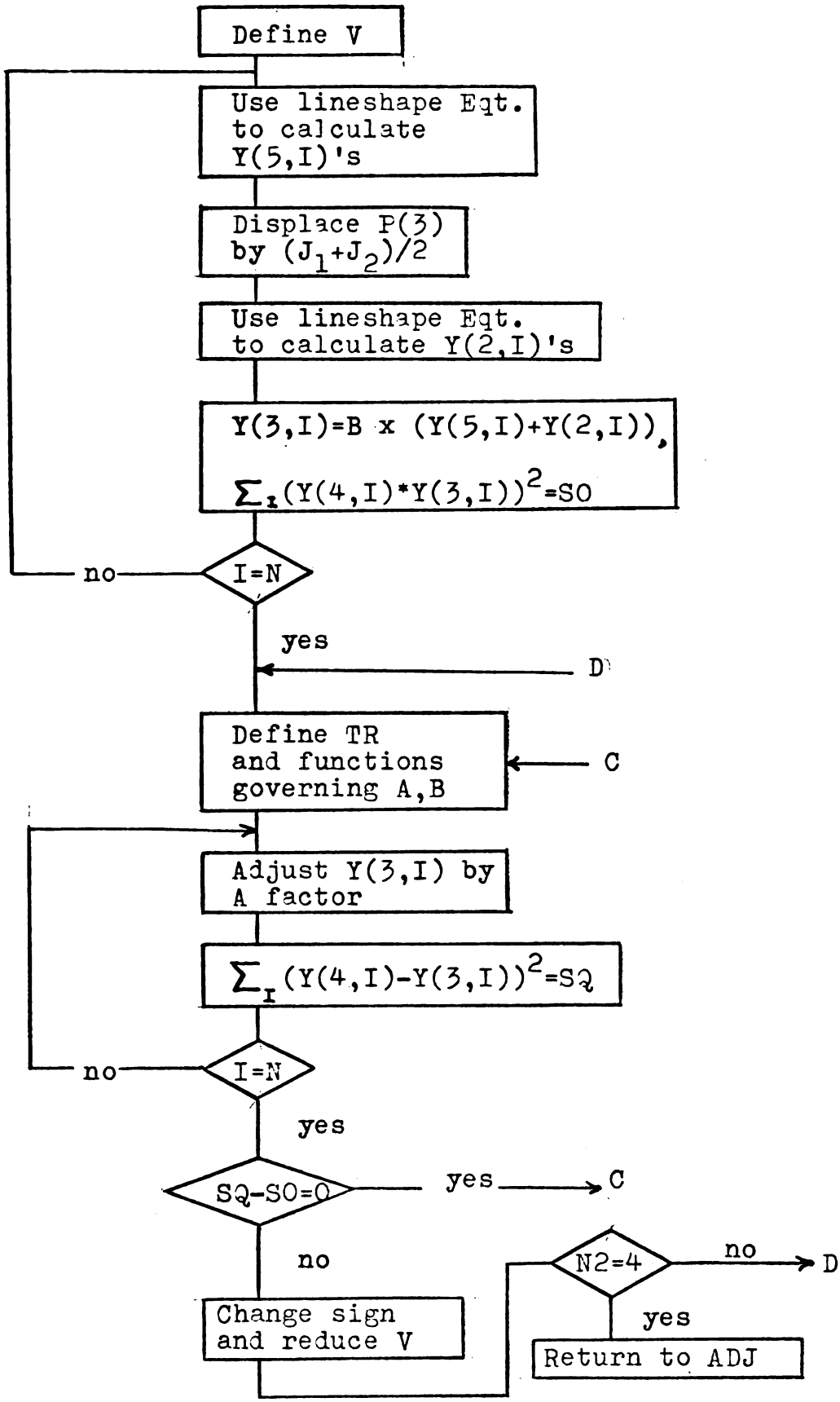
Define V
Use lineshape Eqt. to calculate Y(5,I)'s
Displace P(3) by $(J_1+J_2)/2$
Use lineshape Eqt. to calculate Y(2,I)'s
Y(3,I)=B x (Y(5,I)+Y(2,I)),
$\sum_I (Y(4,I)*Y(3,I))^2=SO$
I=N
no
yes
D
Define TR and functions governing A,B
C
Adjust Y(3,I) by A factor
$\sum_I (Y(4,I)-Y(3,I))^2=SQ$
I=N
no
yes
SQ-SO=0
yes
C
no
N2=4
no
D
yes
Change sign and reduce V
Return to ADJ

```
      PROGRAM NMR FIT
      COMMON X, Y, P, C, B, SO, TRYS, N, K, J, L, TR, BO, TA, TB
      DIMENSION X(200),Y(6,100),P(6),C(6),B(1),BO(6)
C     THIS PROGRAM IS TO FIT THE EXPERIMENTAL DOUBLET OF DISUBSTITUTED
C     AMIDE OR ANY TWO SITE EXCHANGE PROBLAM
C     X IS THE FREQUENCY IN CYCLES  AND Y IS IN RELATIVE INTENSITY
C     P(1) IS THE TAU P(2) IS THE RELATIVE POPULATION OF THE TWO SITES
C     P(3) IS THE CENTER OF THE TWO PEAKS P(4) P(5) P(6) ARE THE
C     PEAK SEP ,HALF OD THE LINDWIDTHES AT THE ABSENCE OF EXCHANGE
    1 FORMAT (I3,A8,1E10.0)
   10 READ 1,N,COMPOUND,P(3)
    3 FORMAT (5E10.0)
      READ 3, P(1),P(2),P(4),P(5),P(6)
      P(4)=P(4)*6.2832*1.025
    4 FORMAT (*1DATA OF SPECTRUM *A8)
      PRINT 4,COMPOUND
    5 FORMAT (6E10.3)
      PRINT 5,P(1),P(2),P(3),P(4),P(5),P(6)
   22 FORMAT(/*     PK NO    CONST NO      CONST          ADJ           INT
     1    SO              TR         TRIALS*/)
      PRINT 22
      IF (N.LE.0) GO TO 15
      DO 11, I=1,N,4
    2 FORMAT (8E10.3)
      READ 2,X(I),Y(4,I),X(I+1),Y(4,I+1),X(I+2),Y(4,I+2),X(I+3),Y(4,I+3)
   11 CONTINUE
      SO = 1.0
      TRYS = 25.0
      P=0.5
      BO=0.4
      C(1)=0.2 $ C(2)=0.005 $ C(3)=0.02
      C(4)=0.02 $ C(5)=0.02 $ C(6)=0.02
      DO 14 NB=1,10
      DO 14 K=1,6
      CALL ADJ
   14 CONTINUE
    7 FORMAT (*     X OBS      Y CAL      Y OBS     Y DIFF *)
      PRINT 7,
    8 FORMAT (1F10.1,4F10.5)
      DO 33, I=1,N
      PRINT 8, X(I),Y(3,I),Y(4,I),Y(6,I)
   33 CONTINUE
    6 FORMAT(///*LOGTAU=*, F10.3)
      A=ALOG10(P(1))
      PRINT 6,A
      GO TO 10
   15 CONTINUE
      END
```

```
      SUBROUTINE ADJ
      COMMON X, Y, P, C, B, SO, TRYS, N, K, J, L, TR, BO, TA, TB
      DIMENSION X(200),Y(6,100),P(6),C(6),B(1),BO(6)
      TRIALS = 0.0
      T = 999999.9
      V=1.0+C(K)
      DO 8 N1 = 1,2
    3 CONTINUE
      CALL SIZE
      TO = T
      T = SO
      TRIALS = TRIALS + 1.0
      IF  (TRIALS - TRYS) 5,9,9
    5 CONTINUE
      IF (T - TO)6,7,7
    6 CONTINUE
      P(K)=P(K)*V
      GO TO 3
    7 CONTINUE
      C(K) =-C(K)
      V=1.0 + C(K)
      P(K)=P(K)*V
    8 CONTINUE
    9 CONTINUE
      C(K)=C(K)*TRIALS/10.0
    1 FORMAT (I6,I10,4X,4E12.4,2F6.0)
      PRINT 1,J,K,P(K),C(K),B,SO,TR,TRIALS
      RETURN
      END
      SUBROUTINE SIZE
      COMMON X, Y, P, C, B, SO, TRYS, N, K, J, L, TR, BO, TA, TB
      DIMENSION X(200),Y(6,100,,P(6),C(6),B(1),BO(6)
      S=0.0
      V=0.025*(B-BO)/ABSF(B-BO)
      BO=B
      CONTINUE
      DO 11 I = 1,N
      R=X(I)-P(3)
      R=R*6.2832*1.025
      TB=1./(P(6)*6.2832*1.025)
      TA=1./(P(5)*6.2832*1.025)
      PP=P(1)*(1./(TA*TB)-R*R+(P(4)/2.)*P(4)/2.)+(1.-P(2))/TB+P(2)/TA
      G=P(1)*(R-P(4)*(P(2)*2.-1.)/2.)
      RR=R*(1.+P(1)*(1./TA+1./TB))+P(1)*P(4)*(1./TB-1./TA)/2.+
     1P(4)*(P(2)*2.-1.)/2.
      Y(5,I)=(PP*(1.+P(1)*P(2)/TB+P(1)*(1.-P(2))/TA)+
     1G*RR)/(PP*PP+RR*RR)
      J1=0.7 $J2=0.3
```

```
      RS=X(I)-(P(3)+(J1+J2)/2.)
      RS=RS*6.2832*1.025
      PT=P(1)*(1./(TA*TB)-RS*RS+((P(4)-J1+J2)/2.)*((P(4)-J1+J2)/2.))+
     1(1.-P(2))/TB+P(2)/TA
      QQ=P(1)*(RS-(P(4)-J1+J2)*(P(2)*2.-1.)/2.)
      RT=RS*(1.+P(1)*(1./TA+1./TB))+P(1)*(P(4)-J1+J2)*(1./TB-1./TA)/
     12.+(P(4)-J1+J2)*(P(2)*2.-1.)/2.
      Y(2,I)=(PT*(1.+P(1)*P(2)/TB+P(1)*(1.-P(2))/TA)+
     1QQ*RT)/(PT*PT+RT*RT)
      Y(3,I)=B*(Y(5,I)+Y(2,I))
      Y(6,I)=Y(4,I)-Y(3,I)
      SQ=Y(6,I)*Y(6,I)
      S=S+SQ
      J=2
   11 CONTINUE
      GO TO 4
    4 CONTINUE
      TR=0.0
      DO 8 N2 = 1,4
      A = 1.0 + V
    5 CONTINUE
      B=B*A
      SO = S
      S = 0.0
      TR=TR+1.0
      DO 6 I = 1,N
      Y(3,I)=Y(3,I)*A
      Y(6,I)=Y(4,I)-Y(3,I)
      SQ=Y(6,I)**2
      S = S + SQ
    6 CONTINUE
      IF (S - SO) 5,7,7
    7 CONTINUE
      V=-V*0.25
    8 CONTINUE
      RETURN
      END
*RUN,10,10000,1
```

APPENDIX II

NMRPLOT

The purpose of this program is to calculate and plot out the spectrum from a given set of line-shape parameters corresponding to those from the program **NMRFIT** which best fit the experimental spectrum. The program can plot out spectra on the same scale as those obtained experimentally, so the calculated and observed spectra can be compared by superimposing one on the other.

Description of symbols:

KAPPA identifies the spectrum.
KSCALE is the scale factor. If it is 1, the plot has a 50 cycle/sec sweep width, and if it is 2 a 100 cycle/sec sweep width.
YY is the highest intensity, in centimeters, of the experimental spectrum. This will set the upper limit of the calculated spectrum.
RECORD is the compound name.
TAU is the inverse of twice of the rate constant.
PA is the fractional population for the low field peak.
R and **S** are the half width at half half height of the two doublet peaks in the absence of exchange.
FR is the peak separation of the doublet in the absence of exchange.
CEN is the center position of the doublet.
TOTAL is the calculated intensity.

Notes:

1) In order to produce the spectrum which best fits the experimental one the line shape parameters should be taken from the output of **NMRFIT**.
2) Before the plotter starts, the pen is at the right hand side of the paper.

3) The statement **CALL PLOT** (200,X,3) requests the total number of inches desired for all the spectra to be plotted. In this case, the request is 200 inches.

4) If more than one spectrum is desired, the data cards for the additional spectra should be provided in the same order as given in the comment statements at the beginning of the program.

5) The program will correct the frequency readings by a calibration factor, such as 1.025 in the statements 333 and 5. This quantity means that 1 cycle/sec. is equal to 1.025 cm. This factor is dependent on the instrument.

Flow Chart for NMRPLOT

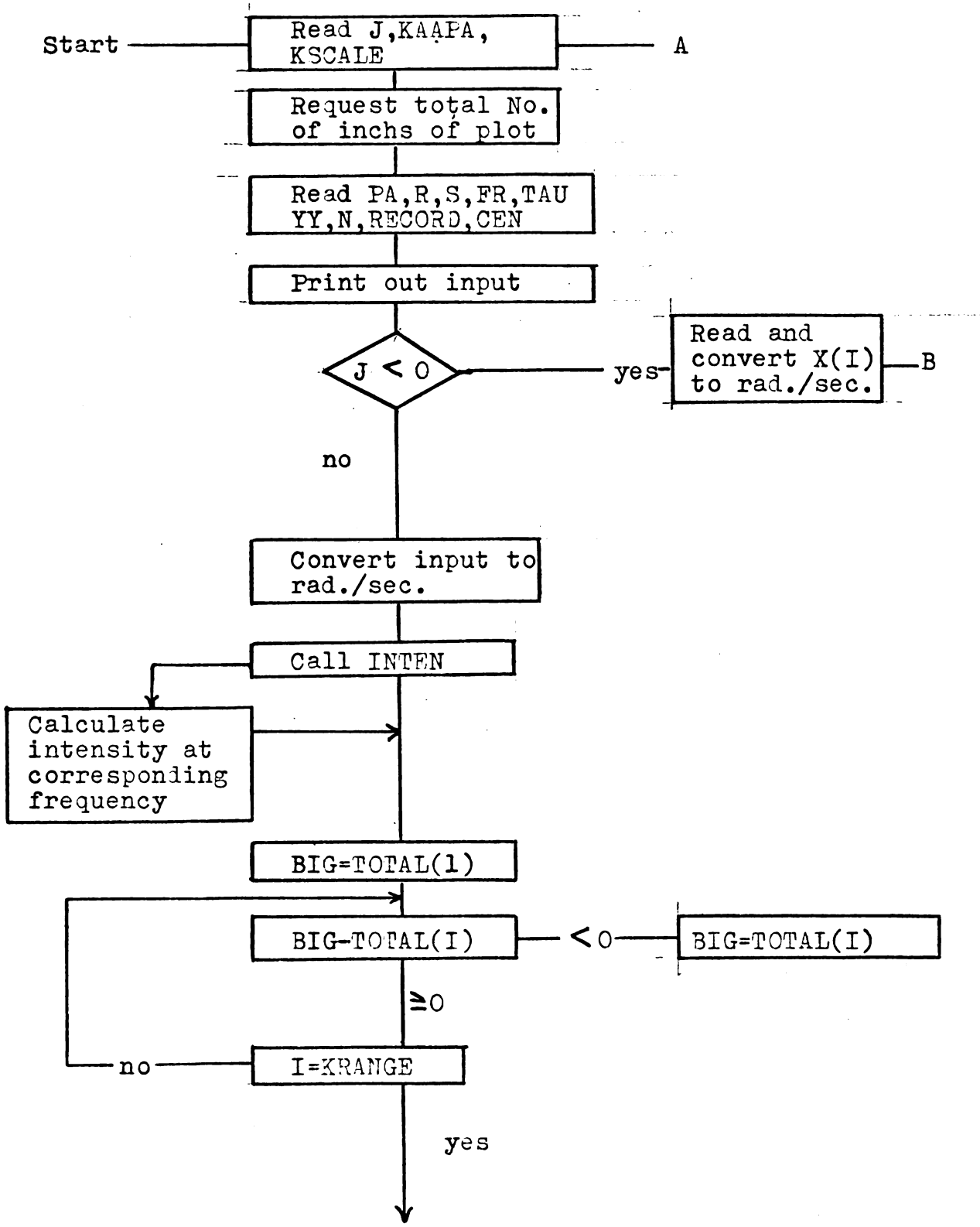

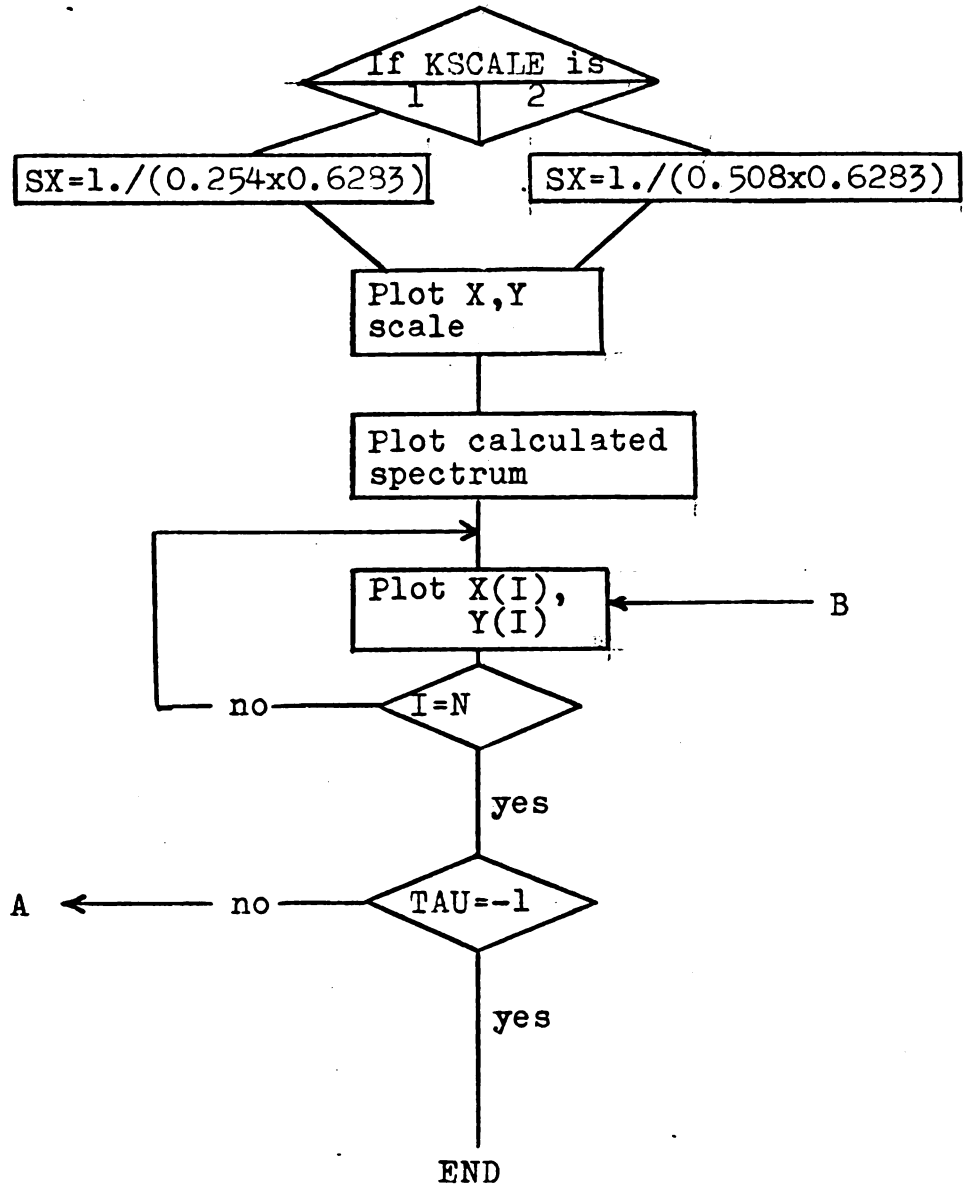
If KSCALE is
1
2
SX=1./(0.254x0.6283)
SX=1./(0.508x0.6283)
Plot X,Y scale
Plot calculated spectrum
Plot X(I), Y(I)
B
no
I=N
yes
A
no
TAU=-1
yes
END

```
      PROGRAM NMRPLOT
      DIMENSION TOTAL(5000),KAPPA(10),XC(100),Y(100),X(100),CEN(1)
      COMMON TOTAL
C     IF J IS 111  EXPT PTS WILL BE INCLUDED
C     IF J IS ZERO ,1ST DATA CARD US BLANK,EXPT PTS NOT READ IN
C     1ST CARD IS J
C     2ND CARD IS IDENTIFICATION OF SPECTRUM
C     3RD 1 FOR 50 CYCLE SWEEPT WIDTH,2 FOR 100 CYCLE S.W.
C     4TH CARD TAU AND YY WHICH IS THE HIGHEST EXPT. POINT IN CM
C     R.S.FR. AS PRINT/OUT FROM NMRFIT
C     5TH PA,R,S,FR WHICH ARE POPULATION,LINE WIDTHS AND PEAK SEP.
C     AT THE ABSENCE OF ROTATION
C     6TH NUMBER OF SPECTRA,RECORD=COMPD NAME,POSITION OF CENTER OF TWO
C     PEAKS
C     7TH X,Y,S ARE THE RELATIVE FREQUENCY AND INTENSITY IS CENTMETER
C     FOR MORE THAN ONE SPECTRA, REPEAT THE ABOVE ORDER
    2 FORMAT (4E10.0)
    4 FORMAT (2E10.0)
    6 FORMAT (10A8)
    8 FORMAT (I1)
   32 FORMAT (8E10.3)
  334 FORMAT (I3)
  750 FORMAT (/,4H PA=E11.5,5X,4H PB=E11.5,5X,
     13H R=E12.6,2X,3H S=E12.6,2X,10H PEAK SEP=E11.5)
  751 FORMAT (/,5H TAU=F12.6)
      READ 334,J
    9 READ 6, KAPPA
      READ 8, KSCALE
      PRINT 6, KAPPA
      CALL PLOT (400,X,3)
      CALL PLOT (0.0,0.0,0.0,100.,100.)
       CALL PLOT (0.0,-20.,2,100.,100.)
    3 READ 4,TAU,YY
      IF (TAU) 88,9,1
    1 READ 2,PA,FR,R,S
      PB=1.-PA
      PRINT 750, PA,PB,R,S,FR
      IF (J.LE.0) GO TO 333
  101 FORMAT (I3,A8,1F10.0)
  100 READ 101,N,RECORD,CEN
      DO 31,I=1,N,4
      READ 32,X(I),Y(I),X(I+1),Y(I+1),X(I+2),Y(I+2),X(I+3),Y(I+3)
C     XC IS X COORD CALCUD FROM READIN X
   31 CONTINUE
      DO 333, I=1,N
      XC(I)=(FR/1.025-(CEN/1.025-X(I)))*6.2832
  333 CONTINUE
C     CONVERT CYCLES/SEC. TO RADIANS/SEC.
```

```
      FR=FR/1.025
      S=S*6.2832/1.025
      R=R*6.2832/1.025
    5 PRINT 751, TAU
      PB=1.-PA
      P=PA-PB
      W=PA*R+PB*S
      Q=1.+TAU*(R+S)
      VM=-FR
      YM=2.*FR
      KRANGE=YM/0.125
    7 DO 10 I=1,KRANGE
      CALL INTEN(TAU,R,S,FR,W,P,Q,TOTAL(I),VM,PA,PB)
   10 VM=VM+0.125
      BIG=TOTAL(1)
      DO 20 I=2,KRANGE
      IF(BIG-TOTAL(I)) 25,20,20
   25 BIG=TOTAL(I)
   20 CONTINUE
      YY=YY*100./2.54
      SY=YY/BIG
      GO TO (21,22), KSCALE
   21 SX=1./(0.254*0.62832)
C     THIS IS SCALED TO 1 CYCLE/CM.
      GO TO 30
   22 SX=1./(0.508*0.62832)
C     THIS IS SCALED TO 2 CYCLES/CM.
   30 CALL PLOT (0.0,0.0,0.0,100.,100.)
      X=0
      DO 11 I=1,9
      X=X+5.0/2.54
      CALL PLOT (0.0,X,1,100.,100.)
      CALL PLOT (0.1,X,1,100.,100.)
   11 CALL PLOT (0.0,X,1,100.,100.)
      CALL PLOT (0.0,0.0,1,100.,100.)
      Y=0
      DO 222 I=1,10
      Y=Y+1.
      CALL PLOT (Y,0.,1,100.,100.)
      CALL PLOT (Y,0.1,1,100.,100.)
  222 CALL PLOT (Y,0.0,1,100.,100.)
      CALL PLOT (0.0,0.0,1,100.,100.)
      VIM=0.125
      DO 76 I=1,KRANGE
      CALL PLOT (TOTAL(I),VIM,1,SY,SX)
      VIM=VIM+0.125
   76 CONTINUE
      CALL PLOT (0.0,0.0,2,SY,SX)
```

```
      CALL PLOT (0.0,0.0,0.0,100.,SX)
      IF (J.LE.0) GO TO 335
      DO 77 I=1,N
      Y(I)=Y(I)/2.54
      CALL PLOT (Y(I),XC(I),2,100.,SX)
      CALL PLOT (0.0,0.0,0.0,100.,100.)
      CALL PLOT (0.05,0.0,2,100.,100.)
      CALL PLOT (0.05,0.05,1)
      CALL PLOT (-0.05,0.05,1)
      CALL PLOT (-0.05,-0.05,1)
      CALL PLOT (0.05,-0.05,1)
      CALL PLOT (0.05,0.0,1)
      CALL PLOT (0.0,0.0,2)
      CALL PLOT (Y(I),XC(I),0,100.,SX)
   77 CONTINUE
      CALL PLOT (0.0,0.0,2,100.,SX)
  335 CALL PLOT (0.0,0.0,0.0,100.,100.)
      CALL PLOT (11.5,0.0,2,100.,100.)
      GO TO 3
   88 CALL PLOT (0.0,0.0,-1,SY,SX)
   89 END
      SUBROUTINE INTEN(TAM,R,S,FR,W,P,Q,TOTAL,F,PA,PR)
      X=FR/2.
      PIN=TAM*(R*S-F*F+X*X)+W
      QIN=TAV*(F-P*X)
      RIN=F*Q+TAM*X*(S-R)+P*X
      PIR=PIN*PIN+RIN*RIN
      TOTAL=(PIN*(1.+TAV*(PR*P+PA*S))+QIN*RIN)/PIR
      END
*RUN,1,29,2100,1

 TEST DATA FOR AN UNSYMMETRICAL DOUBLET
1
```

APPENDIX III

NMRTAU

In this program the rate constants for exchange between the two sites are calculated. The program consists of two parts. The first part of the calculation is based on Woodbrey's intensity-ratio method and the second part of the calculation is based on Gutowsky's peak-separation method (13). No correction for overlap of the doublet components is included in this program because the observed line widths are small in comparison to the peak separation of the doublet. The inputs are the observed lineshape parameters, intensities at two maxima and central minimum, peak separations at each temperature and in absence of exchange, and the temperatures at which spectra were taken. The output is a list of temperatures and the corresponding 1/(2 rate constant) or $1/\tau$ values and the energy barrier and the frequency factor obtained by each method.

Description of symbols:

TEM is the experimental temperature in ^{o}C.
BIG is the relative intensity of the first maximum.
SMA is the relative intensity of the central minimum.
BIGG is the relative intensity of the second maximum.
SPE is the peak separation at TEM.
FR is the peak separation in the absence of exchange.

TAM is the inverse of twice of the rate constant from the peak-separation method.
TAU is the inverse of twice of the rate constant from the intensity-ratio method.
ENG and EN are the energy barriers in kcal/mole from the intensity-ratio and peak-separation methods, respectively.
FRE and FE are the logarithms of the frequency factors from the intensity-ratio and peak-separation methods, respectively.

Flow Chart for NMRTAU

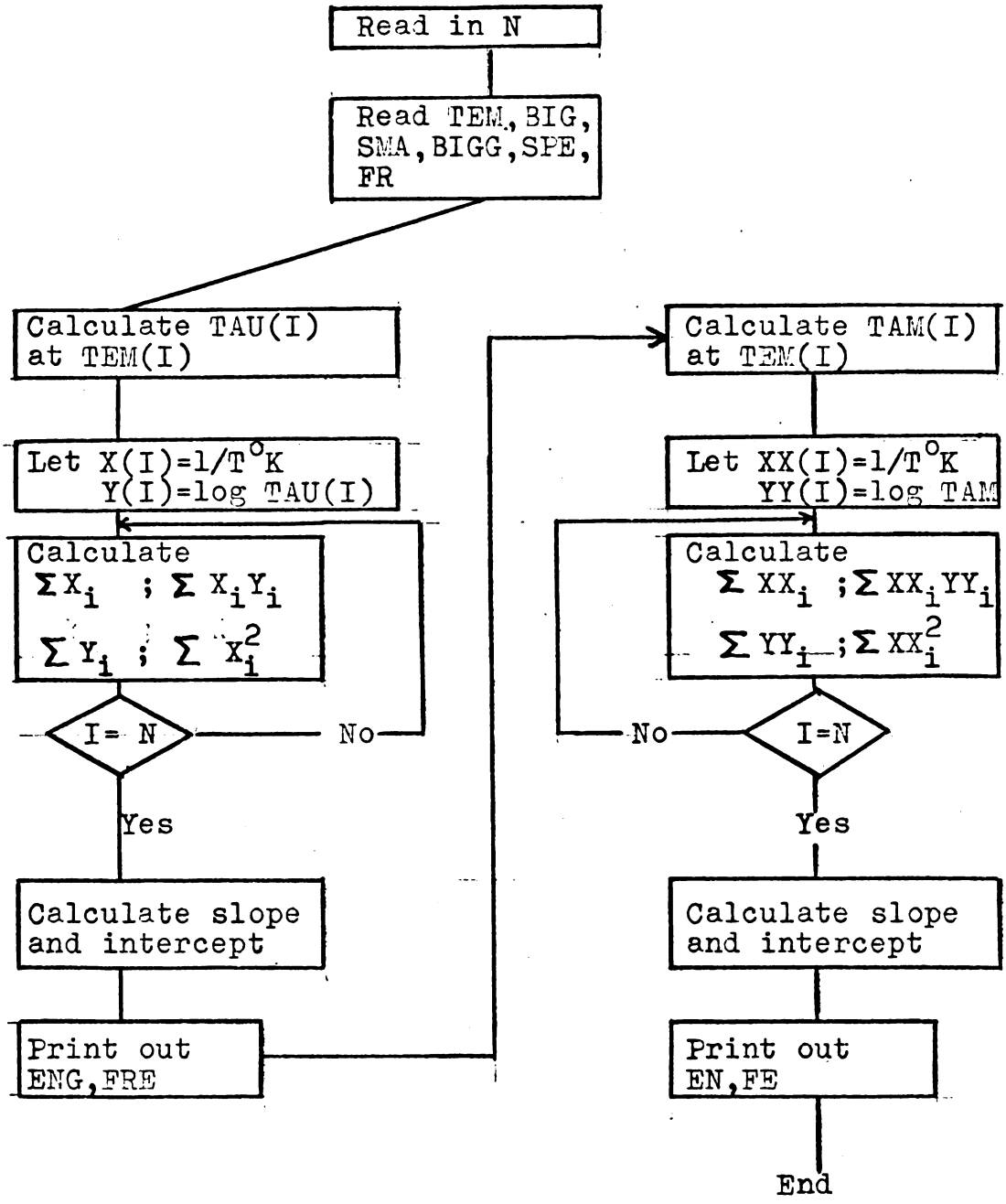

```
      PROGRAM NYRTAU
C     THIS GIVES ENERGY AND FREQUENCY BY INT RATIO AND PEAK SEP
      DIMENSION TAU(100),FR(100),RA(100),SMA(100),BIG(100),BIGG(100),
     1SPE(100),TEM(100),SUMX(50),SUMY(50),SUMXY(50),SUMX2(50),A(50),
     2B(50),ENG(50),FRE(50),TAU(100),EN(100),EE(100),
     3SUX(50),SUY(50),SUXY(50),SUX2(50),
     4X(50),Y(50),XX(50),YY(50)
    1 FORMAT(I2)
    2 FORMAT(6E10.0)
C     ENG AND FRE ARE FROM INT RATIONMETHOD
C     L IS THE NUMBER OF SPECTRA TO BE CALCULATED
      DO 14, L=1,14
      READ 1,N
      IF(N.LE.0)GO TO 100
      DO 10, I=1,N
C     TEMP IN CETIGRADE, INTENSITIES ARE RELATIVE LENGTH
C     SPE AND FR ARE IN CYCLES
      READ 2, TEM(I),BIG(I),SMA(I),BIGG(I),SPE(I),FR(I)
   10 CONTINUE
   33 FORMAT (14HBY INT RATIO,   //)
      PRINT 33
      DO 11, I=1,N
      RA(I)=(BIG(I)+BIGG(I))/(2.*SMA(I))
      TAU(I)=SQRTF(RA(I)+SQRTF(RA(I)**2.-RA(I)))/
     1(3.1416*FR(I)*1.4142)
    3 FORMAT (*TAU(*I2*)=*,E9.3,5X,*TEM(*I2*)=*,E9.3)
      PRINT 3,I,TAU(I),I,TEM(I)
      X(I)=1./(TEM(I)+273.2)
      Y(I)=ALOG10(TAU(I))
   11 CONTINUE
C     LEASR SQUARE APPLICATION
      SUMX=0.
      SUMY=0.
      SUMXY=0.
      SUMX2=0.
      DO 4, I=1,N
      SUMX=SUMX+X(I)
      SUMY=SUMY+Y(I)
      SUMXY=SUMXY+X(I)*Y(I)
    4 SUMX2=SUMX2+X(I)**2
      EN=N
C     A IS THE SLOPE AND B IS THE INTECEPTION
      A=(EN*SUMXY-SUMX*SUMY)/(EN*SUMX2-SUMX**2)
      B=(SUMY*SUMX2-SUMXY*SUMX)/(EN*SUMX2-SUMX**2)
      ENG(L)=2.3*1.987*A
      FRE(L)=B
    5 FORMAT (//*ENG(*I2*)=*,E10.3,5X,*FRE(*I2*)=*,E10.3,///)
      PRINT 5,L,ENG(L),L,FRE(L)
```

```
C       BY PEAK SEP METHOD
   99 FORMAT (12HBY PEAK SEP,  //)
      PRINT 99
      DO 13, I=1,N
      TAM(I)=1./(1.4142*3.1416*SQRTF(FR(I)**2.-SPF(I)**2.))
    9 FORMAT (*TAY(*I2*)=*,F10.3,5X,*TEY(*I2*)=*,F10.3)
      PRINT 9,I,TAM(I),I,TEM(I)
      XX(I)=1./(TEY(I)+273.2)
      YY(I)=ALOG10(TAM(I))
   13 CONTINUE
C       LEAST SQURE APPLICATION
      SUX=0.
      SUY=0.
      SUXY=0.
      SUX2=0.
      DO 6, I=1,N
      SUX=SUX+XX(I)
      SUY=SUY+YY(I)
      SUXY=SUXY+XX(I)*YY(I)
    6 SUX2=SUX2+XX(I)**2
      FNN=N
C       AA IS SLOPE,BB IS INTECEPT
      AA=(FNN*SUXY-SUX*SUY)/(FNN*SUX2-SUX**2)
      BB=(SUY*SUX2-SUX*SUXY)/(FNN*SUX2-SUX**2)
      EN(L)=2.3*1.987*AA
      EE(L)=BB
    7 FORMAT (//*EN(*I2*)=*,F10.3,5X,*EE(*I2*)=*,F10.3,///)
      PRINT 7,L,EN(L),L,EE(L)
   14 CONTINUE
  100 CONTINUE
      END
*RUN,1,3000,1
```